8-10-2021

Unprecedented DNA Photocleavage Mediated by Quinolinium Pentamethine Carbocyanine Dyes in the NIR Wavelength Range

Effibe O. Ahoulou
odetteffibe@yahoo.fr

Unprecedented DNA Photocleavage Mediated by Quinolinium Pentamethine Carbocyanine Dyes in the NIR Wavelength Range

by

Effibe Ahoulou

Under the Direction of Kathryn B. Grant, PhD

A Thesis submitted in Partial Fulfillment of the Requirements for the Degree of

Master of Science

in the College of Arts and Sciences

Georgia State University

2021

ABSTRACT

Here we report the DNA photocleavage abilities of near-infrared (NIR) quinolinium pentamethine carbocyanine dyes substituted with either bromine, chlorine, or hydrogen at the *meso*-carbon position. We are interested in developing these cyanine dyes as treatment agents in photodynamic cancer therapy because they can be activated to selectively kill diseased cells with NIR light that deeply penetrates biological tissues. UV-visible, CD, and fluorescence spectra show that the brominated quinolinium cyanine dyes **4** and **KI2** are stable in aqueous buffer and bind to DNA in a non-intercalative manner both externally and in the DNA minor groove. Reactions run in the presence and absence of fluorescent probes and chemical additives reveal that irradiation of dye **4** and **KI2** with 707–759-nm and 830-905 nm NIR light respectively generates Type I $OH^{\bullet}$ radicals that form direct strand breaks in plasmid DNA in high yield.

INDEX WORDS: PDT, Cyanine, Dye, Quinolinium, DNA binding, ROS, Hydroxyl radicals, Singlet oxygen, Photocleavage, DNA binding, SOSG, HPF, Non-intercalative, Groove binding, Intercalation, Near-infrared

Unprecedented DNA Photocleavage Mediated by Quinolinium Pentamethine Carbocyanine Dyes in the NIR Wavelength Range

by

Effibe Ahoulou

Committee Chair: Kathryn B. Grant

Committee: Maged Henary

Dabney Dixon

Electronic Version Approved:

Office of Graduate Services

College of Arts and Sciences

Georgia State University

August 2021

DEDICATION

I dedicate this thesis to both my father, Gerard N'gatta Ahoulou and my mother, Josephine Mokoubo Mosson, for the constant support and encouragement that they have always provided on my behalf. Words cannot even express my gratitude towards them for all they have done for me. To my siblings, uncles Mathieu N'gatta, and Mathias N'gatta, I thank them so much for their thoughtfulness, support, and encouragement. To my father, whom I affectionately call "grand G" you know what? I say millions of thanks to you, the road was long, but you never missed your support on my behalf through this journey. You have always shown me what a father can do for his daughter. Thank you for that because, without your support, I would not have been here in my academic career and complete this masters project. It is difficult to invest in an education from an associate degree level to the master level. Nevertheless, it is feasible, and you proved it. I salute and pay you a huge respect to you for that. To all my friends, thank you for your time and encouragement.

ACKNOWLEDGEMENTS

I want to thank all individuals who demonstrated a vital contribution to my scientific research progress and my accomplishments in graduate school. I would like to tell you that I greatly appreciate your help because I would not have made it happen on time without it. I would like to thank Professor Kathryn B. Grant for all her support and encouragement throughout my scientific work. Thank you for believing in me and providing me the opportunities that challenged me to think further. As a graduate student, I have learned a lot from her throughout my studies under her supervision. Her insightful and expert guidance has tremendously impacted my life not only academically but also socially and personally. With her inner guidance, I can say I am readier to continue my career.

Similarly, I would like to express my gratitude towards my thesis committee members, Professors Dabney Dixon and Maged Henary, for their valuable support and advice. Also, I tremendously appreciate your insightful comments. To the Georgia State University Department of Chemistry faculty members and staff, thank you for your support and help. To my friend Daniel Ouedraogo, thank you for being there for me at all costs; I appreciate your dedicative support and encouragement for me to make it through this journey and successfully complete this thesis. Least but not last, I would like to thank all my lab mates for their support during graduate school, mainly to Dr. Kanchan Basnet, whose research project was related to mine, and Dr. M. Sadegh Safiarian for their contributions throughout this thesis project. I would like to thank my other lab mates, Victoria Milian, Lynda Kouomou, Aikohi Ugboya, David Brewer, Carine Seudieu, and Karen Phan for making me have an exciting and memorable graduate school experience at Georgia State University.

TABLE OF CONTENTS

LIST OF TABLES

LIST OF FIGURES

LIST OF ABBREVIATIONS

PDT	=	Photodynamic therapy
ROS	=	Reactive oxygen species
PS	=	Photosensitizer
HpD	=	Hematoporphyrin
5-ALA	=	5-Aminolevulinic acid
MAL	=	Methyl aminolevulinate
MB	=	Methylene blue
NIR	=	Near-infrared
LED	=	Light emitting diode
UV	=	Ultraviolet
CT DNA	=	Calf thymus DNA
DAPI	=	4′,6-diamidino-2-phenylindole
DMEM	=	Dulbecco's Modified Eagle Media
DMSO	=	Dimethyl sulfoxide
DPBS	=	Dulbecco's phosphate-buffered saline
ICD	=	Induced circular dichroism
ICG	=	Indocyanine green
OY	=	Oxazole yellow
TAE	=	Tris-acetate-EDTA
TO	=	Thiazole orange
EtBr	=	Ethidium bromide
EDTA	=	Ethylenediaminetetraacetic acid

D_2O	=	Deuterium oxide
HPF	=	Hydroxyphenyl fluorescein
SOSG	=	Singlet oxygen sensor green

1 PHOTODYNAMIC THERAPY A THERAPEUTIC APPROACH: DNA PHOTOCLEAVAGE AND DNA-CYANINE DYE INTERACTIONS

1.1 Photodynamic Therapy

Photodynamic therapy (PDT) is a form of light treatment to cure various diseases, including cancer. PDT is commonly performed as an outpatient procedure.[1] It requires the intravenous, oral, or topical application of a drug called a photosensitizer (PS) into the body.[2] Light is then used to activate the PS in targeted tissues, resulting in the localized production of cytotoxic reactive oxygen species. The treatment can be performed before or after radiotherapy, surgery, cryotherapy, chemotherapy, and surgery or in combination without compromising the other treatment modalities.[3] Unlike conventional therapies, such as chemotherapy and radiotherapy, PDT is non-invasive with low cytotoxicity and has high effectiveness.[4] PDT is selective and can accurately target the affected areas without compromising surrounding healthy cells. It is a repeatable procedure with moderate side effects and can be administered over a short time period.[5] PDT is a promising treatment that has grown speedily over the past years. Though PDT was initially reported to treat various skin conditions, including actinic keratoses (AK) and localized patch-stage cutaneous T-cell lymphoma with the limitation of deep light penetration issues, it has shown potential in the treatments of several diseases.[6, 7] PDT is used to cure head and neck, bladder, esophageal, skin, and cavity cancers.[8, 9] Also, it can enhance the survival rate of patients with cancerous diseases. Chhatre and co-workers reported a significant decrease in the mortality rate of Stage III and Stage IV non-small cell lung cancer (NSCLC) patients who received treatment with a combination of PDT and chemotherapy.[10]

Nowadays, PDT is employed in several fields: in urology, dermatology, gastroenterology, and ophthalmology.[11] In dentistry, PDT has lately been used as an alternative procedure in

periodontal care to eliminate bacteria from infected areas during root canal treatment.[12, 13] It has been applied to disinfect dentin and oral tissues. We can infer that PDT applications are broad.

1.1.1 History of Photodynamic Therapy

Light therapy, classically known as heliotherapy dates to antiquity, where light was used to treat psoriasis, rickets, and vitiligo.[14] In ancient Greece, daylight exposure was utilized as a way to cure various skin conditions. Light therapy was further developed by Niels Finsen, a Danish physician and scientist. As a physician, he worked extensively with various light sources to treat several diseases. In 1903, Finsen received a Nobel prize for using carbon arc phototherapy to treat skin tuberculosis.[15] His work encouraged other scientists such as von Tappeiner to use light as a therapeutic system to treat diseases. Von Tappeiner was the first scientist to conduct scientific PDT clinical trials by treating patients with basal cell carcinoma through the combination of dyes and exposure to either sunlight or arc-lamp light.[16] Von Tappeiner and co-workers also led an experiment where they observed that protozoans stained with acridine orange were destroyed upon their exposure to bright light.[17] Many other studies were further driven towards PDT in which von Tappeimer employed dyes and light to treat tuberculosis, syphilis, and tumors. During his numerous studies, he observed that oxygen was one of the main requirements of the treatment and coined the term “photodynamic therapy”.[18, 19] The modern era of PDT began in 1960 with a study, which led to the discovery of a porphyrin-based photosensitizer, hematoporphyrin derivative (HpD), by Lipson and Schwartz[20] at the Mayo Clinic. They observed fluorescence of neoplastic lesions and phototoxicity effects upon the injection of crude hematoporphyrin into the skin during surgery.[21]

In the 1970s, Dougherty clinically investigated the translational relevance for PDT using HpD to treat various tumors. HpD was selectively localized in tumors [20, 22] making PDT initially

a promising treatment for cancer. Soon after, in 1993, the first regulatory approval PDT agent, porfimer sodium (Photofrin®), originated in Canada for the treatment of bladder desease.[22] Since then, many other PDT agents have been synthesized as derivatives of the initially discovered PS agent. Consequently, numerous new PS have followed and gained clinical approval worldwide to image and treat various cancers and other diseases.

1.2 Components and Principle of PDT

PDT involves the administration of a PS into the targeted tissues. The procedure can be defined in two stages. During the first stage, the PS accumulates into the affected tissue upon its administration. In the second stage, the PS is exposed to light with low energy and a specific wavelength leading to its activation.[23] PDT requires three principal components: a PS, light, and oxygen.[24] Each component plays an essential role in PDT treatment. Hence, proper identification and choice of the components are vital.

1.2.1 Photosensitizing Agents

An ideal PS should be a pure, stable PS agent, and water-soluble.[25] However, for better tissues penetration, the light absorption of the PS should ideally lie within the infra-red region of the electromagnetic spectrum with a range of 650-850 nm, called the “therapeutic window”.[26] Near-infrared (NIR) photosensitizers are strongly recommended, and are ideal PDT agent candidates because they can absorb light that is easily transmitted through biological tissues, such as skin and blood.[27] The PS should possess minimal dark toxicity and an excellent cytotoxic effect after its photoactivation. The selected PS should have should efficiently produce ROS.[28] Also, the PS should have a good accumulation and retention into the target cells.

The PS should exhibit a high extinction coefficient and quantum yield for ROS production.[29] Also, an optimum PS concentration and the PS uptake into the cancerous cells are

critical parameters in achieving an effective PDT treatment.[30, 31] However, PS, light penetration, and oxygen perfusion vary per person based on the type of tissues, making it difficult to accurately predict PDT effects.[32] Photosensitizers are sometimes categorized as anti-microbial or anticancer drugs with structural features that differ from each other. Anti-cancer photosensitizers are mostly lipophilic with less or neutral overall charge. In contrast, anti-microbial photosensitizers tend to have pronounced cationic charges, making them better candidates in targeting Gram-negative bacteria.[33] Photosensitizers containing tetrapyrrole structures make the largest group of photosensitizers employed in cancer treatment. These photosensitizers have tetrapyrrole backbones, which are naturally derived from chlorophyll, heme, and bacteriochlorophyll. This type of photosensitizer can further be divided into four main classes: porphyrins, chlorins, bacteriochlorin, and phthalocyanine derivatives. Examples of porphyrin-based photosensitizers are hematoporphyrin (HpD), porfimer sodium (Photofrin®), protoporphyrin-IX with precursors 5-aminolevulinicacid (5-ALA or Levulan®) and methyl aminolevulinate (MAL or Metvix®). Temoporfin (Foscan®), verteporfin (Visudyne®), and talaporfin (Laserphyrin®) constitute the chlorins family, while Redaporfin (LUZ-11®) is a bacteriochlorin (Figure 1.1).[33] Besides tetrapyrroles, other groups include synthetic dyes, such as phenothiazinium dyes (*e.g.,* methylene blue, toluidine blue, and nile bleu), squaraines, transition metal complex dyes, and cyanine dyes (*e.g.*, merocyanines and cationic cyanine dyes).[34] HpD and photofrin were the first regulatorily approved PDT agents by the FDA and are broadly used worldwide. In 2003, the FDA clinically approved porfimer sodium for the treatment of Barrett's esophagus. Temoporfin is sold in Europe for the treatment of head and neck squamous cell carcinoma. Talaporfin is mainly used in Japan for the treatment of lung cancer.[35, 36]

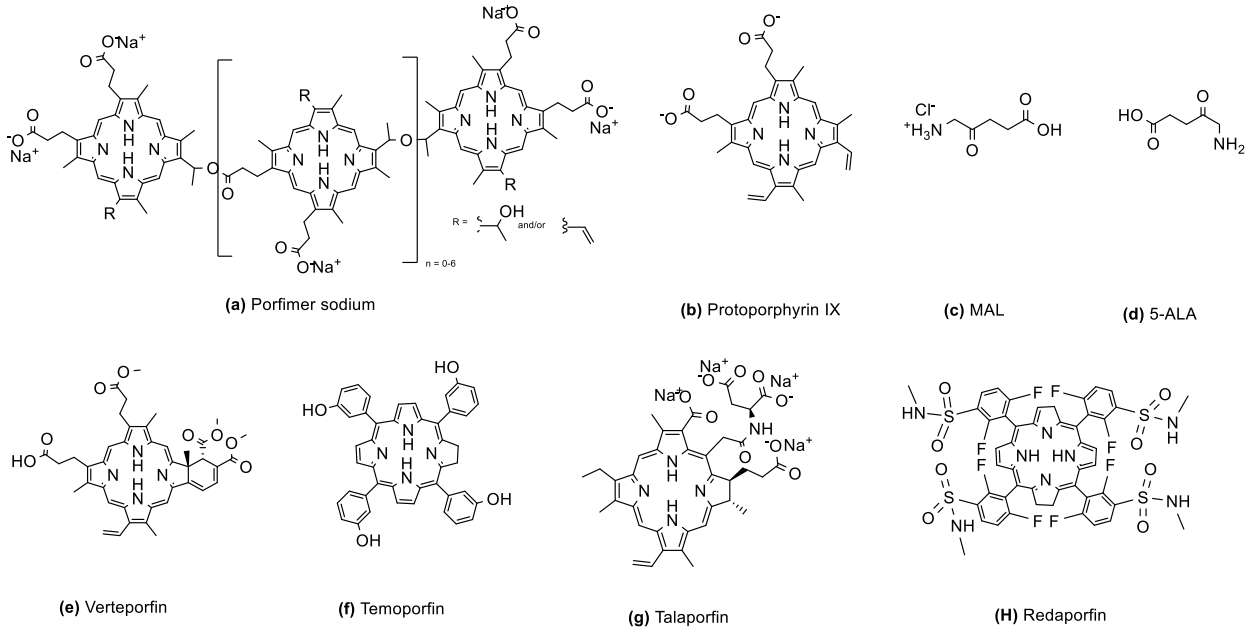

Figure 1.1: Examples of PDT agents.

Although may drugs have been discovered and successfully used in PDT, only a few of these PDT agents have been approved so far. Thus, porfimer sodium, 5-ALA, MAL, and verteporfin have been approved in the USA by FDA.[36] Though these PSs have been widely used to treat malignant and non-malignant diseases, they have some limitations, involving the need to be activated by red light that is absorbed by biological tissues.

1.2.2 Light Sources

An appropriate light source with a specific wavelength to activate the PS agent is needed in PDT. The type of light used must have a wavelength that correlates with the light absorption of the PS to optimize activation.[37] Preferably, the light wavelength is in the therapeutic range because the energy present in the photons at this range is high enough to excite the ground state PS to an excited state while being readily transmitted through biological tissues. Different light sources have been employed. Thus, lamps, lasers, and light-emitting diodes (LEDs) are the main types of light sources used in PDT applications. Notably, lamps, light-emitting diodes, diode lasers, carbon

dioxide lasers (CO_2), metal vapor lasers, potassium titanyl phosphate (KTP)-dye, and argon-dye laser systems are used during PDT.[38]

The first light sources employed in PDT were conventional lamps that utilized filters.[39] Though conventional light sources are easy to use and relatively affordable, they had some drawbacks for PDT treatment because they produce thermal effects. Also, it is difficult to determine the proper amount of the delivered light using these lamps. Lasers are now the most common light type used in PDT. Lasers are the most convenient because they can be directly applied through optic fiber cables to deliver light to the affected cells in the body compared to the other light sources. They are mostly not affordable, but they emit light with defined monochromatic wavelengths that can be easily determined. Lasers exhibit a maximum photoactivation efficiency due to their monochromatic light.

Lasers have high efficiency that is above 90%, which is coupled to a single optical fiber.[40] Wilson clinically evaluated the effect of laser light in treating periodontal disease using the PDT procedure. In the study, he performed treatment by applying laser light in combination with methylene blue and toluidine blue as PS agents to kill oral bacteria.[41] Diode lasers are currently the standard light source for many PDT applications that surpass KTP-dye systems. Unlike standard lasers, diode lasers are semiconducting light sources that do not require optical configurations. Diode lasers are small, easy to install, and affordable.[42]

A CO_2 laser can be utilized to treat basal cell carcinoma (BCC), squamous cell carcinoma (SCC), and Bowen's diseases through superficial vaporization of the tumors.[43] It can alternatively treat malignant skin tumors through excision or vaporization; however, it has shown some drawbacks. This light type was described not extensively to benefit from the effect of recurrence and survival rates.[44]

An alternative light source is the LED. LEDs have been used in PDT in the past few years for their many advantages. LEDs produce light through the luminescence process. The light produced by the LEDs can be electronically monitored in different ways.[45] They are small, which eases their portability. Also, they have high light output and low energy.

Lasers are by far the most used light source employed in PDT practice. Still, one must consider aspects and factors that can affect the choice of light type during the clinical practice of PDT modalities. Unfortunately, some PSs and light sources fail to fulfill the complete requirements to achieve a successful PDT procedure due to light depth limitations. As a result, PDT is more effective for small tumors and superficial skin lesions.[1] The selection of light depends on the nature of the PS in use and the location of the disease.

1.3 Mechanism of PDT Action

PDT reaction initiates a biological response that causes the selective localized destruction of the targeted tissues. Before the light activation, the PS is in its ground singlet state form. Upon irradiation of the PS by a light with a specific wavelength, the PS undergoes a series of photochemical transformations. This light activation of the PS leads to a change in its electronic state, making it move to higher energy levels. In the first place, the PS moves from a low energy ground singlet state to the excited singlet state. Hence, the PS is no longer in its initial form but instead becomes an excited singlet state PS. The unstable photosensitizer can have different fates during relaxation. The photosensitizer can lose its energy by emitting light through a phenomenon known as fluorescence or heat production (internal conversion).[46] Alternatively, the single excited-state photosensitizer can undergo a spin inversion, intersystem crossing (ISC) process to reach the more stable excited triplet state (T_1) with parallel spins of unpaired electrons.[33] The excited triplet state photosensitizer ($^3PS^*$) can alternatively relax back to its ground state by emitting photons via

phosphorescence or undergo a PDT reaction. T_1 is relatively long-lived with a lower energy[47] that provides photosensitizers their ability to photodynamically react with macromolecules.

In the excited triplet state, the formation of highly localized reactive oxygen species (ROS) in the affected tissues is triggered by two mechanisms. In the presence of ground state triplet oxygen ($^3O_2$), the $^3PS^*$ can either undergo electron transfer (type I) or energy transfer (type II) pathways to generate ROS. In the type I reaction, $^3PS^*$ reacts with nearby electrons donating substrates by accepting an electron. Thus, the triplet state photosensitizer anion radical ($^3PS^{\bullet -*}$) reacts with ground-state triplet oxygen ($^3O_2$), resulting in superoxide anion radical ($O_2^{\bullet -}$) production.[48, 49] The superoxide anion radical possesses a half-life that is less than a second. It is spontaneously converted to the relatively stable molecule hydrogen peroxide (H_2O_2) either nonenzymatically or via superoxide dismutase (SOD).[50] Hydrogen peroxide, in turn, generates hydroxyl radicals ($^{\bullet}OH$) by reducing the ferrous iron (Fe^{2+}) through an oxidation reaction known as Fenton chemistry[51, 52](Figure 1.2). Hydrogen peroxide is not a free radical, but it acts as a precursor of hydroxyl radicals. The hydroxyl radical is highly reactive and extremely short-lived. Thus, it reacts in proximity to its formation site with biomolecules, mainly due to its unpaired electron and highly positive redox potential.[53, 54] As described earlier, for both type I and type II processes, the PS undergoes intersystem crossing to reach the excited triplet state. In the type II pathway, energy is transferred from the excited triplet state $^3PS^*$ to generate highly reactive excited singlet state oxygen ($^1O_2$). The intracellular targets of $^1O_2$ are also located near the site of PS accumulation due to its very short lifetime in the cells.[55] The overall PDT mechanism results in the formation of

Type I hydroxyl radicals and Type II singlet oxygen and II can oxidize various macromolecules, such as proteins, nucleic acids, and lipids.[56]

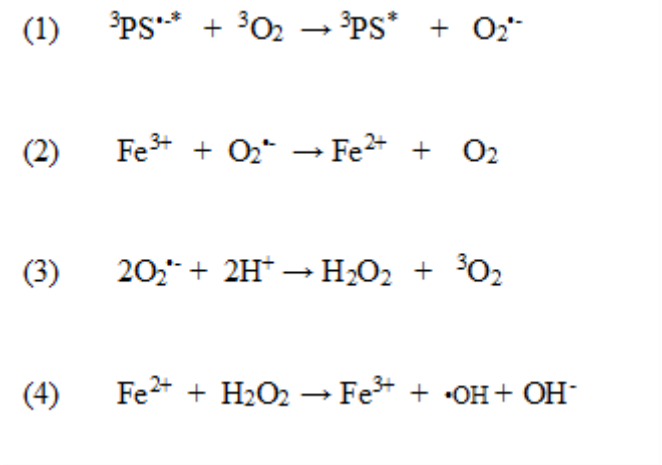

Figure 1.2: Hydroxyl radical generation through Fenton Chemistry.

These ROS induce oxidative damage to DNA through the single-strand break (SSB) or alkali-labile lesions. The damage to biological molecules results in the target tissue cell death through apoptosis and necrosis as described in the next section of this paper.[57] Type II energy transfer is known to be the leading cause of tumor tissue damage in PDT.

1.3.1 Tissues Destruction Pathways

PDT has been reported to potentially target mitochondria, endoplasmic reticulum (ER), plasma membrane, lysosomes,[58] and nuclei of tumor cells. The phototoxicity effect of PDT is produced via photodamage to the target cells. In PDT, cancerous cells are destroyed in two pathways. The destruction can occur through both programmed cell death (apoptotic or non-apoptosis) and non-programmed cell death (necrosis).[59, 60] However, the degree to which cell death is triggered during PDT's tumor destruction depends on the type of PS and its dosimetry, its intracellular localization, oxygen levels, type of light source, and affected tissue type.[61]

Tumor cell death can occur through necrosis, a randomly uncontrolled process initiated by stimuli, such as toxic trauma or physical damage.[62] Necrosis is morphologically characterized by the swelling of cytoplasm and organelles such as the endoplasmic reticulum, mitochondria, and the disruption of the plasma membrane.[62]

Apoptosis in PDT as a cell death mechanism has a broad efficacy for various types of tumors. Apoptosis is the main form of cell death following PDT in different experimental situations employing different PSs and cell types.[63] Cells undergo apoptosis in response to either extrinsic or intrinsic mediators causing morphological (*e.g.*, cell shrinkage) and biochemical (*e.g.*, activation of caspases) changes. Apoptotic cell death is regulated by the stimulation of hydrolytic enzymes such as nucleases and proteases, leading to DNA damage and the alteration of intracellular structures.[63, 64] Tumor necrosis factor (TNF), a pro-inflammatory cytokine, plays essential roles in cell proliferation, survival, differentiation, and death.[65] During apoptosis, cell surface receptors from TNF are stimulated, triggering the activation of caspase-8 through scaffolding proteins.[66, 67] Caspase-8 activates downstream effector caspases, for instance, caspase-3, committing the cell to apoptosis.[68] Roughly two-thirds of caspases in humans have been identified to function in apoptosis. Other characteristic aspects of the apoptosis pathway can be explained through caspase-mediated cleavage of substrates.[69] In contrast, autophagy may be an alternative cell death in PDT. However, little is known about the non-apoptosis (autophagy) in PDT.

1.4 Reactive Oxygen Species Production

Nature has made it possible for ROS to be naturally generated inside living organisms. ROS are byproducts of cellular respiration and photosynthesis in plants. Under physiological

conditions, they play fundamental roles in regulating metabolism, homeostasis, cell signaling, and memory development.[70] ROS are produced either from endogenous or exogenous sources.

1.4.1 Endogenous ROS Generation

In mammalian cells, ROS are produced by enzymes mainly from cytoplasmic membrane nicotinamide adenine dinucleotide phosphate (NADPH) oxidase and the electron transport of mitochondria respiratory chain. ROS can be produced by organelles, such as mitochondria, and peroxisomes.[70] Ground state triplet oxygen ($^3O_2$) has a unique molecular structure and is abundant within the cell. These characteristics confer oxygen its legibility to accept electrons from the normal oxidative metabolism process by inducing the production of ROS within the cell.[71] In plants, ROS, notably $^1O_2$, are naturally generated during photosynthesis. In the presence of light, oxygen, and chlorophyll, excited triplet state oxygen is converted to $^1O_2$. It was reported that $^1O_2$ was the main ROS produced in *Arabidopsis* cells at a high light level.[72] Also, any stress conditions that disturb the harvest of chlorophyll-binding proteins can form uncoupled chlorophyll molecules that can act as singlet oxygen-producing PS.

1.4.2 Exogeneous ROS Production

Various agents can generate ROS, such as environmental pollutants, solar irradiation of nitrate (NO_3^-) and nitrite (NO_2), heavy metals, certain drugs (*e.g.*, cyclosporine, gentamycin, and bleomycin).[73, 74] For instance, hydroxyl radicals can be produced via a modification reaction process between ozone (O_3) and chlorophyll, where O_3 acts as an electron acceptor and receives an electron from the photoexcited chlorophyll.[74] An alternative source of ROS production is through the photochemical type I and II mechanisms, as previously discussed.

1.5 Damage Effects of ROS

Because ROS production is detrimental to biomolecules, it is related to numerous pathological diseases.[75] ROS production can lead to a phenomenon known as oxidative stress due to an imbalance between ROS production and antioxidant defenses. This oxidative stress can lead to oxidative damage to a wide range of macromolecules.[76] ROS production inside the body can be harmful to biomolecules such as proteins, nucleic acids, and lipids. DNA and RNA are often negatively impacted by stress. However, DNA is the main target. It was reported that oxidized nucleotides, such as deoxythioguanosine (dTG) and 8-hydroxy2-deoxyguanosine (8-oxo-dG), are found to be increased during oxidative stress induced by UV radiation or free radical damage.[76]

1.6 Cellular Defense Against ROS

Cellular detoxification is essential to survival in aerobic conditions. The fate of ROS as signaling or damaging molecules depends significantly on the equilibrium existing between ROS levels and antioxidants in the cell.[77] Inside cells, ROS levels are naturally regulated through enzymatic processes or non-enzymatic molecules, causing antioxidants formation. Many genes encode either antioxidant enzymes SOD, catalase, peroxidases, glutathione S-transferase (GST) or enzymes that facilitate antioxidant enzymes biosynthesis, such as glutamyl cysteine synthetase, a key component of glutathione biosynthesis.[78] Moreover, cellular damage triggered by ROS is mitigated DNA or protein repair mechanisms by a replacement of damaged cellular components.[79] In eukaryotic cells, SOD initiates the detoxification process through the dismutation of superoxide anion to form hydrogen peroxide. Then, catalase, an enzyme that is found in peroxisomes, converts H_2O_2 to oxygen and water. Glutathione peroxidase, a selenium-containing enzyme, catalyzes the degradation of hydrogen peroxide and peroxides to alcohols. Glutamyl-cysteinyl-glycine (GSH), known as glutathione, is a tripeptide and an important intracellular defense molecule, which plays

a fundamental role against the toxic effects of ROS. Glutathione exists in two different forms: glutathione disulfide (GSSG) is termed as the oxidized glutathione, and the reduced glutathione is GSH.[80] Alternatively, in plants, two main enzyme classes, chloroplast kinases and phosphatases, regulate photosynthetic activity and redox state during environmental changes to avoid damage caused by ROS.[81] Various vitamins, such as vitamin A, C, and E possess antioxidant properties.[82] However, the effect and the proper concentration of these vitamins to detoxify ROS are major concerns. Glutathione (GSH) and vitamins are non-enzymatic molecules that can act as antioxidants by reducing ROS.

1.7 DNA-Small Molecules Interactions

Small molecules such as drugs and dyes can act as ligands by binding to nucleic acids. Cyanine dyes can bind to the DNA helix due to their versatile structural features. The interaction between dyes and the DNA helix results in the formation of a DNA-dye duplex. Drugs can mainly bind to DNA through reversible noncovalent binding via one or more major binding modes: intercalative binding, groove (minor or major) binding, and external binding.

1.7.1 Intercalative Binding

In general, intercalators stack between DNA base pairs by creating a separation distance of approximately 3.4 Å, representing van der Waals thickness of each intercalating moiety.[83] As a result, the DNA helix is elongated or unwound when intercalators are bound to DNA.[84] Also, small molecules that possess a planar structure or planar aromatic ring can bind to DNA in an intercalative fashion by horizontally inserting themselves in the hydrophobic part of the dsDNA base pairs.[85] Stacking of these molecules into the DNA base pairs leads to a formation of a complex, stabilized by π-π stacking interactions between the drug and DNA.[84, 85] The binding of intercalators such as cyanine dyes favors rigidity, consequently promoting stability. Also,

intercalators can increase DNA viscosity upon binding. Becker and Norden carried out a study in which they observed an increase in DNA viscosity caused by DNA helix elongation upon binding of anthracene derivatives as intercalators.[86] Methylene blue, ethidium bromide (EtBr), and acridine orange have been found to intercalate DNA.[87] Cationic polycyclic aromatic hydrocarbons (PAHs), as well as those derived from pyrene and anthracene have also been found to bind to DNA in an intercalative manner.[86] Some intercalators can be used as inhibitors of DNA replication of cancer cell growth during chemotherapy since they can covalently bind to DNA upon chemical activation. Adriamycin, daunorubicin, and dactinomycin are examples of intercalators that can be used as DNA replication inhibitors.

1.7.2 Groove Binding

Small molecules that have relatively flexible structures are generally groove binders. Also, cationic molecules with unfused aromatic rings such as distamycin, mitomycin, netropsin, Hoechst 33258, methyl green, pentamidine, and some cyanine dyes bind in a DNA groove.[88, 89] For groove binding, ligands selectively bind either in the minor groove or the major groove of DNA. The homodimeric cyanine TOTO (thiazole orange) selectively binds in the dsDNA minor groove by promoting stability of the dye-DNA complex.[90] In this type of binding, the ligand occupies the place of water molecules along the grooves of DNA. Unlike intercalation, groove binding does not alter DNA conformation and is stabilized by hydrogen bonds and van der Waals interactions.[91] Minor groove binders prefer AT rich sequence due to their narrow minor groove width. Dissimilarly, intercalators show no preference for binding to A:T but have a slight preference for binding to GC rich sequence.[88] In a study by Zimmer and co-workers in the early 1970s, netropsin was found to show binding specificity for A:T base pairs compared to intercalators.[92] Also, molecules that bind in the DNA grooves may sometimes display increased fluorescence signatures

compared to intercalators. For instance, the fluorescence emission of the intercalator EtBr was found to be 24-fold higher upon binding to DNA, while for the groove binder Hoechst 33258, fluorescence increased by 140-fold in the presence of DNA.[93]

1.7.3 External, Electrostatic Binding

During external DNA binding, the negatively charged phosphodiester groups on the DNA backbone interact with a positive-charged dye via electrostatic interactions. External DNA binders are positively charged ligands that can occupy the place of cations, such as sodium ion (Na^+) and magnesium ion (Mg^{2+}), responsible for physiological DNA helix stabilization. As a result, the electrostatic interaction between the cationic part of the binder and the negatively charged phosphate oxygen of DNA dislocates cations, which eventually leads to external binding. [94]

1.8 DNA Photocleavage

DNA photocleavage is an oxidative phenomenon that can either oxidize the sugar residues or nucleobases leading to the degradation of nucleotides and subsequently forming DNA fragmentation.[95] Thermodynamically, the hydrogens located on the 1', 3', 4', and 5'carbons of the DNA deoxyribose sugar are possible target of hydrogen abstraction.[95, 96] Some chromophores are reported to cause DNA cleavage by sensitizing the production of hydroxyl radicals that abstract hydrogen atom from deoxyribose.[97]Singlet oxygen also cleaves DNA directly. *In vitro*, damaged DNA fragments can be separated and analyzed by agarose gel electrophoresis.[98, 99]

In this thesis, pUC19 DNA, a circular double-stranded plasmid derived from *E. coli* containing 2,686 base pairs (bp)[100, 101] was used as the plasmid DNA in all the photocleavage studies. The plasmid was cloned and purified by alkaline lysis, a DNA purification method that generally yields of more than 90% of supercoiled DNA.[102] DNA bands visualized on a non-denaturingagarose gel can be in three different forms: supercoiled, linear, and nicked. The

supercoiled form, the native DNA conformation, is caused by overtwisting of the double helix DNA strands. Linear DNA bands are observed on the gel when the breakage occurs at the same location on opposite DNA strands. Yet, linear DNA band is not always seen on the electrophoresis gel, which is the case when the cut of the opposite DNA strands happens at different locations from each other. In this case, nicked DNA is formed, relaxing the supercoiled conformaton.[102] The observation of this type of DNA band on a gel is an indicative of cleaved DNA. By using light, DNA photocleavage can be controlled in temporal and spatial ways. The photocleavage efficiency depends greatly on the binding affinity of the photonuclease and its binding site on the DNA.[103]

1.9 DNA Cleaving Agents

DNA photocleaving agents also known as "photonucleases" have given rise to great interest and discoveries because they exhibit impressive potential in therapeutic applications.[103] Photonuclease are compounds that directly interact with DNA and then upon their irradiation with an appropriate light source cause an immediate dsDNA scission event.[95] Many photonuclease have been intensively studied by researchers.

1.9.1 Types of Photonucleases

In 2016, Grant and coworker published a review article with the emphasis on DNA cleaving photosensitizers in which a broad range of long wavelength DNA cleaving agents was discussed. In general, photonucleases can be classified as metal complex photonucleases or organic photonucleases.[35] The incorporation of a bivalent metal such, as iron (II), copper (II), cobalt (II), zinc (II), or nickel (II) to form metal complexes has proved to bring about DNA photocleavage activities. The Grant group reported DNA photocleavage mediated by a copper-based photo-nuclease in 2017.[104] Also, Roy and co-workers studied the visible light DNA photocleavage of bivalent transition metal complexes [M (TpPh)(B)](ClO_4), where M designates

Co (II), Ni (II), Cu (II), or, Zn (II), TpPh is anionic tris(3-phenylpyrazolyl)borate, B represents 1,10-phenanthroline, or dipyridoquinoxaline, respectively in the visible light range.[105] They found that cobalt and copper metal complexes caused high DNA cleavage yields. Similarly, some anticancer agents have shown therapeutic efficacy because they have metal cations incorporated into them. Besides the use of bivalent cationic metal complexes to induce DNA strand breaks, some other transition metals have shown a promising properties towads therapeutic treatments. Metal complex photosensitizers containing ruthenium (II), platinum (IV), ruthenium (II), iridium (III), and rhodium (III) have been studied for their DNA photocleavage abilities.[35, 106-111] Although many transition metal complexes have drawn attention, Ru (II) complex-based DNA cleaving agents are perhaps the most studied. Hergueta-Bravo and co-workers reported the ability of four Ru (II) photosensitizers to photocleave double-stranded DNA upon irradiation.[108] The DNA photocleavage efficiency of a metal complex depends on its structure.[103] Numerous metal complex photonuclease have been intensively studied and have shown promising outcomes for therapeutic. Nevertheless, metals are found often to be too toxic for pharmaceutical formulations because the metal ions dissociated from the photonuclease complexes and then interfere with biological processes.[106]

On the other hand, organic compounds such as anthraquinone and cyanine dyes can photocleave DNA strands.[112] Henary, Grant, and co-workers have developed and studied numerous cyanine dyes that exhibit the ability of cleaving dsDNA in the infrared wavelength range upon irradiation.[112, 113]

1.10 Cyanine Dyes

Cyanine dyes are a class of synthetic organic dyes. The use of cyanine dyes began with the synthesis of blue solid cyanine dye by Williams in 1856.[87] He developed numerous dyes for color

photography and fluorescent probes for biomolecules. Cyanine dyes were further applied in high energy lasers and digital image storage.[114] Since then, cyanine dyes have been widely used as fluorescent probes to label nucleic acids and proteins due to the powerful properties they own. Likewise, they are currently playing vital roles in medical, chemical, and biological fields due to their low dark-cytotoxicity and excellent phototoxicity. They often have a high binding affinity to biomolecules such as DNA and proteins. In a study, Biver and co-workers determined the binding constant of two cyanine dye-DNA complexes with overall constants of 10^4 M^{-1}.[114] Furthermore, cyanine dyes often possess large extension coefficients of $\varepsilon_{max} > 10^4$ M^{-1} cm^{-1}, moderate quantum yields, and photostability[115, 116] in the visible and near-infrared regions of the electromagnetic spectrum.[90] They exhibit an excellent fluorescence upon staining any solutions or tissues. Additionally, cyanine dyes are being used as photosensitizing agents in our study of DNA interactions due to their excellent biological and photochemical properties. They generally consist of two nitrogen containing aromatic rings that share a positive charge via a central and conjugated linking unit called a polymethine bridge (Figure 1.3).

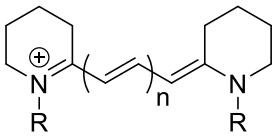

Cyanine Dyes Generic Structure

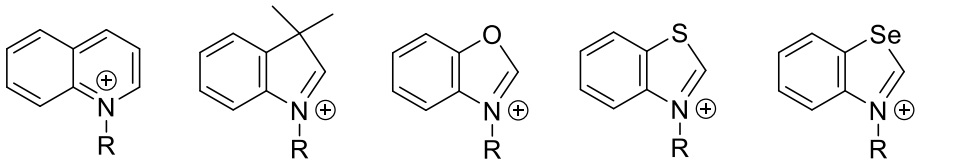

Quinoline Indole Benzoxazole Benzothiazole Benzselenazole

Figure 1.3: Cyanine dyes generic structure and common heterocyclic moieties. R refers to substituent and n, the number of conjugated carbons forming the polymethine bridge.

The heterocyclic system of cyanine dyes is identified to be quinoline, indole, benzoxazole, benzothiazole, and benzselenazole among others (Figure 1.3).[87, 115, 117] The polymethine bridge can be modified to stabilize the dyes and tune their absorption properties.[118] Aromaticity and the delocalized positive charge of cyanine dyes through the polymethine bridge enable them to bind to DNA[116] through intercalation, groove and/or external modes based on the structure of the dye. Cyanine dyes interact with each other in solution through their π-electron systems to form aggregate.[90] The addition of biomolecules to a solution containing cyanine dyes can lead to a change in dye aggregation state as it binds to the biomolecule.

1.11 Summary and Purpose of Research

In this thesis, the DNA interactions and photocleavage of a series of pentamethine carbocyanine dyes synthesized by Maged Henary, our collaborator, are studied by employing chemical, biochemical, and biophysical techniques, such as plasmid DNA cloning, as well as agarose gel electrophoresis, and UV-visible, fluorescence, and circular dichroism spectroscopies.

The cyanine dyes under investigation are 2-quinolinium and 4-quinolinium pentamethine (di)carbocyanine dyes *meso*-substituted either with hydrogen or chlorine or bromine atoms (Figure 1.4). Pentamethine dyes are polymethine dyes that belong to the cyanine family. We are interested in developing cyanine dyes for use in photodynamic cancer therapy because they can be activated with near-infrared light that can transmit deeply through biological tissues.

This study aims to determine the stability of the cyanine dyes in different media and evaluate their interactions with DNA. A main focus is the DNA photocleavage abilities of the cyanine dyes in the NIR wavelength range. Ultimately, we investigate ROS formation to identify and monitor the free radicals production and other reactive molecules generated by the dyes during DNA photocleavage reactions. Chapter 2 of our study focuses on DNA photocleavage in the NIR range by two synthesized 2-quinolinium dicarbocyanine dyes *meso*-substituted with either hydrogen or bromine. Chapter 3 centers on developing unprecedented DNA photocleavage above 830 nm by a series of 4-quinolinium pentamidine carbocyanine dyes with either bromine, chlorine, or hydrogen at the *meso*-carbon position. Chapter 4 of this thesis summarizes conclusions and considers future directions of research.

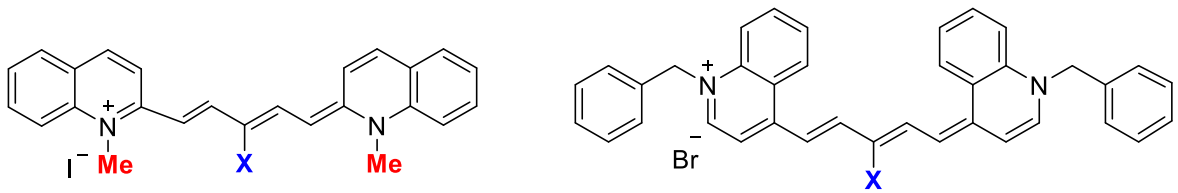

3: X = H
4: X = Br

KI2: X = Br
KI3: X = Cl
KI4: X = H

Figure 1.4: Structures of 2-quinolinium and 4-quinolinium pentamethine carbocyanine dyes (**3** and **4; KI2**, **KI3**, and **KI4**) under study.

1.12 References

1. Capella, M. A.; Capella, L. S. A light in multidrug resistance: photodynamic treatment of multidrug-resistant tumors. *Journal of biomedical science.* **2003,** *10* (4), 361-6.
2. Akens, M. K.; Hardisty, M. R.; Wilson, B. C.; Schwock, J.; Whyne, C. M.; Burch, S.; Yee, A. J. Defining the therapeutic window of vertebral photodynamic therapy in a murine pre-clinical model of breast cancer metastasis using the photosensitizer BPD-MA (Verteporfin). *Breast Cancer Research and Treatment.* **2010,** *119* (2), 325-33.
3. Agostinis, P.; Berg, K.; Cengel, K. A.; Foster, T. H.; Girotti, A. W.; Gollnick, S. O.; Hahn, S. M.; Hamblin, M. R.; Juzeniene, A.; Kessel, D.; Korbelik, M.; Moan, J.; Mroz, P.; Nowis, D.; Piette, J.; Wilson, B. C.; Golab, J. Photodynamic therapy of cancer: an update. *CA A Cancer Journal for Clinicians.* **2011,** *61* (4), 250-81.
4. Plotino, G.; Grande, N. M.; Mercade, M. Photodynamic therapy in endodontics. *International Endodontic Journal.* **2019,** *52* (6), 760-774.
5. Park, Y. K.; Park, C. H. Clinical efficacy of photodynamic therapy. *Obstetrics & Gynecology Science.* **2016,** *59* (6), 479-488.
6. Kendall, C. A.; Morton, C. A. Photodynamic therapy for the treatment of skin disease. *Technology in cancer research & treatment.* **2003,** *2* (4), 283-8.
7. Fien, S. M.; Oseroff, A. R. Photodynamic therapy for non-melanoma skin cancer. *Journal of the National Comprehensive Cancer Network : JNCCN.* **2007,** *5* (5), 531-40.
8. Biel, M. A. Photodynamic therapy treatment of early oral and laryngeal cancers. *Photochemistry and photobiology.* **2007,** *83* (5), 1063-8.
9. Dougherty, T. J. An update on photodynamic therapy applications. *Journal of clinical laser medicine & surgery.* **2002,** *20* (1), 3-7.
10. Chhatre, S.; Vachani, A.; Allison, R. R.; Jayadevappa, R. Survival Outcomes with Photodynamic Therapy, Chemotherapy and Radiation in Patients with Stage III or Stage IV Non-Small Cell Lung Cancer. *Cancers (Basel).* **2021,** *13* (4).
11. Zhao, B.; He, Y. Y. Recent advances in the prevention and treatment of skin cancer using photodynamic therapy. *Expert Review of Anticancer Therapy.* **2010,** *10* (11), 1797-809.
12. Prazmo, E. J.; Kwasny, M.; Lapinski, M.; Mielczarek, A. Photodynamic Therapy As a Promising Method Used in the Treatment of Oral Diseases. *Advances in Clinical and Experimental Medicine.* **2016,** *25* (4), 799-807.
13. Mohammadi, Z.; Jafarzadeh, H.; Shalavi, S.; Kinoshita, J. I. Photodvnamic Therapy in Endodontics. *The journal of contemporary dental practice.* **2017,** *18* (6), 534-538.
14. Daniell, M. D.; Hill, J. S. A history of photodynamic therapy. *The Australian and New Zealand journal of surgery.* **1991,** *61* (5), 340-8.
15. Møller, K. I.; Kongshoj, B.; Philipsen, P. A.; Thomsen, V. O.; Wulf, H. C. How Finsen's light cured lupus vulgaris. *Photodermatology, photoimmunology & photomedicine.* **2005,** *21* (3), 118-24.
16. Hönigsmann, H. History of phototherapy in dermatology. *Photochemical and Photobiological Sciences.* **2013,** *12* (1), 16-21.
17. Dai, T.; Fuchs, B. B.; Coleman, J. J.; Prates, R. A.; Astrakas, C.; St Denis, T. G.; Ribeiro, M. S.; Mylonakis, E.; Hamblin, M. R.; Tegos, G. P. Concepts and principles of photodynamic therapy as an alternative antifungal discovery platform. *Frontiers in Microbiology.* **2012,** *3*, 120.

18. Spikes, J. D. The origin and meaning of the term “photodynamic” (as used in “photodynamic therapy”, for example). *Journal of Photochemistry and Photobiology B: Biology.* **1991,** *9* (3), 369-371.
19. Steinbauer, J. M.; Schreml, S.; Kohl, E. A.; Karrer, S.; Landthaler, M.; Szeimies, R. M. Photodynamic therapy in dermatology. *Journal of the German Society of Dermatology : JDDG.* **2010,** *8* (6), 454-64.
20. Lee, C. N.; Hsu, R.; Chen, H.; Wong, T. W. Daylight Photodynamic Therapy: An Update. *Molecules.* **2020,** *25* (21).
21. Dougherty, T. J.; Gomer, C. J.; Henderson, B. W.; Jori, G.; Kessel, D.; Korbelik, M.; Moan, J.; Peng, Q. Photodynamic therapy. *Journal of the National Cancer Institute.* **1998,** *90* (12), 889-905.
22. Luby, B. M.; Walsh, C. D.; Zheng, G. Advanced Photosensitizer Activation Strategies for Smarter Photodynamic Therapy Beacons. *Angewandte Chemie (International ed. in English).* **2019,** *58* (9), 2558-2569.
23. Issa, M. C.; Manela-Azulay, M. Photodynamic therapy: a review of the literature and image documentation. *Anais brasileiros de dermatologia.* **2010,** *85* (4), 501-11.
24. Dąbrowski, J. M.; Pucelik, B.; Regiel-Futyra, A.; Brindell, M.; Mazuryk, O.; Kyzioł, A.; Stochel, G.; Macyk, W.; Arnaut, L. G. Engineering of relevant photodynamic processes through structural modifications of metallotetrapyrrolic photosensitizers. *Coordination Chemistry Reviews.* **2016,** *325*, 67-101.
25. Kim, M. M.; Darafsheh, A. Light Sources and Dosimetry Techniques for Photodynamic Therapy. *Photochemistry and photobiology.* **2020,** *96* (2), 280-294.
26. Dąbrowski, J. M.; Arnaut, L. G. Photodynamic therapy (PDT) of cancer: from local to systemic treatment. *Photochemical and Photobiological Sciences.* **2015,** *14* (10), 1765-80.
27. Smith, A. M.; Mancini, M. C.; Nie, S. Second window for in vivo imaging. *Nature Nanotechnology.* **2009,** *4* (11), 710-711.
28. Konopka, K.; Goslinski, T. Photodynamic therapy in dentistry. *Journal of Dental Research.* **2007,** *86* (8), 694-707.
29. Juarranz, A.; Jaén, P.; Sanz-Rodríguez, F.; Cuevas, J.; González, S. Photodynamic therapy of cancer. Basic principles and applications. *Clinical & translational oncology : official publication of the Federation of Spanish Oncology Societies and of the National Cancer Institute of Mexico.* **2008,** *10* (3), 148-54.
30. Banerjee, S. M.; MacRobert, A. J.; Mosse, C. A.; Periera, B.; Bown, S. G.; Keshtgar, M. R. S. Photodynamic therapy: Inception to application in breast cancer. *Breast.* **2017,** *31*, 105-113.
31. Van Straten, D.; Mashayekhi, V.; de Bruijn, H. S.; Oliveira, S.; Robinson, D. J. Oncologic Photodynamic Therapy: Basic Principles, Current Clinical Status and Future Directions. *Cancers (Basel).* **2017,** *9* (2), 19.
32. Celli, J. P.; Spring, B. Q.; Rizvi, I.; Evans, C. L.; Samkoe, K. S.; Verma, S.; Pogue, B. W.; Hasan, T. Imaging and Photodynamic Therapy: Mechanisms, Monitoring, and Optimization. *Chemical reviews.* **2010,** *110* (5), 2795-2838.
33. Abrahamse, H.; Hamblin, M. R. New photosensitizers for photodynamic therapy. *Biochemical Journal.* **2016,** *473* (4), 347-64.
34. O’Connor, A. E.; Gallagher, W. M.; Byrne, A. T. Porphyrin and Nonporphyrin Photosensitizers in Oncology: Preclinical and Clinical Advances in Photodynamic Therapy. *Photochemistry and photobiology.* **2009,** *85* (5), 1053-1074.

35. Li, Z.; Grant, K. B. DNA photo-cleaving agents in the far-red to near-infrared range – a review. *RSC Advances.* **2016,** *6* (29), 24617-24634.
36. Wachowska, M.; Muchowicz, A.; Firczuk, M.; Gabrysiak, M.; Winiarska, M.; Wańczyk, M.; Bojarczuk, K.; Golab, J. Aminolevulinic Acid (ALA) as a Prodrug in Photodynamic Therapy of Cancer. *Molecules.* **2011,** *16* (5), 4140-4164.
37. Singh, S.; Nagpal, R.; Manuja, N.; Tyagi, S. P. Photodynamic therapy: An adjunct to conventional root canal disinfection strategies. *Australian endodontic journal: the journal of the Australian Society of Endodontology Inc.* **2015,** *41* (2), 54-71.
38. Brancaleon, L.; Moseley, H. Laser and non-laser light sources for photodynamic therapy. *Lasers in medical science.* **2002,** *17* (3), 173-86.
39. Ackroyd, R.; Kelty, C.; Brown, N.; Reed, M. The history of photodetection and photodynamic therapy. *Photochemistry and photobiology.* **2001,** *74* (5), 656-69.
40. Wilson, B. C.; Patterson, M. S. The physics, biophysics and technology of photodynamic therapy. *Physics in medicine and biology.* **2008,** *53* (9), R61-109.
41. Wilson, M. Photolysis of oral bacteria and its potential use in the treatment of caries and periodontal disease. *The Journal of applied bacteriology.* **1993,** *75* (4), 299-306.
42. Breskey, J. D.; Lacey, S. E.; Vesper, B. J.; Paradise, W. A.; Radosevich, J. A.; Colvard, M. D. Photodynamic therapy: occupational hazards and preventative recommendations for clinical administration by healthcare providers. *Photomed Laser Surgery.* **2013,** *31* (8), 398-407.
43. Karrer, S.; Szeimies, R. M.; Hohenleutner, U.; Landthaler, M. Role of lasers and photodynamic therapy in the treatment of cutaneous malignancy. *American journal of clinical dermatology.* **2001,** *2* (4), 229-37.
44. Landthaler, M.; Szeimies, R. M.; Hohenleutner, U. Laser therapy of skin tumors. *Recent results in cancer research. Fortschritte der Krebsforschung. Progres dans les recherches sur le cancer.* **1995,** *139*, 417-21.
45. Mang, T. S. Lasers and light sources for PDT: past, present and future. *Photodiagnosis Photodynamic Therapy.* **2004,** *1* (1), 43-8.
46. Cramer, S. W.; Chen, C. C. Photodynamic Therapy for the Treatment of Glioblastoma. *Frontiers in surgery.* **2019,** *6*, 81.
47. Zhang, Q.; He, J.; Yu, W.; Li, Y.; Liu, Z.; Zhou, B.; Liu, Y. A promising anticancer drug: a photosensitizer based on the porphyrin skeleton. *RSC medicinal chemistry.* **2020,** *11* (4), 427-437.
48. Halliwell, B. Free radicals and antioxidants - quo vadis? *Trends in pharmacological sciences.* **2011,** *32* (3), 125-30.
49. Turrens, J. F. Mitochondrial formation of reactive oxygen species. *Journal of Physiology.* **2003,** *552* (Pt 2), 335-344.
50. Grant, J. J.; Loake, G. J. Role of reactive oxygen intermediates and cognate redox signaling in disease resistance. *Plant Physiology.* **2000,** *124* (1), 21-29.
51. Castano, A. P.; Demidova, T. N.; Hamblin, M. R. Mechanisms in photodynamic therapy: part one-photosensitizers, photochemistry and cellular localization. *Photodiagnosis and Photodynamic Therapy.* **2004,** *1* (4), 279-293.
52. Zepp, R. G.; Faust, B. C.; Hoigne, J. Hydroxyl radical formation in aqueous reactions (pH 3-8) of iron(II) with hydrogen peroxide: the photo-Fenton reaction. *Environmental Science & Technology.* **1992,** *26* (2), 313-319.

53. Pospíšil, P.; Prasad, A.; Rác, M. Mechanism of the Formation of Electronically Excited Species by Oxidative Metabolic Processes: Role of Reactive Oxygen Species. *Biomolecules.* **2019,** *9* (7).
54. Di Meo, S.; Reed, T. T.; Venditti, P.; Victor, V. M. Role of ROS and RNS Sources in Physiological and Pathological Conditions. *Oxidative Medicine and Cellular Longevity.* **2016,** *2016*, 1245049-1245049.
55. Moan, J.; Berg, K. The photodegradation of porphyrins in cells can be used to estimate the lifetime of singlet oxygen. *Photochemistry and photobiology.* **1991,** *53* (4), 549-53.
56. Gutteridge, J. M.; Halliwell, B. Free radicals and antioxidants in the year 2000. A historical look to the future. *Annals of the New York Academy of Sciences.* **2000,** *899*, 136-47.
57. Breen, A. P.; Murphy, J. A. Reactions of oxyl radicals with DNA. *Free Radical Biology and Medicine.* **1995,** *18* (6), 1033-1077.
58. Dos Santos, A. F.; de Almeida, D. R. Q.; Terra, L. F.; Baptista, M. S.; Labriola, L. Photodynamic therapy in cancer treatment - an update review. *Journal of Cancer Metastasis and Treatment.* **2019,** *5*, 25.
59. Allison, R. R.; Moghissi, K. Photodynamic Therapy (PDT): PDT Mechanisms. *Clinical Endoscopy.* **2013,** *46* (1), 24-29.
60. Reginato, E.; Wolf, P.; Hamblin, M. R. Immune response after photodynamic therapy increases anti-cancer and anti-bacterial effects. *World Journal of Immunology.* **2014,** *4* (1), 1-11.
61. Scherer, K. M.; Bisby, R. H.; Botchway, S. W.; Parker, A. W. New Approaches to Photodynamic Therapy from Types I, II and III to Type IV Using One or More Photons. *Anti-cancer agents in medicinal chemistry.* **2017,** *17* (2), 171-189.
62. Jan, R.; Chaudhry, G.-E. S. Understanding Apoptosis and Apoptotic Pathways Targeted Cancer Therapeutics. *Advanced Pharmaceutical Bulletin.* **2019,** *9* (2), 205-218.
63. Allegra, A.; Pioggia, G.; Tonacci, A.; Musolino, C.; Gangemi, S. Oxidative Stress and Photodynamic Therapy of Skin Cancers: Mechanisms, Challenges and Promising Developments. *Antioxidants (Basel, Switzerland).* **2020,** *9* (5).
64. Poon, I. K. H.; Hulett, M. D.; Parish, C. R. Molecular mechanisms of late apoptotic/necrotic cell clearance. *Cell Death & Differentiation.* **2010,** *17* (3), 381-397.
65. Wang, X.; Lin, Y. Tumor necrosis factor and cancer, buddies or foes? *Acta Pharmaceutica Sinica.* **2008,** *29* (11), 1275-1288.
66. Wallach, D.; Varfolomeev, E. E.; Malinin, N. L.; Goltsev, Y. V.; Kovalenko, A. V.; Boldin, M. P. Tumor necrosis factor receptor and Fas signaling mechanisms. *Annual review of immunology.* **1999,** *17*, 331-67.
67. Almeida, R. D.; Manadas, B. J.; Carvalho, A. P.; Duarte, C. B. Intracellular signaling mechanisms in photodynamic therapy. *Biochimica et biophysica acta.* **2004,** *1704* (2), 59-86.
68. Oleinick, N. L.; Morris, R. L.; Belichenko, I. The role of apoptosis in response to photodynamic therapy: what, where, why, and how. *Photochemical & Photobiological Sciences.* **2002,** *1* (1), 1-21.
69. Hengartner, M. O. The biochemistry of apoptosis. *Nature.* **2000,** *407* (6805), 770-776.
70. Collin, F. Chemical Basis of Reactive Oxygen Species Reactivity and Involvement in Neurodegenerative Diseases. *International Journal of Molecular Sciences.* **2019,** *20* (10).
71. Auten, R. L.; Davis, J. M. Oxygen Toxicity and Reactive Oxygen Species: The Devil Is in the Details. *Pediatric Research.* **2009,** *66* (2), 121-127.
72. Laloi, C.; Havaux, M. Key players of singlet oxygen-induced cell death in plants. *Frontiers in Plant Science.* **2015,** *6*, 39.

73. Pizzino, G.; Irrera, N.; Cucinotta, M.; Pallio, G.; Mannino, F.; Arcoraci, V.; Squadrito, F.; Altavilla, D.; Bitto, A. Oxidative Stress: Harms and Benefits for Human Health. *Oxidative Medicine and Cellular Longevity.* **2017,** 8416763-8416763.
74. Gligorovski, S.; Strekowski, R.; Barbati, S.; Vione, D. Environmental Implications of Hydroxyl Radicals (•OH). *Chemical reviews.* **2015,** *115* (24), 13051-13092.
75. Zhou, Z.; Song, J.; Nie, L.; Chen, X. Reactive oxygen species generating systems meeting challenges of photodynamic cancer therapy. *Chemical Society Reviews.* **2016,** *45* (23), 6597-6626.
76. Lobo, V.; Patil, A.; Phatak, A.; Chandra, N. Free radicals, antioxidants and functional foods: Impact on human health. *Pharmacognosy Reviews.* **2010,** *4* (8), 118-126.
77. Sharma, P.; Jha, A. B.; Dubey, R. S.; Pessarakli, M. Reactive Oxygen Species, Oxidative Damage, and Antioxidative Defense Mechanism in Plants under Stressful Conditions. *Journal of Botany.* **2012,** *2012*, 1-26.
78. Lushchak, V. I. Free radicals, reactive oxygen species, oxidative stress and its classification. *Chemico- Biological Interactions.* **2014,** *224*, 164-75.
79. Mittler, R. ROS Are Good. *Trends in plant science.* **2017,** *22* (1), 11-19.
80. Sies, H. Glutathione and its role in cellular functions. *Free radical biology & medicine.* **1999,** *27* (9-10), 916-21.
81. Suzuki, N.; Koussevitzky, S.; Mittler, R.; Miller, G. ROS and redox signalling in the response of plants to abiotic stress. *Plant, cell & environment.* **2012,** *35* (2), 259-70.
82. Forrester Steven, J.; Kikuchi Daniel, S.; Hernandes Marina, S.; Xu, Q.; Griendling Kathy, K. Reactive Oxygen Species in Metabolic and Inflammatory Signaling. *Circulation Research.***2018,** *122* (6), 877-902.
83. Coury, J. E.; McFail-Isom, L.; Williams, L. D.; Bottomley, L. A. A novel assay for drug-DNA binding mode, affinity, and exclusion number: scanning force microscopy. *Proceedings of the National Academy of Sciences of the United States of America.* **1996,** *93* (22), 12283-6.
84. Sischka, A.; Toensing, K.; Eckel, R.; Wilking, S. D.; Sewald, N.; Ros, R.; Anselmetti, D. Molecular mechanisms and kinetics between DNA and DNA binding ligands. *Biophysical Journal.* **2005,** *88* (1), 404-11.
85. Aleksić, M. M.; Kapetanović, V. An overview of the optical and electrochemical methods for detection of DNA - drug interactions. *Acta chimica Slovenica.* **2014,** *61* (3), 555-73.
86. Becker, H. C.; Norden, B. DNA binding mode and sequence specificity of piperazinylcarbonyloxyethyl derivatives of anthracene and pyrene. *Journal of American Chemical Society.* **1999,** *121* (51), 11947-11952.
87. Armitage, B. A.. Cyanine Dye-DNA Interactions: Intercalation, Groove Binding, and Aggregation. In *DNA Binders and Related Subjects*. **2005**; pp 55-76.
88. Ogulchansky, T. Y.; Losytskyy, M. Y.; Kovalska, V. B.; Lukashov, S. S.; Yashchuk, V. M.; Yarmoluk, S. M. Interaction of cyanine dyes with nucleic acids. XVIII. Formation of the carbocyanine dye J-aggregates in nucleic acid grooves. *Spectrochimica Acta Part A: Molecular and Biomolecular Spectroscopy.* **2001,** *57* (13), 2705-15.
89. Kellett, A.; Molphy, Z.; Slator, C.; McKee, V.; Farrell, N. P. Molecular methods for assessment of non-covalent metallodrug-DNA interactions. *Chemical Society Reviews.* **2019,** *48* (4), 971-988.
90. Yarmoluk, S. M.; Kovalska, V. B.; Kryvorotenko, D. V.; Balanda, A. O.; Ogul'chansky, T. Interaction of cyanine dyes with nucleic acids. XXV. Influence of affinity-

modifying groups in the structure of benzothiazol-4-[2,6-dimethylpyridinium] dyes on the spectral properties of the dyes in the presence of nucleic acids. *Spectrochimica Acta Part A: Molecular and Biomolecular Spectroscopy.* **2001,** *57* (7), 1533-40.
91. Phadte, A. A.; Banerjee, S.; Mate, N. A.; Banerjee, A. Spectroscopic and viscometric determination of DNA-binding modes of some bioactive dibenzodioxins and phenazines. *Biochemistry and Biophysics Reports.* **2019,** *18*, 100629.
92. Nanjunda, R.; Wilson, W. D. Binding to the DNA minor groove by heterocyclic dications: from AT-specific monomers to GC recognition with dimers. *Current Protocols in Nucleic Acid Chemistry.* **2012,** *Chapter 8*, Unit8 8.
93. Palchaudhuri, R.; Hergenrother, P. J. DNA as a target for anticancer compounds: methods to determine the mode of binding and the mechanism of action. *Current opinion in biotechnology.* **2007,** *18* (6), 497-503.
94. De Almeida, S. M. V.; Ribeiro, A. G.; de Lima Silva, G. C.; Ferreira Alves, J. E.; Beltrão, E. I. C.; de Oliveira, J. F.; de Carvalho, L. B. J.; Alves de Lima, M. D. C. DNA binding and Topoisomerase inhibition: How can these mechanisms be explored to design more specific anticancer agents? *Biomedicine & Pharmacotherapy.* **2017,** *96*, 1538-1556.
95. Armitage, B. Photocleavage of Nucleic Acids. *Chemical reviews.* **1998,** *98* (3), 1171-1200.
96. Da Ros, T.; Spalluto, G.; Boutorine, A. S.; Bensasson, R. V.; Prato, M. DNA-photocleavage agents. *Current pharmaceutical design.* **2001,** *7* (17), 1781-821.
97. Li, Z. Y.; Grant, K. B. DNA photo-cleaving agents in the far-red to near-infrared range - a review. *Rsc Advances.* **2016,** *6* (29), 24617-24634.
98. Chadalavada, D. M.; Bevilacqua, P. C. Analyzing RNA and DNA folding using temperature gradient gel electrophoresis (TGGE) with application to in vitro selections. *Methods in enzymology.* **2009,** *468*, 389-408.
99. Lee, P. Y.; Costumbrado, J.; Hsu, C. Y.; Kim, Y. H. Agarose gel electrophoresis for the separation of DNA fragments. *Journal of Visualized Experiments.* **2012,** (62).
100. Vieira, J.; Messing, J. The pUC plasmids, an M13mp7-derived system for insertion mutagenesis and sequencing with synthetic universal primers. *Gene.* **1982,** *19* (3), 259-68.
101. Yanisch-Perron, C.; Vieira, J.; Messing, J. Improved M13 phage cloning vectors and host strains: nucleotide sequences of the M13mpl8 and pUC19 vectors. *Gene.* **1985,** *33* (1), 103-119.
102. Feliciello, I.; Chinali, G. A modified alkaline lysis method for the preparation of highly purified plasmid DNA from Escherichia coli. *Analytical Biochemistry.* **1993,** *212* (2), 394-401.
103. Bindu, P. J.; Mahadevan, K. M.; Satyanarayan, N. D.; Ravikumar Naik, T. R. Synthesis and DNA cleavage studies of novel quinoline oxime esters. *Bioorganic & Medicinal Chemistry Letters.* **2012,** *22* (2), 898-900.
104. Williams, D. E.; Fischer, C. M.; Kassai, M.; Gude, L.; Fernández, M.-J.; Lorente, A.; Grant, K. B. An unlikely DNA cleaving agent: A photo-active trinuclear Cu(II) complex based on hexaazatriphenylene. *Journal of Inorganic Biochemistry.* **2017,** *168*, 55-66.
105. Roy, S.; Patra, A. K.; Dhar, S.; Chakravarty, A. R. Photosensitizer in a Molecular Bowl and its Effect on the DNA-Binding and -Cleavage Activity of 3d-Metal Scorpionates. *Inorganic Chemistry.* **2008,** *47* (13), 5625-5633.
106. Monro, S.; Colón, K. L.; Yin, H.; Roque, J., 3rd; Konda, P.; Gujar, S.; Thummel, R. P.; Lilge, L.; Cameron, C. G.; McFarland, S. A. Transition Metal Complexes and Photodynamic

Therapy from a Tumor-Centered Approach: Challenges, Opportunities, and Highlights from the Development of TLD1433. *Chemical reviews.* **2019,** *119* (2), 797-828.
107. Gopalakrishnan, D.; Srinath, S.; Baskar, B.; Bhuvanesh, N. S. P.; Ganeshpandian, M. Biological and catalytic evaluation of Ru (II)-p-cymene complexes of Schiff base ligands: Impact of ligand appended moiety on photo-induced DNA and protein cleavage, cytotoxicity and C-H activation. *Applied Organometallic Chemistry.* **2019,** *33* (3).
108. Hergueta-Bravo, A.; Jimenez-Hernandez, M. E.; Montero, F.; Oliveros, E.; Orellana, G. Singlet oxygen-mediated DNA photocleavage with Ru(II) polypyridyl complexes. *Journal of Physical Chemistry B.* **2002,** *106* (15), 4010-4017.
109. Li, Z.; Burya, S. J.; Turro, C.; Dunbar, K. R. Photochemistry and DNA photocleavage by a new unsupported dirhodium (II,II) complex. *Philosophical Transactions: Mathematical, Physical and Engineering Sciences.* **2013,** *371* (1995), 20120128.
110. Sitlani, A.; Long, E. C.; Pyle, A. M.; Barton, J. K. DNA photocleavage by phenanthrenequinone diimine complexes of rhodium(III): shape-selective recognition and reaction. *Journal of American Chemical Society.* **1992,** *114* (7), 2303-2312.
111. Weynand, J.; Moreno-Betancourt, A.; Loiseau, F.; Berthet, N.; Defrancq, E.; Elias, B. Redox-Active Bis-Cyclometalated Iridium (III) Complex as a DNA Photo-Cleaving Agent. *Inorganic Chemistry.* **2020,** *59* (4), 2426-2433.
112. Ahoulou, E. O.; Drinkard, K. K.; Basnet, K.; St Lorenz, A.; Taratula, O.; Henary, M.; Grant, K. B. DNA Photocleavage in the Near-Infrared Wavelength Range by 2-Quinolinium Dicarbocyanine Dyes. *Molecules.* **2020,** *25* (12).
113. Basnet, K.; Fatemipouya, T.; St Lorenz, A.; Nguyen, M.; Taratula, O.; Henary, M.; Grant, K. B. Single photon DNA photocleavage at 830 nm by quinoline dicarbocyanine dyes. *Chemical Communications (Camb).* **2019,** *55* (84), 12667-12670.
114. Biver, T.; De Biasi, A.; Secco, F.; Venturini, M.; Yarmoluk, S. Cyanine dyes as intercalating agents: kinetic and thermodynamic studies on the DNA/Cyan40 and DNA/CCyan2 systems. *Biophysical Journal.* **2005,** *89* (1), 374-83.
115. Wang, L.; Xiang, J.; Sun, H.; Yang, Q.; Yu, L.; Li, Q.; Guan, A.; Tang, Y. Controllable cy3-MTC-dye aggregates and its applications served as a chemosensor. *Dyes and Pigments* **2015,** *122*, 382-388.
116. Ernst, L. A.; Gupta, R. K.; Mujumdar, R. B.; Waggoner, A. S. Cyanine dye labeling reagents for sulfhydryl groups. *Cytometry.* **1989,** *10* (1), 3-10.
117. Ilina, K.; Henary, M., Cyanine Dyes Containing Quinoline Moieties: History, Synthesis, Optical Properties, and Applications. *Chemistry* **2020**.
118. Sovenyhazy, K. M.; Bordelon, J. A.; Petty, J. T. Spectroscopic studies of the multiple binding modes of a trimethine-bridged cyanine dye with DNA. *Nucleic Acids Research.* **2003,** *31* (10), 2561-9.

2 DNA PHOTOCLEAVAGE IN THE NIR WAVELENGTH RANGE BY 2-QUINOLINIUM DICARBOCYANINE DYES

(This chapter is a verbatim as it appears in Ahoulou, E. O., Drinkard, K. K., Basnet, K., St Lorenz, A., Taratula, O., Henary, M., Grant, K. B. DNA Photocleavage in the Near-Infrared Wavelength Range by 2-Quinolinium Dicarbocyanine Dyes. *Molecules*. **2020**, 25, 2926. The manuscript was written by Profs. Kathryn B. Grant, Maged Henary, and Oleh Taratula. The 2-quinolinium dicarbocyanine dyes **3** and **4** were synthesized, and their NMR spectra were taken by Prof. Maged Henary. UV-visible spectra of competitive DNA binding were recorded by Kaitlyn Drinkard. DNA photocleavage, % cleavage, and % inhibition calculations were accomplished by Kanchan Basnet and Kaitlyn Drinkard. Uptake, distribution, and phototoxicity studies were done by Anna Lorenz. All the other experiments were achieved by Effibe Odette Ahoulou.)

2.1 Abstract

Here, we report the synthesis of two pentamethine cyanine dyes containing quinolinium rings and substituted with either hydrogen (**3**) or bromine (**4**) at the *meso* carbon. The electron withdrawing bromine atom stabilizes dye **4** in aqueous buffer, allowing complex formation to occur between the dye and double-helical DNA. UV–visible, CD, and fluorescence spectra recorded at low DNA concentrations suggest that dye **4** initially binds to the DNA as a high-order aggregate. As the ratio of DNA to dye is increased, the aggregate is converted to monomeric and other low-order dye forms that interact with DNA in a non-intercalative fashion. The brominated dye **4** is relatively unreactive in the dark, but, under 707–759 nm illumination, generates hydroxyl radicals that cleave DNA in high yield (pH 7.0, 22 °C). Dye **4** is also taken up by ES2 ovarian carcinoma cells, where it is non-toxic under dark conditions. Upon irradiation of the ES2 cells at 694 nm, the brominated cyanine reduces cell viability from 100 ± 10% to 14 ± 1%. Our results

suggest that 2-quinolinium-based carbocyanine dyes equipped with stabilizing electron withdrawing groups may have the potential to serve as sensitizing agents in long-wavelength phototherapeutic applications.

2.2 Introduction

Originally employed in photography to extend the wavelength range of silver halide emulsions, cyanine dyes are now extensively used in diverse fields ranging from biotechnology to laser technology.[1-3] Carbocyanines are typically composed of two nitrogen-containing heterocyclic aromatic rings that share a positive charge that is delocalized by the movement of electrons through a semi-flexible central polymethine bridge. These features make it possible for the monomeric and/or aggregated forms of many carbocyanine dyes to form stable complexes with double-helical DNA. Modes of cyanine binding, which include intercalation, groove binding, and external electrostatic interactions, depend upon the structure and aggregation state of the dye.[4-7] Many cyanines exhibit excellent optical properties that include high absorption coefficients, high fluorescence quantum yields, and absorption and emission maxima that are easily tuned by alternating terminal heterocyclic groups and by the lengthening the dye's central polymethine chain. For every two methine carbons added to the polymethine unit, absorption is red-shifted by ~100 nm.[1] This has made possible the design and synthesis of a variety of carbocyanine-based nucleic acid fluorescent sensors that absorb and emit light in the visible and/or near-infrared regions of the electromagnetic spectrum.[1, 8, 9] Near infrared excitation wavelengths from 700 to 900 nm are particularly attractive for biological applications because they are efficiently transmitted through biological tissue.[10]

Low cellular toxicity coupled with the ability to absorb and emit near-infrared light has led to the development of indocyanine green (ICG; λ_{ex} = 800 nm; λ_{em} = 810 nm) and other cyanines as

biological agents in the diagnosis and imaging of cancer.[1, 11-14] The fluorophore ICG, approved by the United States Food and Drug Administration in 1956, is routinely used in medical diagnostics to monitor blood flow, and is now under investigation as a tumor-imaging agent. Although ICG and other cyanines are largely employed as fluorescent probes, it has been proposed that they should also be able to serve as effective phototherapeutic agents.[12, 15-18] In photodynamic therapy (PDT), a light source is used to activate a photosensitizing agent (PS) in diseased tissue. This triggers the production of highly localized, short-lived reactive oxygen species (ROS) through the reaction of ground state triplet oxygen ($^3O_2$) with the photosensitizer's triplet excited state ($^3PS^*$).[19-21] Two major ROS are formed. Type 2 energy transfer gives rise to singlet oxygen ($^1O_2$), while in Type 1 electron transfer, superoxide anion radical ($O_2^{\bullet-}$) formation generates highly reactive hydroxyl radicals ($OH^\bullet$) through an H_2O_2 intermediate.[22, 23] With respective diffusion distances of 50–100 [24] and 0.8–6.0 nm [25], $^1O_2$ and $OH^\bullet$ cause highly localized, oxidative damage to DNA and other macromolecules within the irradiated cells.[26] This spatial targeting minimizes side effects, thereby enhancing positive clinical outcomes in the treatment of cancer and other diseases.[27] The clinically approved PDT agents porfimer sodium (Photofrin®), verteporfin (Visudyne®), and talaporfin (Aptocine™) all directly cleave genomic DNA in tissue culture and/or in circulating cells exposed to red light.[20] Because absorption of 700-900 nm irradiation by biological tissues is low, there is now great interest in the development of photosensitizing agents that are activated in the near-infrared wavelength range.[10]

Symmetrical benz[*e*]indolium [28] and 4-quinolinium [29] carbocyanine dyes as well as asymmetrical cyanines based on oxazole yellow (YO) and the YO sulfur analog thiazole orange (TO) [30-33] have been utilized to sensitize DNA photocleavage upon irradiation with visible and/or near-infrared light. Surprisingly, little is understood about the potential of other types of cyanine

dyes to act as DNA photo-cleaving agents and even less is known about their phototherapeutic effects in cancer cells. Using a pentamethine linker to connect two 2-quinolinium rings, here we synthesized two symmetrical dicarbocyanine dyes that exhibit strong near infrared photo-nuclease activity (707 to 759 nm hv, pH 7.0: **3** and **4** in Scheme 1). In particular, *meso* brominated dye **4** photo-cleaves DNA in high yield and becomes highly cytotoxic to ES2 ovarian carcinoma cells when exposed to 694 nm illumination.

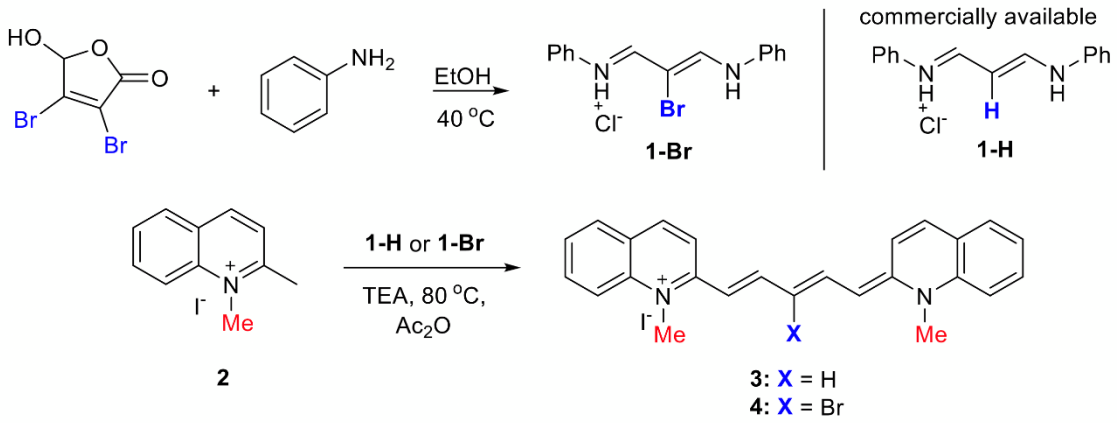

Figure 2.1: Syntheses of 2-quinolinium pentamethine carbocyanine dyes **3** and **4**.

2.3 Results and Discussion

As shown in Figure 2.1, the syntheses of the two pentamethine carbocyanine dyes **3** and **4** was conducted according to published synthetic procedures.[28, 34-38] The 2-quinolinium rings were selected to promote DNA binding interactions [39] and a central pentamethine bridge was employed to red-shift dye absorption. In aqueous solutions, cyanine dyes, especially those with long polymethine chains, are predisposed to lose color over time due to spontaneous dye auto-oxidation (no hv).[40] To render the dye a poorer reducing agent and thereby increase dye stability, the *meso* hydrogen atom in the pentamethine bridge of **3** was replaced with electron withdrawing bromine (**4**). The positioning of a halogen at the polymethine *meso*-carbon was also anticipated to introduce

a “heavy atom effect” in which ROS production and DNA photocleavage might be enhanced by increasing the rate of intersystem crossing between the photosensitizer’s singlet and triplet excited states [41].[41] The brominated linker, **1**-**Br** (Figure 2.1), was thereby created by gently heating mucobromic acid with aniline in dry ethanol until the starting material was consumed according to TLC.[34] The pentamethine quinolinium cyanine dyes were then synthesized by adding 2 equiv of the previously synthesized salt **2**, to either linker **1**-**H**, for dye **3**, or **1**-**Br**, to produce dye **4**. The two dyes **3** and **4** were precipitated with diethyl ether and recrystallized from methanol.[28]

2.3.1 UV-visible Spectrophotometry: Dye Stability and DNA Interactions

In our first set of experiments, UV–visible spectra were recorded as a function of time. Dyes **4** and **3** were found to be stable in DMSO, displaying steady absorption at λ_{max} values of 693 (**4**, X = Br) and 715 nm (**3**, X = H) over 30 min (Figure 2.2A,B). When moved to aqueous buffer, the dyes’ 693- and 715-nm peaks were replaced by new blue-shifted maxima at 532 (**4**) and 699 nm (**3**) (Figure 2.2C,D). In contrast to DMSO, autooxidation of dye **3** (X = H) in the aqueous buffer was indicated by extensive absorption loss over time. Substitution of the *meso* hydrogen for electron withdrawing Br stabilized absorption, showing that dye **4** (X = Br) was considerably less susceptible to oxidation. Upon the addition of calf thymus (CT) DNA to the aqueous buffered solutions, the peak positions, and intensities of dyes **4** and **3** were markedly altered. Both dyes were stabilized by the DNA, especially in the case of **4** (X = Br), which, in contrast to **3**, exhibited a net absorption gain over 30 min rather than a net absorption loss (Figure 2.2E,F).

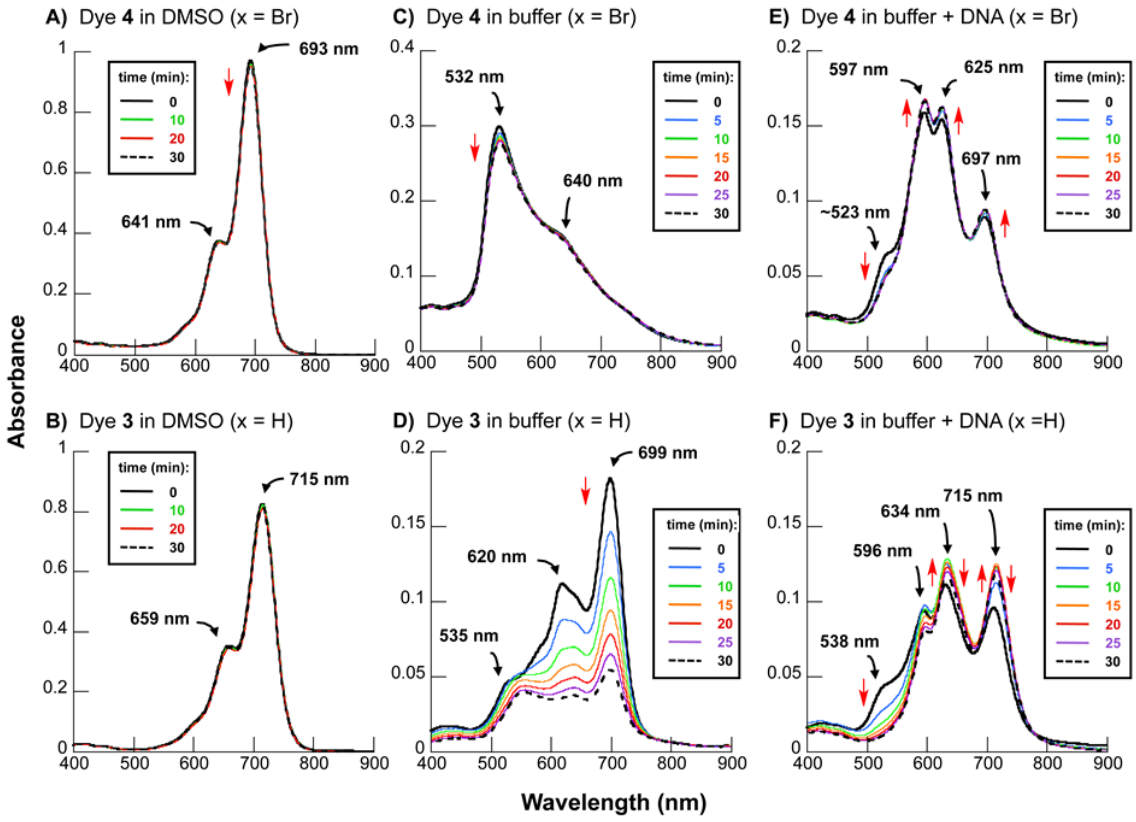

Figure 2.2: UV–visible spectra of recorded over 30 min for 10 μM of dyes **4** and **3** in: (**A**), (**B**) DMSO; (**C**), (**D**) 10 mM sodium phosphate buffer pH 7.0; and (**E**), (**F**) 10 mM sodium phosphate buffer pH 7.0 and 150 μM bp CT DNA (22 °C).

2.3.2 DNA Photocleavage in the Near-Infrared Wavelength Range

Our next goal was to determine whether cyanine dyes **4** and **3** could act as photo-nucleases under physiological conditions of temperature and pH. With the development of phototherapeutic agents in mind, we employed a near-infrared 741-nm LED medical lamp (0.3 W/cm^2) with a 707–759-nm spectral output overlapping DNA-bound dye absorption (Figure 2.2E,F). In a preliminary experiment, solutions containing 38 μM bp of pUC19 plasmid DNA in the absence and presence of 25 μM of dye were either irradiated for 60 min or kept in the dark (10 mM sodium phosphate buffer pH 7.0, 22 °C). Upon exposure to the near-infrared light, the reaction containing the brominated dye (**4**) generated very high levels of DNA strand scission (Lane 2 in Figure 2.3).

Photocleavage yields were intermediate in the case of unstable H-substituted counterpart **3** (Lane 3) and low for negative control reactions that were either kept in the dark (Lanes 4 and 5 in Figure 2.3) or irradiated in the absence of dye (Lane 1).

The superior stability and DNA-cleaving activity exhibited by brominated cyanine **4** encouraged us to study this dye further. (Cyanine **3** was no longer employed due to the propensity of this dye to degrade in aqueous solutions (Figure 2.2D,F).) In our next experiment, reactions containing 24 μM of **4** and 38 μM bp of pUC19 plasmid DNA were irradiated over intervals of time ranging from 0 to 120 min (10 mM sodium phosphate buffer pH 7.0, 22 °C; Figure 2.4). DNA cleavage was sensitized by the dye in a yield of 43 ± 6% after 5 min of irradiation and in increasing yield until approaching a plateau at ~60 min (88 ± 7% cleavage). We then lowered the reaction temperature from 22 °C to 10 °C and tested different amounts of dye (10 mM sodium phosphate buffer pH 7.0, hν 60 min; Figure 2.5). At the lower temperature, strong DNA photocleavage was observed. Yields ranged from 75 ± 17% for 3 μM of dye **4** up to 99 ± 1% at a dye concentration of 48 μM.

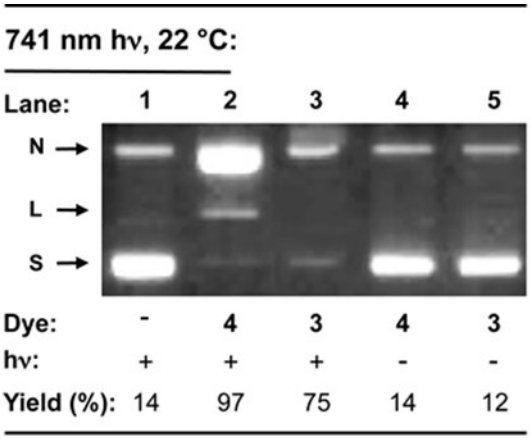

Figure 2.3: Ethidium bromide stained 1.5% agarose gel showing photo-cleavage of pUC19 plasmid DNA upon irradiation with a 741-nm LED lamp (0.3 W/cm^2; spectral output 707–759 nm). Reactions contained 10 mM sodium phosphate buffer pH 7.0 and 38 μM bp DNA in the absence and presence of 25 μM of dyes **4** and **3** (60 min hν at 22 °C). Parallel control reactions containing dye were kept in the dark (lanes **4** and **5**). Abbreviations: L, linear; N, nicked; S, supercoiled.

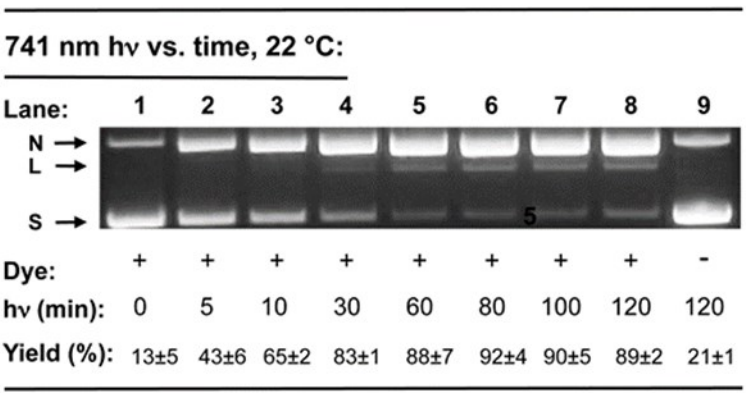

Figure 2.4: A representative agarose gel showing photo-cleavage as a function of time for 38 μM bp pUC19 DNA in 10 mM sodium phosphate buffer pH 7.0 (22 °C). Individual reactions in the presence and absence of 24 μM of dye **4** were irradiated with a 741-nm LED lamp (0.3 W/cm^2; spectral output 707–759 nm) for time intervals ranging from 0 to 120 min. Data points are averaged over 2–3 trials. Errors represent standard deviation. Abbreviations: N, nicked; S, supercoiled.

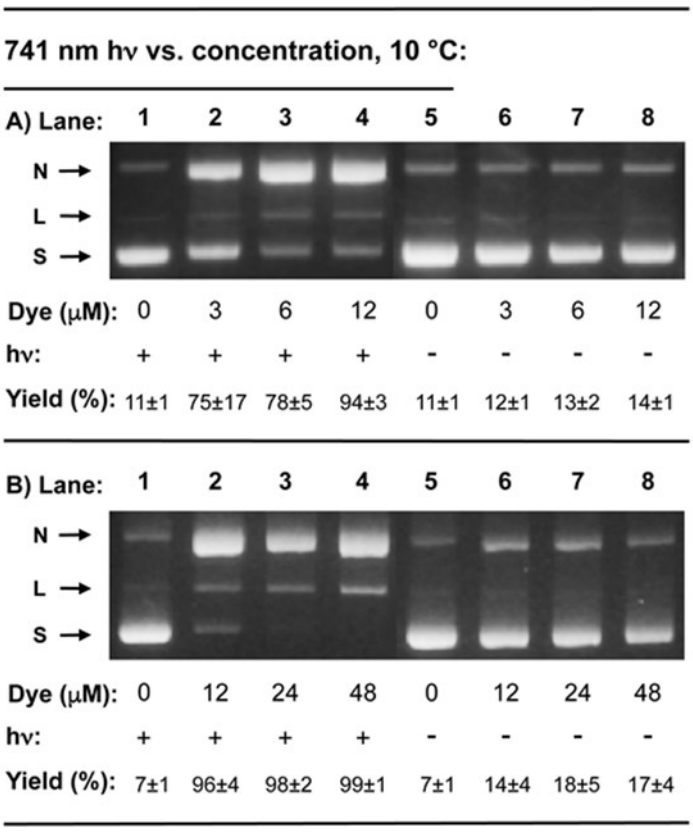

Figure 2.5: Representative agarose gels showing photocleavage of 38 μM bp pUC19 DNA in the presence of dye **4** concentrations ranging: (**A**) 0–12 μM; and (**B**) 0–48 μM (10 mM sodium phosphate buffer pH 7.0, 10 °C). Reactions were either irradiated with a 741-nm LED lamp (0.3

W/cm^2; spectral output 707–759 nm) for 60 min or kept in the dark. Data points are averaged over 2–3 trials. Errors represent standard deviation. Abbreviations: N, nicked; S, supercoiled.

2.3.3 Spectrophotometric Analyses of DNA Binding Modes

Aggregation of cyanines in aqueous solution typically involves the formation of cofacial *H*-aggregates with absorption maxima that are hypsochromic with respect to the cyanine monomer, and/or staggered cyanine J-aggregates that display bathochromic absorption.[3] The monomeric as well as aggregated carbocyanines can bind to DNA in minor groove as well as externally, depending on the structure of the dye.[6, 7, 29, 42, 43] Intercalative DNA binding is possible for monomeric cyanines but is highly unlikely in the case of the H and J forms due to self-stacking of the dyes' aromatic rings within the aggregate .[3] To better understand how aggregation effects might be influencing the DNA interactions, additional spectroscopic measurements of brominated cyanine dye **4** were carried out.

2.3.3.1 UV-visible Absorption Spectrophotometry

In our first experiment, absorption titrations were conducted in which small amounts of CT DNA titrant were sequentially added to a solution containing a fixed amount of dye **4** (Figure 2.6). Raising DNA concentration is known to disrupt cyanine aggregation in favor of the formation monomeric dye.[5, 7, 42] These changes in aggregation state are often reflected in the absorption spectra of the dye. This being said, the introduction of CT DNA to **4** produced major cyanine peak positions with λ_{max} values that varied as a function of increasing DNA concentration. In the case of the dye's lowest wavelength peak position at 526 nm, sequential DNA addition gradually shifted the λ_{max} from 526 to 523 nm while significantly decreasing absorption. At the same time, the intensities increased in the case of two major bathochromic peaks with respective λ_{max} values that changed from 619 to 628 nm and from 691 to 697 nm (Figure 2.6A). In DMSO, a polar organic solvent that promotes monomer formation [6, 29, 44], dye **4** absorbs strongly at 693 nm (Figure 2.2A).

When moved to buffered water, a highly polar solvent that supports dye aggregation, the 693-nm peak was no longer observed and was replaced by a major absorption band at 532 nm (no DNA; Figure 2.2C). These effects suggest that the hypsochromic "526–523-nm" feature in the absorption titration shown in Figure 2.6A represents either free or DNA-bound *H*-aggregated dye, while the "691–697-nm" peak corresponds to a DNA-bound dye monomer. At very high DNA concentrations (Figure 2.6B), the height of a ~599 nm shoulder in the absorption titration spectra in Figure 2.6A became a more prominent spectral feature with λ_{max} values that ranged from 596 to 600 nm. The absorption of this "596–600-nm" band in the high DNA concentration range initially increased but then substantially decreased relative to a concomitant net increase in "619–628-nm" absorption (Figure 2.6B). These trends suggest that the "596–600-nm" and "619–628-nm" spectral features in the absorption titrations shown in Figure 2.6B represent two distinct DNA bound dye species, possibly dimers or low-order aggregates.

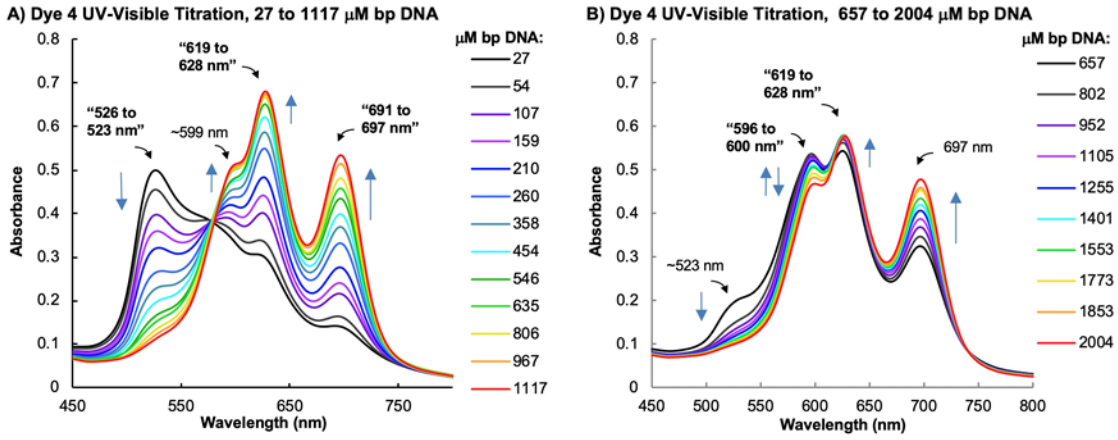

Figure 2.6: UV–visible absorption titration spectra at 22 °C of 20 µM of dye **4** in the presence of 10 mM sodium phosphate buffer pH 7.0 and CT DNA concentrations ranging: (**A**) 27–1117 µM bp; and (**B**) 657–2004 µM bp. All absorption spectra are corrected for sample dilution.

2.3.3.2 Circular Dichroism

Circular dichroism (CD) represents a convenient and informative tool for gaining knowledge of cyanine dye/DNA interactions. Binding of an achiral cyanine to chiral B-form DNA typically generates an induced circular dichroism (ICD) signal that can reveal information about the dye's DNA binding mode and aggregation state. For example, a bisignate exciton ICD signal is usually indicative of the formation of groove bound [6, 7, 42] or externally bound [43] high- and low-order aggregates as well as adjacent end-to-end cyanine dimers. In contrast, individual groove-bound monomers and groove-bound dimers do not exhibit exciton coupling and instead tend to generate positive ICD signals.[7, 45] The ICDs of cyanine intercalators are relatively weak and are either positive [45] or negative [5, 43, 46], depending on the orientation of the transition moment of the dye relative to the dyad axis of the DNA duplex.[47] This being said, we recorded circular dichroism spectra of brominated dye **4** as a function of increasing CT DNA concentration. The ICD signals generated by binding of the achiral cyanine to the chiral DNA were then plotted against corresponding absorption spectra shown in Figure 2.6A (Figure 2.7A). As expected, dye **4** had no CD signal in the absence of the CT DNA. When the DNA was introduced, however, the CD titration data revealed the formation of an apparent bisignate ICD band indicative of exciton coupling interactions between DNA-bound dye molecules. This bisignate feature is comprised of a positive short wavelength component at 516 nm and a negative long wavelength component that appears to be partially attenuated by a positive ICD signal at 591 nm. The central position of the bisignate band and its intensity as a function of DNA concentration correspond to the hypsochromic "526–523-nm" absorption feature we tentatively attributed to the formation of an H-aggregate (Figures 2.6A and 2.7A). Typically, H-aggregated cyanines bind in the DNA minor groove through the formation of cofacial cyanine dimers that assemble in right-handed, end-to-

end fashion that matches the right-handed curvature of B-form duplex DNA.[6, 7, 48] The hypsochromic "526–523-nm" absorption peak in Figures 2.6A and 2.7A could indeed represent an H-aggregate. However, the ordering of the two components the ICD band, with the positive peak at shorter wavelengths and negative peak at longer wavelengths, points to a left-handed orientation that is inconsistent with the formation a groove-bound complex involving right-handed B-form DNA.[6, 7] The bisignate DNA CD signal in the extended CD spectra shown in Figure 6B confirms that the nucleic acid maintains a right-handed B-form helical shape upon complex formation with dye **4**. We therefore conclude that the peak ordering in the bisignate cyanine ICD band suggests that the "526–523-nm" aggregate may be bound to DNA in an atypical fashion rather than in one of the DNA grooves.[43] In addition to the dye's bisignate ICD, the second prominent feature of the CD titration in Figure 6A is the overlapping positive ICD signal at 591 nm. This peak is closest in position to the "596–600-nm" absorption feature in the high DNA concentration UV–visible titration (Figure 2.6B). Assuming that there is no hidden exciton coupling, the intensity and sign of the 591-nm ICD point to the formation of a cyanine dimer. If exciton coupling is being obscured by overlap with one or more adjacent ICD signals, then a low-order aggregate associated with either the "596–600-nm" or the "619–628-nm" absorption feature might be indicated.

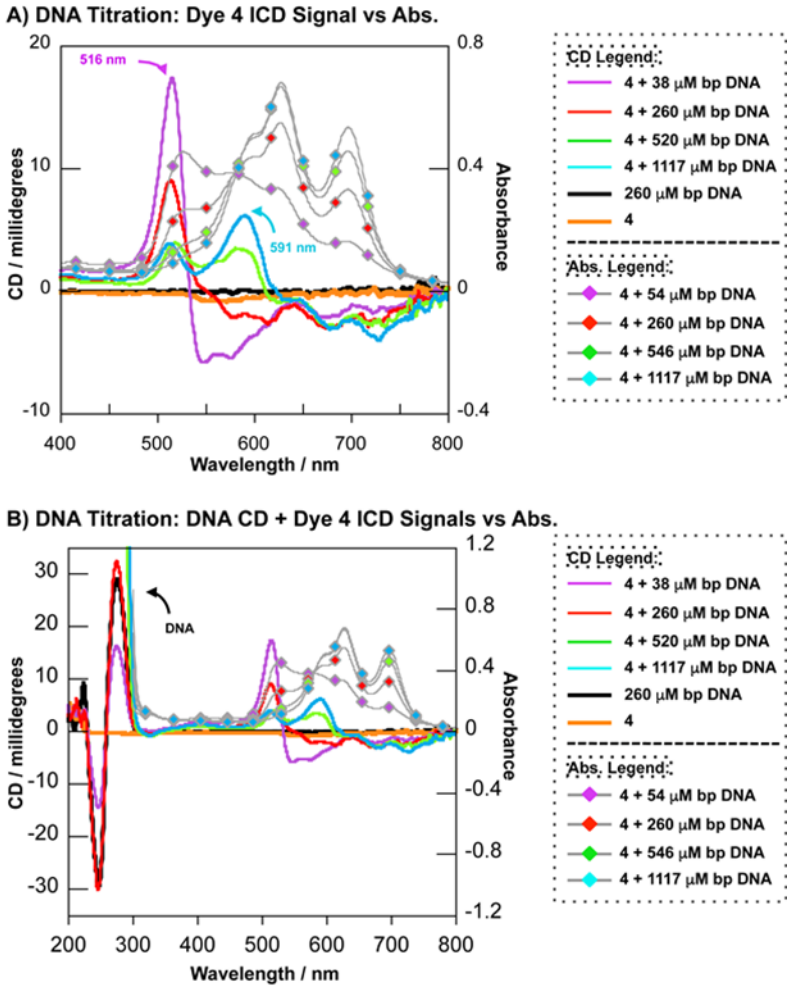

Figure 2.7: Double y-axis plots superimposing CD titration spectra (showing DNA CD and dye **4** induced circular dichroism (ICD) signals) vs. corresponding UV–visible absorption (Abs.) Fluorescence Spectroscopy.

2.3.3.3 Fluorescence Spectroscopy

Figure 2.8A superimposes the absorption spectrum of dye **4** in the presence of 1117 µM bp of CT DNA with fluorescence emission that was generated at excitation wavelengths that overlap the major absorption features of the free (λ_{ex} = 532 and 640 nm; Figure 2.2C) and DNA-bound dye (λ_{ex} = 529, 602, 628, and 697 nm; Figure 2.6). Dye **4** did not fluoresce when the CT DNA was absent (Figure 2.8A). When 1117 µM bp of CT DNA was added to the solution, however, emission was observed only at the λ_{ex} = 529 nm wavelength (blue line in Figure 2.8A). Interestingly, the

corresponding “526–523-nm” absorption feature overlapping this wavelength was of very low intensity and almost completely obscured by other dye absorption features (Figure 2.8A). Based on the UV–visible absorption and ICD results from the preceding two sections, we had tentatively assigned the “526–523-nm” feature to be that of an atypical, high-order dye aggregate that is converted to monomeric and other low-order dye forms as DNA concentration is increased.

In our next set of fluorescence measurements, we excited dye **4** at 529 nm over a range of CT DNA concentrations and superimposed the resulting emission spectra with corresponding absorption spectra from Figure 2.6A (Figure 2.8B). Interestingly, as absorption by the “526–523-nm” DNA bound high-order aggregate increased at the low DNA concentrations, the emission intensity upon 529-nm excitation decreased in an inversely proportional fashion. This suggests that the putative aggregate might be quenching its own fluorescence at high aggregate concentrations. Fluorescence self-quenching of aggregated dyes is a well-known phenomenon that can arise from close packing of dye molecules and is a common occurrence for even widely used fluorophores such as fluorescein and rhodamine .[49, 50] Our results indicate that “diluting” the aggregate by adding DNA lowers its concentration relative to other dye forms. This may partially reverse the self-quenching process, allowing aggregate fluorescence to increase (Figure 2.8B).[50]

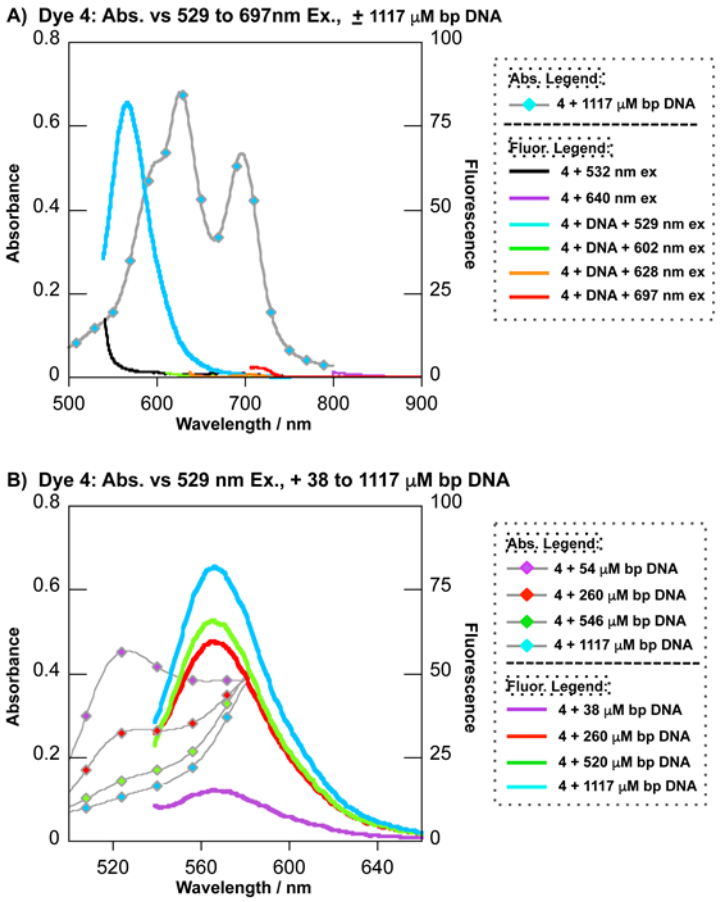

Figure 2.8: Double y-axis plots superimposing dye **4** fluorescence emission spectra (Em) with dye **4** UV–visible absorption (Abs) (22 °C). Samples contained 10 mM sodium phosphate buffer pH 7.0, 10 µM of dye (Em) or 20 µM of dye (Abs) and: (**A**) 1117 µM bp of CT DNA, where the emission spectra were recorded at the excitation wavelengths (Ex) 532 and 640 nm (dye **4**); 529, 602, 628, and 697 nm (dye **4** with DNA); and (**B**) 38–1117 µM bp of CT DNA, where the emission spectra were recorded at an excitation wavelength (Ex) of 529 nm. The absorption spectra are from Figure 5A and in (**B**) are re-plotted from 500 to 580 nm for clarity.

Strong cyanine dye fluorescence is typically observed when the conformational mobility causing rapid non-radiative decay from the singlet excited state of free dye is restricted, i.e., by intercalative DNA binding.[3, 5] While dimeric and aggregated cyanines cannot intercalate, the absence of a fluorescence signal in the case of the "691–697-nm" putative DNA-bound monomer would seem to rule against its ability to interact with DNA by intercalation. The "526–523-nm" high-order aggregate is fluorescent at low dye concentrations, suggesting that there is less

flexibility in its structure compared to the non-fluorescent “596–600-nm” and “619–628-nm” low-order cyanine forms.

2.3.3.4 Competitive DNA Binding

In our next experiment, UV–visible spectrophotometry was used to compare aqueous solutions of dye **4** without and with untreated CT DNA vs. solutions containing a CT DNA preparation that had been pre-equilibrated with the known minor groove binder pentamidine. The results of the pentamidine pre-treatment are shown in Figure 2.9. Addition of the pentamidine increased the ratio of aggregated “526–523-nm” dye absorption relative to the putative low-order and monomeric dye forms absorbing at “619–628-nm” and “691–697-nm”, respectively. Unlike ethidium bromide, which unwinds and lengthens DNA [51], pentamidine makes minimal changes to DNA duplex structure.[52, 53] Taking this into consideration, the experimental results suggest that pentamidine might be reducing the number of dye-accessible minor groove binding sites on the DNA. This could conceivably prevent the “619–628-nm” low-order and “691–697-nm” monomeric dye forms from binding to DNA in the minor groove and at the same time might promote the formation externally bound “526–523-nm” high-order aggregate.

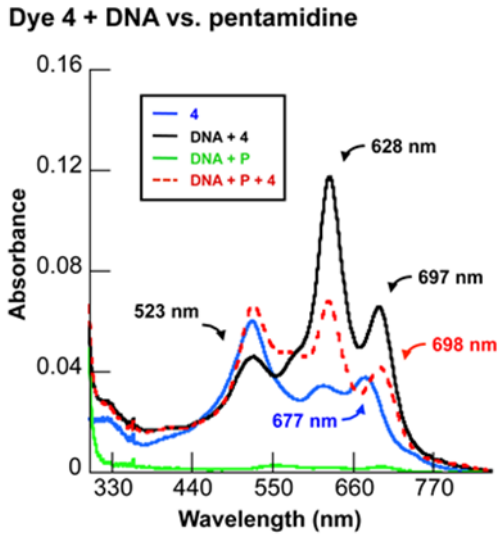

Figure 2.9: UV–visible absorption spectra recorded for: dye **4** without CT DNA (blue lines); dye **4** with CT DNA (black lines); pentamidine (P) with CT DNA (green lines); and dye **4** with DNA pre-equilibrated for one min with pentamidine (red lines). All samples contained 10 mM sodium phosphate buffer pH 7.0 and one or more of the following: 10 µM of dye **4**, 150 µM bp of CT DNA, and 10 µM of pentamidine.

2.3.4 Mechanistic Analysis of Dye-Sensitized DNA Photocleavage

Experiments to probe for cyanine dye-sensitized ROS production were conducted using chemical additives to alter DNA direct strand break formation. Irradiating plasmid DNA reactions in the presence of the $OH^{\bullet}$ scavenger sodium benzoate reduced strand scission by 77 ± 9%, strongly implicating the involvement of Type 1 hydroxyl radicals in dye **4**-sensitized DNA cleavage (Table 1 and Figure S1 in the Supplementary Materials). The metal ion chelating agent EDTA and the hydrogen peroxide reducing enzyme catalase decreased photocleavage yields by ~73%, and ~30%, respectively, pointing to Fenton chemistry as a possible hydroxyl radical source. The mechanism shown in Figure 2.10 can be considered. In this series of reactions, the photosensitizer triplet state of dye **4** reduces ground state triplet oxygen $^3O_2$ by Type 1 electron transfer to yield superoxide anion radicals ($O_2^{\bullet-}$) (Line 1). Then, spontaneous dismutation of the $O_2^{\bullet-}$ gives rise to H_2O_2, which, in the presence of trace Fe(II), triggers the production of hydroxyl radicals ($OH^{\bullet}$) by the Fenton

reaction (Lines 2 and 3).[22, 23] To test for the participation of an alternative ROS pathway involving DNA damage by Type 2 singlet oxygen ($^1O_2$), we replaced H_2O with D_2O, a solvent that produces a 10-fold enhancement in singlet oxygen lifetime.[54] Because levels of dye **4** sensitized DNA strand scission were suppressed by the D_2O rather than undergoing an enhancement, we concluded that it is unlikely that Type 2 singlet oxygen makes a major contribution to dye **4**-sensitized DNA photocleavage.

$$^3PS^* + {}^3O_2 \rightarrow {}^3PS^{*\bullet+} + O_2^{\bullet-} \quad (1)$$

$$2O_2^{\bullet-} + 2H^+ \rightarrow H_2O_2 + {}^3O_2 \quad (2)$$

$$Fe(II) + H_2O_2 \rightarrow HO^\bullet + HO^- + Fe(II) \quad (3)$$

Figure 2.10: Possible mechanism for accounting for dye **4**-sensitized hydroxyl radical formation.[20, 21]

Table 2.1: Inhibition of dye **4** photocleavage induced by chemical additives.[1] Reactions consisting of 38 μM bp of pUC19 plasmid DNA equilibrated with 24 μM of **4** with and without 100 mM sodium benzoate or EDTA, 100 U/μL of catalase, or 72% D_2O (v/v) were irradiated for 60 min with a 741-nm LED lamp (0.3 W/cm^2, spectral output 707–759 nm; 10 mM sodium phosphate buffer pH 7.0). Data were averaged over 2–3 trials with error reported as standard deviation.

Reagents Added	Target	Cleavage Inhibition (%)
Na benzoate	•OH	77 ± 9
D_2O	$^1O_2$	11 ± 0.4
Catalase	H_2O_2	30 ± 10
EDTA	Fe^{2+}, Fe^{3+}/Cu^{1+}, Cu^{2+}	73 ± 8

2.3.5 Uptake, Distribution, and Phototoxicity of Dye 4 in Ovarian Cancer Cells

The cellular internalization efficiency of dye **4** was validated in fluorescence microscopy studies.[55] After incubation of the dye with ES2 ovarian carcinoma cells [56], the intrinsic NIR

fluorescence signal of **4** was visible universally throughout the population of cells within their intracellular cytosolic regions. There was a definitive perinuclearly localization around the Hoescht nuclear stain as well as some overlap indicating possible nuclear uptake (Figure 2.11A). A Calcein AM assay was then used to assess the viability of the cells after treatment with 0.5 μg/mL of the dye in the dark and under light exposure.[57] Our results reveal that, although **4** was non-toxic in the dark at the tested concentration (0.5 μg/mL), the dye was capable of exhibiting substantial phototoxicity to the ES2 cancer cells when exposed to 694-nm light illumination (Figure 2.11B). Of note, the synthesized dye had low dark toxicity (Figure 2.13), with an IC_{50} value of 72.1 μg/mL.

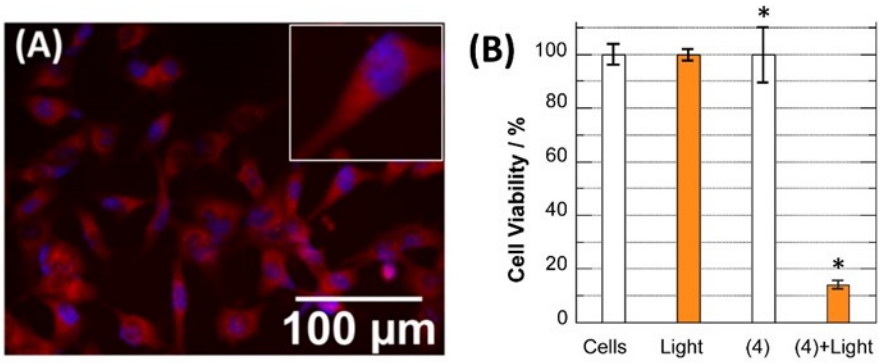

Figure 2.11: (**A**) A representative superimposed fluorescence microscopy image reveals intracellular dye localization (red) in ES-2 ovarian clear cell adenocarcinoma cells after incubation with 0.5 μg/mL of dye **4** for 24 h followed by staining nuclei with Hoechst 33,342 (blue). The enlarged area of one cell within the fluorescence microscopy image. (**B**) ES2 cancer cell viability for: Cells, no treatment; Light, cells exposed to a 694-nm laser (~1.3 W/cm^2) for 5 min; (**4**), cells incubated with dye **4** (0.5 μg/mL = 0.9 μM) for 24 h under dark conditions; and (**4**) + Light, cells incubated with dye **4** (0.5 μg/mL) for 24 h and exposed to a 694-nm laser (1.3 W/cm^2) for 5 min. * $p < 0.05$ when compared with non-treated cells. Error bars represent standard deviation.

2.4 Materials and Methods

2.4.1 General

For the synthesis, all chemicals and solvents were of American Chemical Society grade or HPLC purity and were used as received. HPLC grade acetonitrile (CH_3CN) and water were

purchased from VWR International (West Chester, PA, USA) and American Bioanalytic (Natick, MA, USA), respectively. All other chemicals were from Fisher Scientific (Pittsburgh, PA, USA) and Sigma-Aldrich (Saint Louis, MO, USA). Melting points (mp, open Pyrex capillary) were measured on a Meltemp apparatus and are uncorrected. ^{1}H NMR spectra were recorded on a BrukerAvance (400 MHz) spectrometer(Bruker Corporation, Billerica, MA, USA). Chemical purity was also confirmed using ultra-performance liquid chromatography (UPLC, Waters, Milford, MA, USA) combined with simultaneous evaporative light scattering detection (ELSD), absorbance (photodiode array; PDA), fluorescence, and electrospray time-of-flight (ES-TOF) mass spectrometry (MS) (Waters, Milford, MA, USA).

In the analysis of dye-DNA Interactions, deionized distilled water was used for the preparation of all aqueous solutions. Standard laboratory protocols were employed to clone pUC19 plasmid DNA in XL-1 blue E. coli competent cells (Stratagene, San Diego, CA, USA).[58] The cloned plasmid was then isolated and purified using a QIAfilter Plasmid Mega Kit according to manufacturer's instructions (Qiagen^{TM}, Hilden, Germany, Cat. No. 12263). Sodium phosphate buffer pH 7.0 used in DNA solutions was prepared from sodium phosphate monobasic and sodium phosphate dibasic salts (Thermo Fisher Scientific, Waltham, MA, USA). Sonicated calf thymus (CT) DNA was purchased from Invitrogen (Carlsbad, CA, USA; 10 mg/mL, average size ≤ 2000 bp, Cat. No. 15633-019), while deuterium oxide (99.9%) and agarose were, respectively, obtained from Cambridge Isotope Laboratories and Bio-Rad. All other reagents, including sodium benzoate (99%), dimethyl sulfoxide (DMSO, ≥99.99%), ethidium bromide, pentamidine isethionate salt, and bovine liver catalase were supplied by Sigma-Aldrich. UV–visible absorption spectra and fluorescence emission spectra were respectively acquired using PerkinElmer Lambda 35 (PerkinElmer, Waltham, MA, USA) and a PerkinElmer LS55 spectrophotometers (PerkinElmer,

Waltham, MA, USA). Either a Jasco J-810 (Jasco, Easton, MD, USA) or a Jasco J-1500 CD spectropolarimeter (Jasco, Easton, MD, USA) was employed to record CD and ICD spectra.

2.4.2 Procedures for the Preparation of Dyes 3 and 4

Known compounds **3** and **4** were prepared based on the corresponding published synthetic procedures.[28, 34-38] A mixture of salt **2** (2 equiv); malonaldehyde bisphenylimine monohydrochloride, **1-H**, or the brominated **1-Br** analog (1 equiv); and triethylamine (3 equiv) were refluxed for 3 h in acetic anhydride and then cooled to room temperature. The crude products were precipitated by adding 5 mL of diethyl ether or ethyl acetate to the reaction mixture. Then compounds **3** and **4** were precipitated, filtered, and dried.[28, 34] The final products of dyes **3** and **4** were obtained as pure by crystallization from methanol.

1-methyl-2-((1E,3E)-5-((E)-1-methylquinolin-2(1H)-ylidene)penta-1,3-dien-1-yl)quinolin-1-ium iodide; (**3**); A green powder (56%). ^{1}H NMR (400 MHz, DMSO-*d*6) δ ppm 3.88 (s, 6 H), 6.38 (d, *J* = 12.8 Hz, 2 H), 6.58 (t, *J* = 11.2 Hz, 1 H), 7.43 (m, 2 H), 7.71–7.74 (m, 2 H), 7.79–7.85 (m, 6 H), 7.97–8.04 (m, 4 H) (Figure 2.14).

2-((1E,3Z)-3-bromo-5-((E)-1-methylquinolin-2(1H)-ylidene)penta-1,3-dien-1-yl)-1-methyl-quinolin-1-ium iodide; (**4**); A green powder (49%). ^{1}H NMR (400 MHz, DMSO-*d*6) δ ppm 4.00 (s, 6H), 6.32 (d, *J* = 13.2 Hz, 2 H), 7.53 (t, *J* = 7.6 Hz, 2 H), 7.81 (t, *J* = 7.6 Hz, 2 H), 7.90–7.94 (m, 4H), 8.02 (d, *J* = 8.8 Hz, 2 H), 8.22 (d, *J* = 9.6 Hz, 2 H), 8.34 (d, *J* = 13.2 Hz, 2 H) (Figure 2.15).

2.4.3 DNA Photocleavage

Thirty microliter samples consisting of 3–48 μM of cyanine dye, 38 μM bp of pUC19 plasmid, and 10 mM of sodium phosphate pH 7.0 were either kept in the dark or irradiated from 5 to 120 min with a near-infrared 741-nm LED medical lamp (0.3 W/cm^2, 707–759-nm spectral output;

Larson Electronics, Kemp, TX, USA). Reaction temperature was maintained at 10 or 22 °C by placing the samples in a thermometer-fitted metal block that was heated, kept at room temperature, or immersed in an ice bath during the reaction. In total, 3 μL of electrophoresis loading buffer containing 15.0% (*w*/*v*) ficoll and 0.025% (*w*/*v*) bromophenol blue was added to each sample and 20 μL of the resulting solution were transferred to the wells of 1.5% agarose gel stained with ethidium bromide (0.5 μg/mL, final concentration). Completely loaded gels were electrophoresed at 100 V for 1 h in a Bio-Rad Laboratories gel box containing 1 × tris-acetate-EDTA (TAE) as running buffer and 0.5 μg/mL ethidium bromide. The gels were then visualized at 302 nm with a VWR Scientific LM-20E transilluminator, photographed with a UVP PhotoDoc-It™ Imaging System, and quantitated using ImageJ software. In the case of supercoiled DNA, integrated numerical values were multiplied by a correction factor of 1.22 to account for the decreased affinity of ethidium bromide for supercoiled vs. nicked and linear plasmid forms. The DNA photocleavage yields were then calculated according to the formula:

Percent Photocleavage = [(Linear + Nicked DNA)/(Linear + Nicked + Supercoiled DNA)] × 100.

2.4.4 UV-visible Spectrophotometry

Quartz cuvettes contained either 10 μM of cyanine dye in DMSO or 10 μM of dye in 10 mM of sodium phosphate pH 7.0 buffer without and with 150 μM bp CT DNA. Absorption spectra were recorded at 5-min time intervals from 0 to 30 min (22 °C).

In DNA titration experiments, small volumes of a concentrated aqueous CT DNA solution were successively added to solutions containing 20 μM of cyanine dye **4** in 10 mM sodium phosphate buffer pH 7.0 (500 μL initial volume). After spectra were acquired, absorption readings were corrected for sample dilution. Final CT DNA concentrations ranged from 0 to 2004 μM bp.

In competitive binding experiments, samples contained 10 μM of dye **4** in 10 mM of sodium phosphate pH 7.0 buffer without and with 150 μM bp CT DNA or 150 μM bp CT DNA pre-equilibrated with 10 μM of pentamidine for one min.

2.4.5 Circular Dichroism

Individual CD samples consisted of 10 mM sodium phosphate buffer pH 7.0 with 10 μM of dye and 38–1117 μM of CT-DNA present alone and in combination (2000 μL total volume). Spectra were collected from 800 to 200 nm in 3 mL (1.0 cm) quartz cuvettes (Starna, Atascadero, CA, USA) using the following instrument settings: scan speed, 100 nm/min; response time, 2 s; bandwidth, 0.5 nm; and sensitivity, 100 millidegrees. The temperature was kept constant at 22 °C. Final spectra were averaged over 12 acquisitions.

2.4.6 Fluorescence Spectroscopy

Solutions containing 10 mM sodium phosphate buffer pH 7.0 and 10 μM of cyanine dye 4 in the absence and presence of 38–1117 μM of bp of CT DNA were transferred to 3.0 mL Starna quartz cuvettes (2000 μL, total volume). The samples were excited at an appropriate wavelength ranging from 529 to 697 nm and emission spectra were recorded (22 °C). The scan speed of the spectrophotometer was 100 nm/min, gain was set at medium, and the excitation and emission slit widths were 4.5 nm.

2.4.7 Regent-Induced Changes in DNA Photocleavage

Reactions containing 10 mM of sodium phosphate buffer pH 7.0, 38 μM bp pUC19 plasmid DNA and 24 μM of dye 4 were prepared in the presence and absence of 100 mM of sodium benzoate, 100 U/μL of catalase, 100 mM EDTA, or 72% D_2O (v/v). The reactions were irradiated for 60 min (707–759 nm), resolved on 1.5% non-denaturing agarose gels, visualized, and

quantitated as just described. The percent change in DNA photocleavage was calculated using the following formula, where the additive was either sodium benzoate, catalase, EDTA, or D_2O:

Percent Change in Cleavage = [(% Total of Linear and Nicked DNA with additive – % Total of Linear and Nicked DNA without additive)/(% Total of Linear and Nicked DNA without additive)] × 100.

2.4.8 Cell Line

ES2 human clear cell ovarian carcinoma cell line was obtained from ATCC (Manassas, VA, USA). All cancer cells were cultured in DMEM medium (Sigma, St. Louis, MO, USA) with 10% fetal bovine serum and 1% penicillin–streptomycin (VWR, Visalia, CA, USA). All cells were grown in a humidified atmosphere of 5% CO_2 (*v*/*v*) in air at 37 °C.[56]

2.4.9 Cellular Uptake and Fluorescence Imaging

ES2 cells were plated in 96-well plates at a density of 10×10^3 cells/well and cultured for 24 h. After that, cells were incubated for 24 h in complete DMEM media containing dye **4** (0.5 μg/mL) dissolved in DMSO (<1%). Cells were then washed with DPBS, stained with Hoechst 33342 [29] and the subcellular distribution of the dye was imaged with an BZ-X710 Keyence microscope using DAPI filter and Cy® 7 filter cubes.[55]

2.4.10 Evaluation of Phototherapeutic Effect

ES2 cells were plated in 96-well plates at a density of 10×10^3 cells/well and cultured for 24 h. After that, the cells were incubated in the dark for 24 h in complete DMEM media containing dye **4** (0.5 μg/mL) dissolved in DMSO (<1%). The dye-containing media was then removed, and the cells were rinsed and left in DPBS while being exposed to a 694-nm laser diode light for 5 min (1.3 W/cm^2). After treatment, cells were cultured for 24 h in complete DMEM growth medium prior to viability measurements with Calcein AM as previously described.[57] Non-treated cells, cells

incubated with the same concentration of the dye **4** under dark conditions, and non-treated cells exposed to a 694-nm laser diode for 5 min were used as controls.

2.5 Conclusion

In photodynamic therapy, an ideal DNA photosensitizer should function optimally within a near-infrared phototherapeutic therapeutic window that affords maximum penetration depth of incident light through biological tissue.[10] Here, we showed that symmetrical 2-quinolinium pentamethine carbocyanine dyes substituted with hydrogen (**3**) or bromine (**4**) generate DNA cleavage when irradiated in the near-infrared wavelength range. The electron withdrawing bromine atom promotes DNA interactions by substantially reducing dye autooxidation in aqueous solution. UV–visible, circular dichroism, and fluorescence spectra of the brominated 2-quinolinium pentamethine cyanine (**4**) show that DNA has a major effect on dye aggregation. Low DNA concentrations favor the formation of a high order hypsochromic cyanine aggregate. As DNA concentration is gradually increased, however, the dye **4** aggregate is sequentially converted to a bathochromic dye monomer through intermediate absorbing dimeric and/or low-order aggregated species. The high-order aggregate appears to interact with DNA in an external fashion, while the monomeric and low-order forms of dye **4** may be associating with DNA via its minor groove. The spectroscopic data also suggest that intercalative interactions do not play a major role in DNA binding. Photocleavage reactions run in the presence and absence of radical scavenging agents and other chemical additives reveal that irradiation of the monomeric, DNA-bound form of dye **4** with 707–759-nm near–infrared light generates Type 1 $OH^{\bullet}$ radicals that produce direct strand breaks in plasmid DNA in high yield (pH 7.0, 22 °C). Using fluorescence microscopy, we were able to show that the dye is readily taken up by ES-2 cells where it localizes in the intracellular cytosolic and perinuclear regions and possibly in the cell nuclei. While non-toxic in the dark,

brominated cyanine **4** displayed high levels of phototoxicity over six trials, reducing ES-2 cell viability from 100 ± 10% to 14 ± 1% when irradiated with a 694-nm laser. We will continue to explore and design new 2-quinolinium dicarbocyanine dyes with the aim of developing optimal DNA photosensitizing agents for near-infrared phototherapeutic applications.

2.6 Supplementary Information

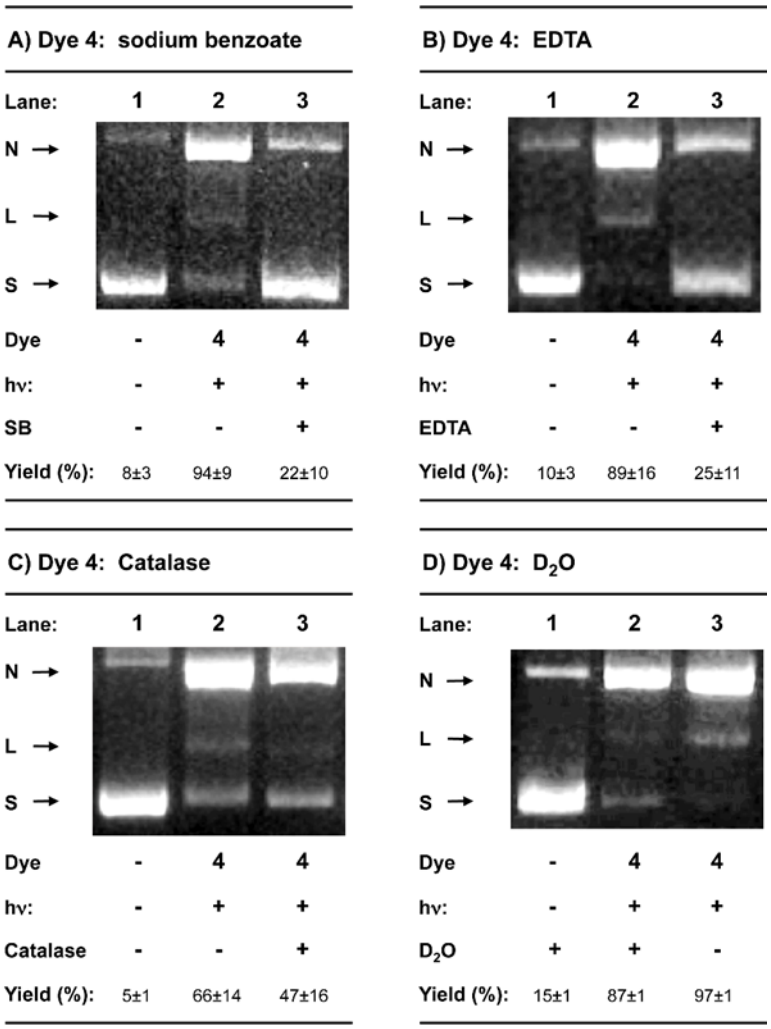

Figure 2.12: Representative agarose gels comparing levels of cyanine dye-sensitized photocleavage of pUC19 plasmid DNA generated in the absence and presence of: (**A**) 100 mM sodium benzoate; (**B**) 100 mM ethylenediaminetetraacetate (EDTA); (**C**) 100 U/μL catalase; (**D**) 72% D_2O (v/v) (741 nm hv for 60 min at 22 °C). All reactions contained 10 mM sodium phosphate buffer pH 7.0, 24 μM of dye **4** and 38 μM bp DNA. Yields are averaged over two to three trials. Errors represent standard deviation. Abbreviations: **L** = linear; **N** = nicked; **S** = supercoiled.

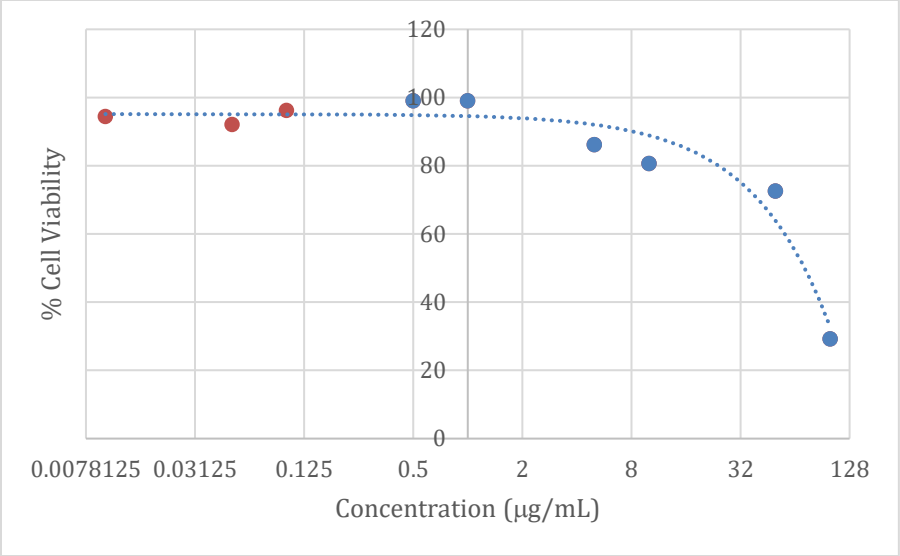

Figure 2.13: Viability of ES2 cells incubated for 24 h under dark conditions with different concentrations of dye **4**. ES2 cells were plated in 96-well plates at a density of 10×10^3 cells/well and cultured for 24 h. After that, the cells were incubated in the dark for 24 h in complete DMEM media containing different concentrations of dye **4** (0.01 - 100 µg/mL) dissolved in DMSO (<1%). The dye-containing media was then removed, and the cells were rinsed with DPBS and cultured for 24 h in complete DMEM growth medium prior to viability measurements with Calcein AM as previously described.[1]

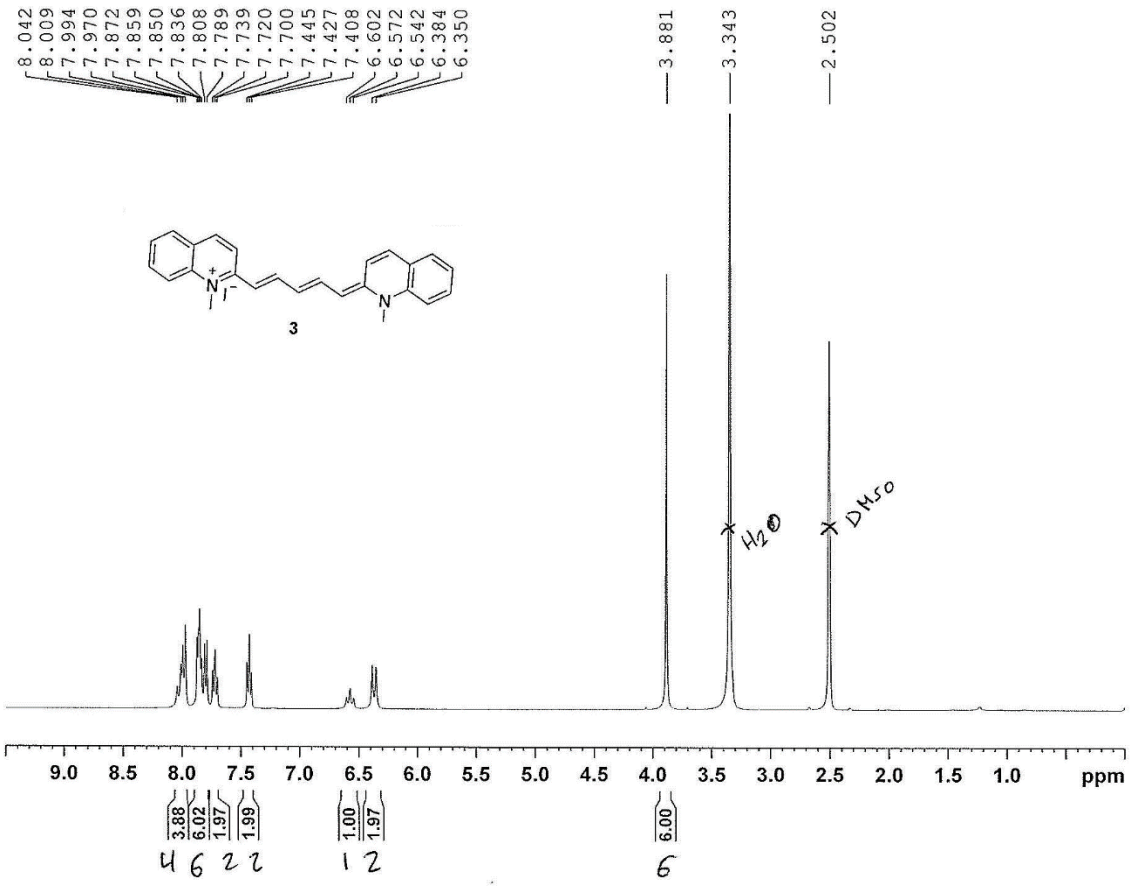

Figure 2.14: ^{1}H NMR spectrum of dye **3**.

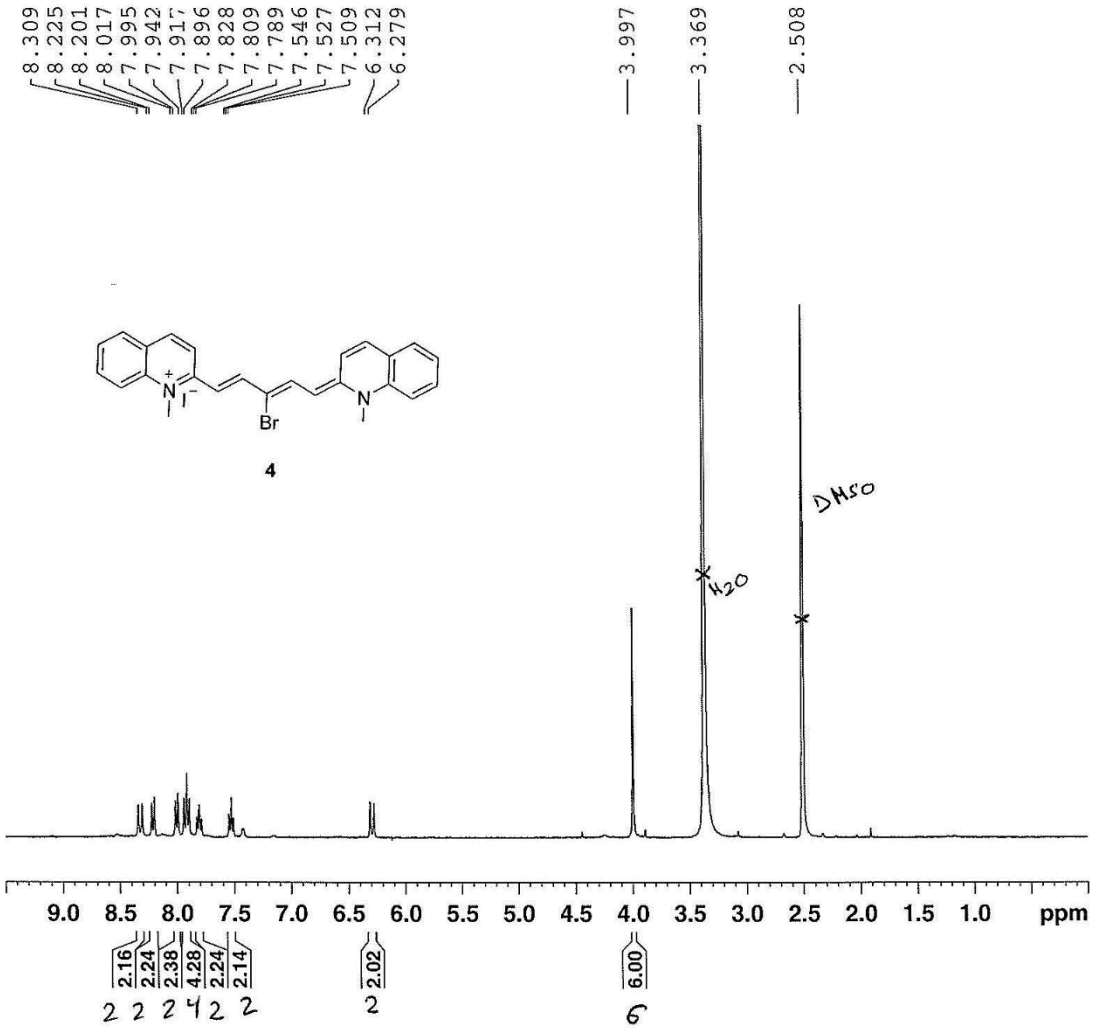

Figure 2.15: ^{1}H NMR spectrum of dye **4**.

2.7 References

1. Sun, W.; Guo, S.; Hu, C.; Fan, J.; Peng, X. Recent Development of Chemosensors Based on Cyanine Platforms. *Chemical reviews.* **2016,** *116* (14), 7768-817.
2. Shindy, H. A. Fundamentals in the chemistry of cyanine dyes: A review. *Dyes and Pigments.* **2017,** *145*, 505-513.
3. Armitage, B. A. Cyanine Dye-Nucleic Acid Interactions. *Heterocyclic Polymethine Dyes.* **2008,** *14*, 11-29.
4. Armitage, B. A. Cyanine Dye–DNA Interactions: Intercalation, Groove Binding, and Aggregation. In *DNA Binders and Related Subjects*. **2005**; pp 55-76.
5. Kawabe, Y.; Kato, S. J. D. Pigments, Spectroscopic study of cyanine dyes interacting with the biopolymer, DNA. *Dyes and Pigments.* **2012,** *95*, 614-618.
6. Garoff, R. A.; Litzinger, E. A.; Connor, R. E.; Fishman, I.; Armitage, B. A. Helical Aggregation of Cyanine Dyes on DNA Templates: Effect of Dye Structure on Formation of Homo- and Heteroaggregates. *Langmuir.* **2002,** *18* (16), 6330-6337.
7. Wang, M.; Silva, G. L.; Armitage, B. A. DNA-Templated Formation of a Helical Cyanine Dye J-Aggregate. *Journal of American Chemical Society.* **2000,** *122* (41), 9977-9986.
8. Boutorine, A. S.; Novopashina, D. S.; Krasheninina, O. A.; Nozeret, K.; Venyaminova, A. G. Fluorescent probes for nucleic Acid visualization in fixed and live cells. *Molecules (Basel, Switzerland).* **2013,** *18* (12), 15357-15397.
9. Wu, H.; Alexander, S. C.; Jin, S.; Devaraj, N. K. A Bioorthogonal Near-Infrared Fluorogenic Probe for mRNA Detection. *Journal of American Chemical Society.* **2016,** *138* (36), 11429-11432.
10. Jacques, S. L., Optical properties of biological tissues: a review. *Physics in medicine and biology* **2013,** *58* (11), R37-61.
11. Keller, D. S.; Ishizawa, T.; Cohen, R.; Chand, M. Indocyanine green fluorescence imaging in colorectal surgery: overview, applications, and future directions. *The lancet. Gastroenterology & hepatology.* **2017,** *2* (10), 757-766.
12. Giraudeau, C.; Moussaron, A.; Stallivieri, A.; Mordon, S.; Frochot, C. Indocyanine green: photosensitizer or chromophore? Still a debate. *Current medicinal chemistry.* **2014,** *21* (16), 1871-97.
13. Xiao, Q.; Chen, T.; Chen, S. Fluorescent contrast agents for tumor surgery. *Experimental and Therapeutic Medicine.* **2018,** *16* (3), 1577-1585.
14. Li, D.-H.; Schreiber, C. L.; Smith, B. D. Sterically Shielded Heptamethine Cyanine Dyes for Bioconjugation and High Performance Near-Infrared Fluorescence Imaging. *Angewandte Chemie International Edition.* **2020,** *59* (29), 12154-12161.
15. Atchison, J.; Kamila, S.; Nesbitt, H.; Logan, K. A.; Nicholas, D. M.; Fowley, C.; Davis, J.; Callan, B.; McHale, A. P.; Callan, J. F. Iodinated cyanine dyes: a new class of sensitisers for use in NIR activated photodynamic therapy (PDT). *Chemical Communications (Camb).* **2017,** *53* (12), 2009-2012.
16. Jing, T.; Fu, L.; Liu, L.; Yan, L. A reduction-responsive polypeptide nanogel encapsulating NIR photosensitizer for imaging guided photodynamic therapy. *Polymer Chemistry.* **2016,** *7*, 951-957.
17. Cao, J.; Chi, J.; Xia, J.; Zhang, Y.; Han, S.; Sun, Y. Iodinated Cyanine Dyes for Fast Near-Infrared-Guided Deep Tissue Synergistic Phototherapy. *American Chemical Society Applied Materials & Interfaces.* **2019,** *11* (29), 25720-25729.

18. Siriwibool, S.; Kaekratoke, N.; Chansaenpak, K.; Siwawannapong, K.; Panajapo, P.; Sagarik, K.; Noisa, P.; Lai, R. Y.; Kamkaew, A. Near-Infrared Fluorescent pH Responsive Probe for Targeted Photodynamic Cancer Therapy. *Scientific Reports.* **2020,** *10* (1), 1283.
19. Ormond, A. B.; Freeman, H. S. Dye Sensitizers for Photodynamic Therapy. *Materials (Basel).* **2013,** *6* (3), 817-840.
20. Li, Z. Y.; Grant, K. B. DNA photo-cleaving agents in the far-red to near-infrared range - a review. *Rsc Advances.* **2016,** *6* (29), 24617-24634.
21. Luby, B. M.; Walsh, C. D.; Zheng, G. Advanced Photosensitizer Activation Strategies for Smarter Photodynamic Therapy Beacons. *Angewandte Chemie-International Edition.* **2019,** *58* (9), 2558-2569.
22. Bonnett, R. Photosensitizers of the porphyrin and phthalocyanine series for photodynamic therapy. *Chemical Society Reviews.* **1995,** *24* (1), 19-33.
23. Ochsner, M. Photophysical and photobiological processes in the photodynamic therapy of tumours. *Journal of photochemistry and photobiology. B, Biology.* **1997,** *39* (1), 1-18.
24. Hatz, S.; Poulsen, L.; Ogilby, P. R. Time-resolved singlet oxygen phosphorescence measurements from photosensitized experiments in single cells: effects of oxygen diffusion and oxygen concentration. *Photochemistry and photobiology.* **2008,** *84* (5), 1284-90.
25. Makrigiorgos, G. M. Detection of chromatin-associated hydroxyl radicals generated by DNA-bound metal compounds and antitumor antibiotics. *Metal ions in biological systems.* **1999,** *36*, 521-45.
26. Pogozelski, W. K.; Tullius, T. D. Oxidative Strand Scission of Nucleic Acids: Routes Initiated by Hydrogen Abstraction from the Sugar Moiety. *Chemical reviews.* **1998,** *98* (3), 1089-1108.
27. Agostinis, P.; Berg, K.; Cengel, K. A.; Foster, T. H.; Girotti, A. W.; Gollnick, S. O.; Hahn, S. M.; Hamblin, M. R.; Juzeniene, A.; Kessel, D.; Korbelik, M.; Moan, J.; Mroz, P.; Nowis, D.; Piette, J.; Wilson, B. C.; Golab, J. Photodynamic therapy of cancer: an update. *CA: A Cancer Journal for Clinicians.* **2011,** *61* (4), 250-81.
28. Mapp, C. T.; Owens, E. A.; Henary, M.; Grant, K. B. Oxidative cleavage of DNA by pentamethine carbocyanine dyes irradiated with long-wavelength visible light. *Bioorganic & Medicinal Chemistry Letters.* **2014,** *24* (1), 214-9.
29. Basnet, K.; Fatemipouya, T.; St Lorenz, A.; Nguyen, M.; Taratula, O.; Henary, M.; Grant, K. B. Single photon DNA photocleavage at 830 nm by quinoline dicarbocyanine dyes. *Chemical Communications (Camb).* **2019,** *55* (84), 12667-12670.
30. Akerman, B.; Tuite, E. Single- and double-strand photocleavage of DNA by YO, YOYO and TOTO. *Nucleic Acids Research.* **1996,** *24* (6), 1080-90.
31. Kanony, C.; Akerman, B.; Tuite, E. Photobleaching of asymmetric cyanines used for fluorescence imaging of single DNA molecules. *Journal of American Chemical Society.* **2001,** *123* (33), 7985-95.
32. Mahon, K. P., Jr.; Ortiz-Meoz, R. F.; Prestwich, E. G.; Kelley, S. O. Photosensitized DNA cleavage promoted by amino acids. *Chemical Communications (Camb).* **2003,** (15), 1956-7.
33. Biton, A.; Ezra, A.; Kasparkova, J.; Brabec, V.; Yavin, E. DNA photocleavage by DNA and DNA-LNA amino acid-dye conjugates. *Bioconjugate Chemistry.* **2010,** *21* (4), 616-21.
34. Nanjunda, R.; Owens, E. A.; Mickelson, L.; Alyabyev, S.; Kilpatrick, N.; Wang, S.; Henary, M.; Wilson, W. D. Halogenated pentamethine cyanine dyes exhibiting high fidelity for G-quadruplex DNA. *Bioorganic & medicinal chemistry.* **2012,** *20* (24), 7002-11.

35. Parton, R. L.; Lenhard, J. R. Dimerization reactions of cyanine radical dications. *The Journal of Organic Chemistry.* **1990,** *55* (1), 49-57.
36. Miyazoe, Y.; Maeda, M. Stimulated Emission from Stimulated emission from 19 polymethine dyes-laser action over the continuous range 710–1060 mμ. *Applied Physics Letters.* **1968,** *12* (5), 206-208.

37. Patnaik, R. L.; Misra, P. K.; Rout, M. K. Application of a free electron molecular orbital model: Absorption spectra of cyanine dyes. *Journal of Indian Chemical Society.* **1976,** *53*, 391-392.

38. Owens, E. A.; Hyun, H.; Tawney, J. G.; Choi, H. S.; Henary, M. Correlating molecular character of NIR imaging agents with tissue-specific uptake. *Journal of medicinal chemistry.* **2015,** *58* (10), 4348-56.
39. Kodama, M.; Tagashira, Y.; Nagata, C. The interaction of pinacyanol with nucleic acids. *Biochimica et biophysica acta.* **1966,** *129* (3), 638-40.
40. Barros, T. C.; Toma, S. H.; Toma, H. E.; Bastos, E. L.; Baptista, M. S. Polymethine cyanine dyes in β-cyclodextrin solution: multiple equilibria and chemical oxidation. *Journal of Physical Organic Chemistry.* **2010,** *23* (10), 893-903.
41. Gorman, A.; Killoran, J.; O'Shea, C.; Kenna, T.; Gallagher, W. M.; O'Shea, D. F. In vitro demonstration of the heavy-atom effect for photodynamic therapy. *Journal of American Chemical Society.* **2004,** *126* (34), 10619-10631.
42. Seifert, J. L.; Connor, R. E.; Kushon, S. A.; Wang, M.; Armitage, B. A. Spontaneous Assembly of Helical Cyanine Dye Aggregates on DNA Nanotemplates. *Journal of American Chemical Society.* **1999,** *121* (13), 2987-2995.
43. Petty, J. T.; Bordelon, J. A.; Robertson, M. E. Thermodynamic Characterization of the Association of Cyanine Dyes with DNA. *The Journal of Physical Chemistry B.* **2000,** *104* (30), 7221-7227.
44. Beckford, G.; Owens, E.; Henary, M.; Patonay, G. The solvatochromic effects of side chain substitution on the binding interaction of novel tricarbocyanine dyes with human serum albumin. *Talanta.* **2012,** *92*, 45-52.
45. Karlsson, H. J.; Bergqvist, M. H.; Lincoln, P.; Westman, G. Syntheses and DNA-binding studies of a series of unsymmetrical cyanine dyes: structural influence on the degree of minor groove binding to natural DNA. *Bioorganic & medicinal chemistry.* **2004,** *12* (9), 2369-84.
46. Nordén, B. Optical studies on complexes between DNA and pseudoisocyanine. *Biophysical chemistry.* **1976,** *6* (1), 31-45.
47. Garbett, N. C.; Ragazzon, P. A. Chaires, J. B. Circular dichroism to determine binding mode and affinity of ligand-DNA interactions. *Nature Protocols.* **2007,** *2* (12), 3166-72.
48. Maj, M.; Jeon, J.; Góra, R. W.; Cho, M. Induced optical activity of DNA-templated cyanine dye aggregates: exciton coupling theory and TD-DFT studies. *The journal of physical chemistry.* **2013,** *117* (29), 5909-18.
49. Zhegalova, N. G.; He, S.; Zhou, H.; Kim, D. M.; Berezin, M. Y. Minimization of self-quenching fluorescence on dyes conjugated to biomolecules with multiple labeling sites via asymmetrically charged NIR fluorophores. *Contrast media & molecular imaging.* **2014,** *9* (5), 355-62.
50. Swiecicki, J. M.; Thiebaut, F.; Di Pisa, M.; Gourdin-Bertin, S.; Tailhades, J.; Mansuy, C.; Burlina, F.; Chwetzoff, S.; Trugnan, G.; Chassaing, G.; Lavielle, S. How to unveil self-

quenched fluorophores and subsequently map the subcellular distribution of exogenous peptides. *Scientific Reports.* **2016,** *6*, 20237.
51. Hayashi, M.; Harada, Y. Direct observation of the reversible unwinding of a single DNA molecule caused by the intercalation of ethidium bromide. *Nucleic Acids Research.* **2007,** *35* (19), e125.
52. Edwards, K. J.; Jenkins, T. C.; Neidle, S. Crystal structure of a pentamidine-oligonucleotide complex: implications for DNA-binding properties. *Biochemistry.* **1992,** *31* (31), 7104-9.
53. Jenkins, T. C.; Lane, A. N. AT selectivity and DNA minor groove binding: modelling, NMR and structural studies of the interactions of propamidine and pentamidine with d(CGCGAATTCGCG)2. *Biochimica et biophysica acta.* **1997,** *1350* (2), 189-204.
54. Merkel, P. B.; Kearns, D. R. Radiationless decay of singlet molecular oxygen in solution. Experimental and theoretical study of electronic-to-vibrational energy transfer. *Journal of American Chemical Society.* **1972,** *94* (21), 7244-7253.
55. Li, X.; Schumann, C.; Albarqi, H. A.; Lee, C. J.; Alani, A. W. G.; Bracha, S.; Milovancev, M.; Taratula, O.; Taratula, O. A Tumor-Activatable Theranostic Nanomedicine Platform for NIR Fluorescence-Guided Surgery and Combinatorial Phototherapy. *Theranostics.* **2018,** *8* (3), 767-784.
56. Schumann, C.; Taratula, O.; Khalimonchuk, O.; Palmer, A. L.; Cronk, L. M.; Jones, C. V.; Escalante, C. A.; Taratula, O. ROS-induced nanotherapeutic approach for ovarian cancer treatment based on the combinatorial effect of photodynamic therapy and DJ-1 gene suppression. *Nanomedicine : nanotechnology, biology, and medicine.* **2015,** *11* (8), 1961-70.
57. Dani, R. K.; Schumann, C.; Taratula, O.; Taratula, O. Temperature-tunable iron oxide nanoparticles for remote-controlled drug release. *AAPS American Association of Pharmaceutical Scientists.* **2014,** *15* (4), 963-72.
58. Sambrook, J.; Ef, F.; Maniatis, T. *Molecular Cloning, 2nd Ed*. 1989.

3 UNPRECENDENTED OXIDATIVE DNA PHOTOCLEAVAGE ABOVE 830 NM MEDIATED BY 4-QUINOLINIUM PENTAMETHINE CARBOCYANINE DYES

3.1 Abstract

This paper presents data describing the DNA interactions of near-infrared (NIR) 4-quinolinium carbocyanine dyes *meso*-substituted either with a bromine, chlorine, or hydrogen atom. UV-visible absorption spectra show that dyes **KI2**, **KI3**, and **KI4** are stable in DMSO and aqueous buffer. The 4-quinolinium dyes absorb light that extends into the near-infrared range between 555 nm and ~980 nm. Addition of increasing amounts of calf thymus (CT) DNA to the aqueous solution results in the conversion of high order H-aggregated dye **KI2** to the monomeric form with a hypsochromic shift. Cyanine dye **KI2** possesses minimal optical signatures by not having any induced CD nor fluorescence signals, suggesting it may externally bind to the DNA backbone. Here, we also report a unique direct strand breakage of pUC19 plasmid DNA by the three symmetrical 4-quinolinium carbocyanine dyes at 830, 850 nm, and/or 905 nm (pH 7.0). Type I hydroxyl radicals display a major involvement in DNA strand breakage by dye **KI2**. To the best of our knowledge, our results represent the first reported case of DNA photocleavage triggered by single-photon excitation of a chromophore at wavelengths above 830 nm. Our data therefore suggest that 4-quinolinium pentamethine carbocyanine dye **KI2** might one day be an important sensitizing agent in photo-therapeutic applications.

3.2 Introduction

Photodynamic therapy is a less invasive treatment approach that requires the combination of a non-toxic photosensitizer with suitable light to generate reactive oxygen species (ROS).[1] Reactive oxygen species are generated in two different pathways. Upon excitation with an appropriate light source, the photosensitizer moves from its ground state to triplet excited state through intersystem crossing from an intermediate excited singlet state. In photodynamic therapy, photosensitizers mostly undergo type II energy transfer where the triplet excited state transfers energy to a ground state triplet oxygen ($^3O_2$) to generate singlet oxygen ($^1O_2$).[2] Alternatively, in the type I process, the triplet excited state can react with $^3O_2$ by transferring electrons to molecular oxygen to generate superoxide anion radicals ($O_2^{\bullet-}$), which spontaneously dismutate to form hydrogen peroxide (H_2O_2) that subsequently gives rise to hydroxyl radical (•OH) via Fenton chemistry.[3, 4] Over the past years, researchers have developed many photosensitizers for phototherapeutic use. These photosensitizers are often derived from porphyrins, chlorins, bacteriochlorins and phthalocyanines, metal complexes, and synthetic organic dyes such as cyanine dyes.[5] Only few of these photosensitizers, such as porfimer sodium (Photofrin®) and verteporfin (Visudyne®) have been clinically approved for the treatment of various diseases. Though, several of these currently used photosensitizers have demonstrated promising outcomes in PDT, majority of them are activated with visible light sources with wavelengths ≤ 689 nm[8] that are readily absorbed by biological tissues. For example, the well-known clinical PDT agent porfimer sodium is activated at ~ 630 nm and exhibits a low absorption coefficient of 1170 M^{-1} cm^{-1} [6, 7] at this wavelength. Due to the tissue penetration issues of light with these photosensitizers, they can only treat superficial skin conditions and diseases. Chromophores that absorb light in near infrared (NIR) are important in photodynamic therapy due to the versatile photochemical

properties they hold. These photosensitizers possess a reduced light scattering effect and absorb in the phototherapeutic window of 650-850 nm, a region that allows an enhanced tissues penetration depth.[9] They can be used as fluorescent probes[10] to enable *in vivo* tumor characterization through tumor visualization.[11] Recent studies have shown a near-infrared cyanine dye based probe for efficiently imaging endogenous hydrogen peroxide.[12]

Long-wavelength cyanine dyes have also been widely investigated as sensitizing agents in photodynamic cancer therapy[13] due to their ability to absorb light in the 650-850 nm near-infrared photo-therapeutic window. Most biological chromophores absorb light minimally in this wavelength range, allowing for a deep penetration of incident irradiation and an efficient activation of the near-infrared photosensitizers. Near-infrared cyanine dyes have high molar absorption coefficients, strong fluorescence, and good photostability. Several studies have reportedly used symmetrical 4-quinolinium[8], 2-quinolinium[14], benz[e]indolium[15]pentamethine carbocyanine dyes, and asymmetrical oxazole yellow (YO) and thiazole orange (TO) based cyanine dyes[16-19] to photocleave DNA in the visible or near-infrared range. However, little is known about the DNA photocleavage ability of other symmetrical cyanine dyes with NIR light.

Here, we report DNA photocleavage activities of three symmetrical 4-quinolinium pentamethine cyanine dyes *meso*-substituted with either a bromine, chlorine, or hydrogen atom (**KI2**, **KI3**, and **KI4**) when irradiated at 830, 850, and 905 nm (Figure 3.1). The brominated carbocyanine dye **KI2** demonstrated a unique ability to form direct DNA strand breaks above 830 nm.

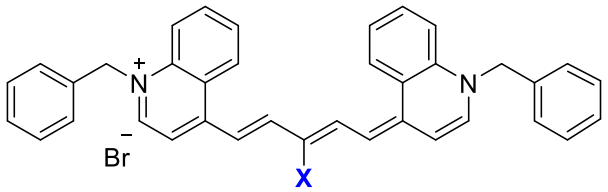

KI2: X = Br
KI3: X = Cl
KI4: X = H

Figure 3.1: Chemical structures of 4-quinolinium pentamethine carbocyanine dyes **KI2**, **KI3**, and **KI4**. All dyes were synthesized and provided by Dr. Maged Henary at the Georgia State University, Department of Chemistry.

3.3 Results and Discussion

3.3.1 Dye Stability and Dye-DNA Interactions

Stability is a vital factor in the determination of photophysical properties of cyanine dyes. Oxidative photodegradation known as photobleaching and self-aggregation are commonly observed with cyanine dyes in solutions.[20, 21] Also, solvent as well as substituents can affect the stability and aggregation of the cyanine dyes. To validate the properties of the symmetrical 4-quinolinium pentamethine carbocyanine dyes under study, a UV-visible spectroscopic assay of the dyes was accessed in different media as a function of time as follows.

3.3.1.1 UV-visible Time Course

In the first part of our study, UV-visible absorption spectra were recorded with 10 μM of dyes **KI2**, **KI3**, and **KI4** in DMSO, and in 10 mM of sodium phosphate buffer at pH 7.0 in the presence and absence of 150 μM bp calf thymus (CT) DNA at time intervals up to 30 min at 22 °C (Figure 3.2). Dyes **KI2**, **KI3**, and **KI4** in aqueous buffer absorb light between 555 and ~ 980 nm with absorption maxima at 671, 684, and 707 nm, respectively. In the presence of DNA, the aggregation patterns of dyes **KI2** and **KI3** change. **KI2** aggregates differently, leading to the formation of a new peak that is noticed at 582 nm, which corresponds to its absorption maximum.

The chlorinated dye **KI3** in presence of DNA exhibits a maximum absorption intensity that is observed at 680 nm. Generally, interaction between cyanine dyes and DNA leads to dye-DNA complex formation, which often offers the dye a great stability towards auto-oxidation. However, DNA seems not to completely stabilize all the dyes, and this might be explained by the degree to which dyes **KI2** , **KI3** and **KI4** interact with DNA. Substituents such as electron withdrawing groups often promote great stability by discouraging dye auto-oxidation[14, 22], which is observed with both the brominated and chlorinated dyes **KI2** and **KI3**. When the free dyes **KI2**, **KI3**, and **KI4** are recorded in DMSO, the formation of high monomeric bands is observed (Figure 3.2 A, D, G) at 804 nm, 808 nm, and 828 nm, respectively. It is apparent that DMSO stabilizes all the dyes compared to aqueous buffer (Figure 3.2 A, D, G).

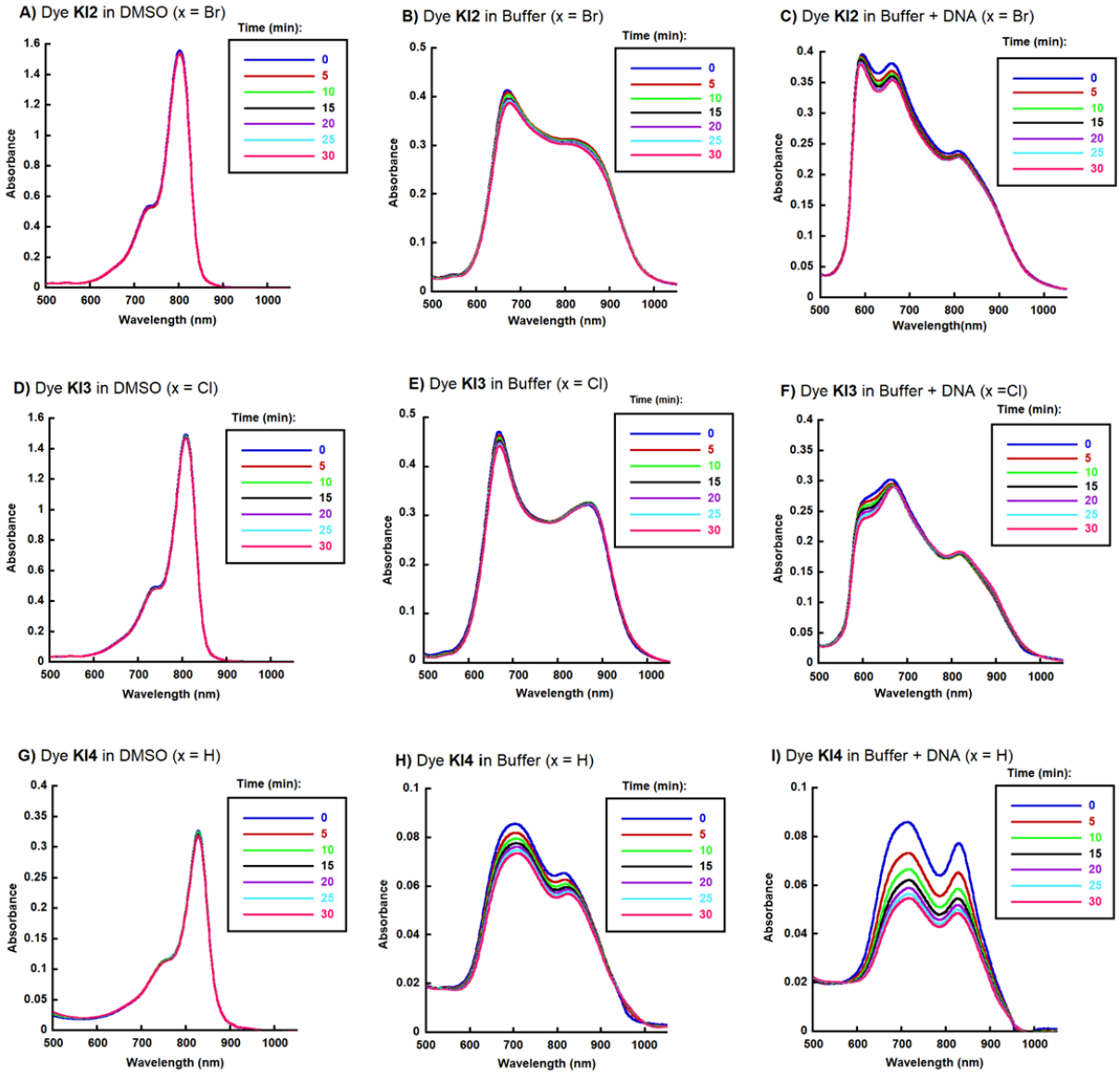

Figure 3.2: UV-visible spectra recorded over 30 min for 10 µM of 4-quinolinium pentamethine carbocyanine dyes **KI2, KI3,** and **KI4** in: **(A), (D), (G)** DMSO; **(B), (E), (H)** 10 mM sodium phosphate buffer pH 7.0; **(C), (F), (I)** 10 mM sodium phosphate buffer pH 7.0 and 150 µM CT DNA (22 °C).

Upon addition of DNA to the aqueous buffer, the absorption of dyes **KI2** and **KI3** changes with a blue shift in their wavelength (Figure 3.3 A, B), which suggests that the dyes may interact with the DNA. In contrast, dye **KI4** seems not to interact with DNA at all (Figure 3.3 C). Additionally, the overlay of previously recorded **KI2** UV-visible spectra from (Figure 3.3 A) at 0

min consisting of 10 mM sodium phosphate pH 7.0 and 10 µM dye **KI2** in presence and absence of 150 µM bp (22 °C) shows a blue-shifted (hypsochromic) absorption with a dye-DNA bound monomer formation at 582 nm (Figure 3.3). This blue shifted peak at 582 nm may be due to the formation of DNA-bound aggregate (Figure 3.3). Upon addition of calf thymus DNA to the aqueous solution, the peaks of dyes **KI2** and **KI3** exhibit a minimal hypsochromic shift as shown in Figure 3.3 A, B. This blue-shift and change in the aggregation is an indication of dye-DNA interaction.

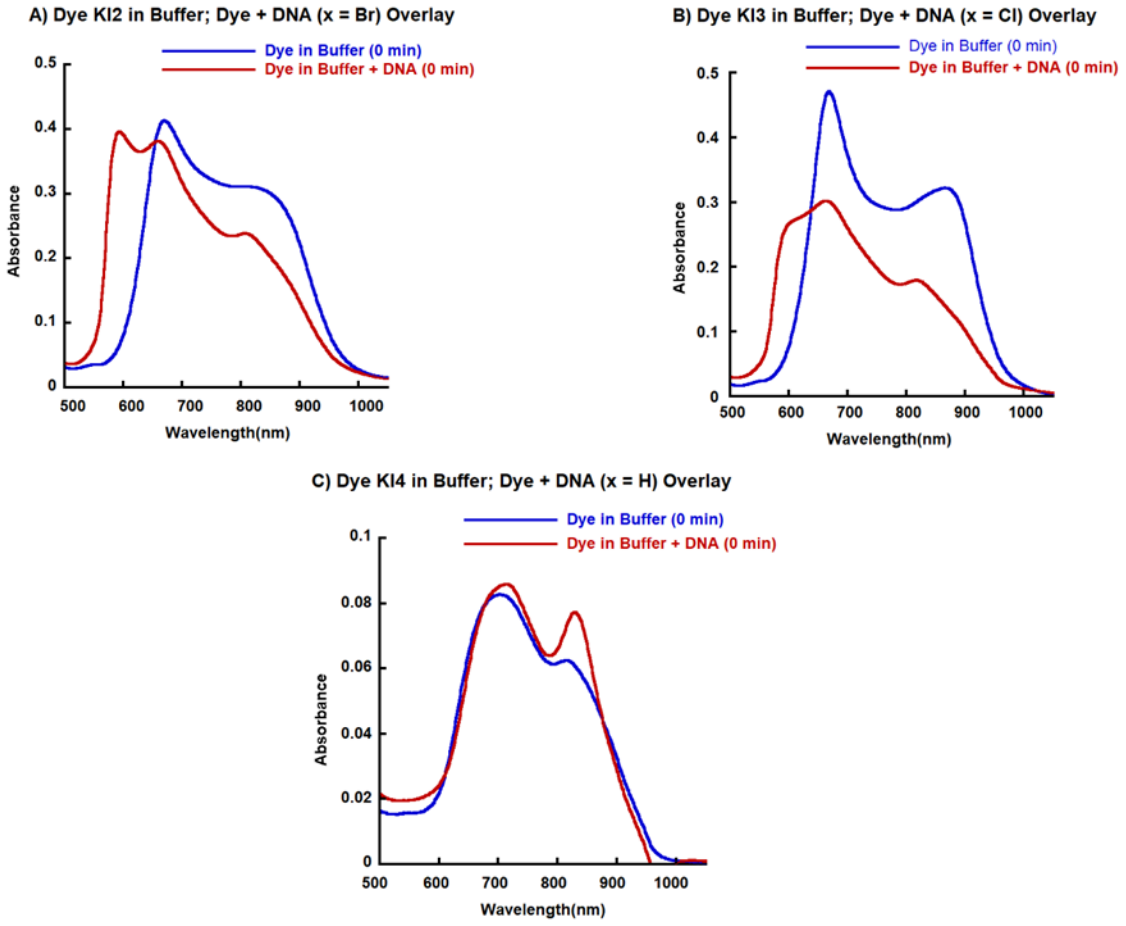

Figure 3.3: UV-visible Overlay spectra at 0 min for 10 µM of dyes **KI2**, **KI3**, and **KI4** in 10 mM sodium phosphate buffer pH 7.0 and 150 µM CT DNA (22 °C).) with: **(A)** is an overlaid spectra of 1B,C; **(B)** is an overlaid spectra of 1E,F; and **(C)** is an overlaid spectrum of 1H,I.

The data show that dyes **KI2** and **KI3** are relatively stable under all conditions (in DMSO, aqueous buffer, and when CT DNA is added) at a time interval of 0 up to 30 min except for dye **KI4**. Unlike dyes **KI2** and **KI3**, the *meso*-substituted hydrogen dye **KI4** seems to auto-oxidize in aqueous buffer even in the presence of CT DNA, suggesting low stability. Notwithstanding data suggest that 830 nm, 850 nm, and 905 nm lasers light could be utilized to irradiate the dye-DNA complexes in photocleavage reactions. Our next experiment will focus on further examining the interactions between dye **KI2** and DNA.

3.3.1.2 UV-visible Absorption Titration

Cyanine dyes have the ability to interact with biomolecules such as DNA and proteins. The interaction between **KI2** with DNA is investigated in this part of our study. We recorded UV-visible absorption spectra of the dye upon the addition of small volumes of an aqueous solution of 13,088 μM bp CT DNA to a sample containing 20 μM of the cyanine dye **KI2** in 10 mM sodium phosphate pH 7.0 at 22 °C with an initial volume of 500 μL (Figure 3.4). The final CT DNA concentrations present in the sample ranged from 34 μM bp up to 1328 μM bp. The result confirms clear evidence of an interaction between the dye and DNA (Figure 3.4).

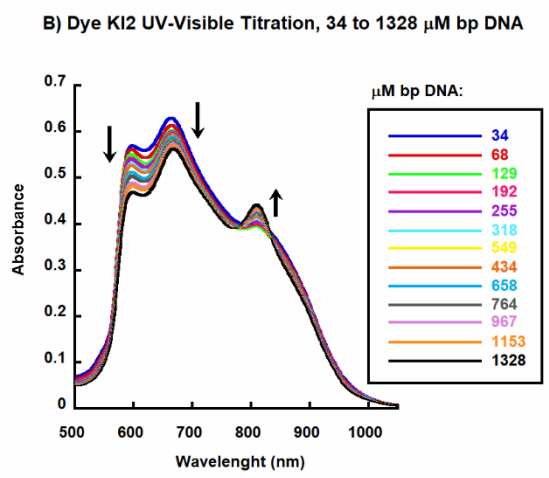

Figure 3.4: Representative UV-visible absorption at 0 min overlay and titration spectra of dye **KI2**. Samples contained 20 µM dye, 10 mM sodium phosphate buffer pH 7.0 in the presence of increasing CT DNA concentrations from 34 up to 1328 µM bp with all absorption spectra corrected for sample dilution (22 ºC).

When an increasing concentration of DNA is added to the aqueous buffer solution containing dye **KI2**, the dye aggregation pattern changes. Yet, this interaction between the dye and DNA is minimal compared to other quinolinium cyanine dyes studied by our research group.[8, 14] As the concentration added of CT DNA increases, the intensities of the absorption bands at ~ 598 and 664 nm decrease. While the monomeric band at 809 nm increases in intensities (Figure 3.4). Some monomeric cyanine dyes have a preference of intercalating to DNA during their interaction, while other cyanine dyes are minor groove binders.[15] However, the UV-vis, these data do not provide sufficient information about the DNA cleavage ability and the DNA binding mode of **KI2**. Our results suggests that dye **KI2** interacts with dsDNA and may bind to DNA as an H-aggregated and a monomer. In our next study, the DNA photocleavage ability of the dyes will be tested in the NIR using 830, 850, and 905 nm light emitting diode lasers (LEDs) that will target the DNA bound monomeric dye **KI2** observed in Figure 3.3 A).

3.3.2 DNA Photocleavage

We began our investigation of the dyes under study to oxidatively photocleave DNA by first comparing dyes **KI2**, **KI3,** and **KI4** DNA photocleavage at 850 nm.

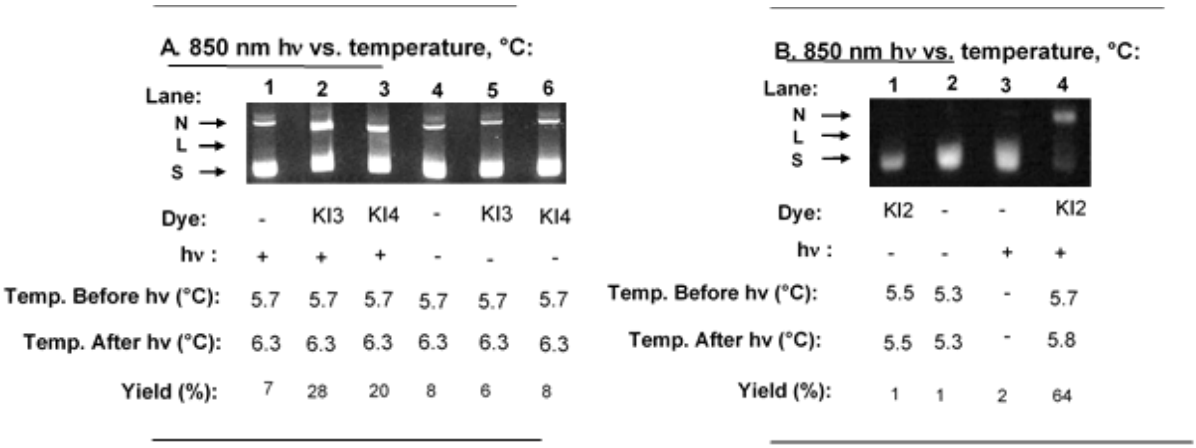

Figure 3.5: Representative ethidium bromide stained 1.3% agarose gel showing pUC19 plasmid DNA photocleavage. Reactions contained 10 mM sodium phosphate buffer pH 7.0, 38 μM bp pUC19 plasmid DNA in the presence and absence of 20 μM dyes **KI2**, **KI3**, and **KI4**. Individual reactions were irradiated for 30 min with laser light power of 100 mW at 850 nm or kept in the dark. A metal block holding the samples was immersed in an ice bath during the reactions. Sample temperature before and after the reaction was recorded a with non-contact of the infrared thermometer. Abbreviations: Temp, temperature; N, nicked; L, linear; S, supercoiled.

DNA photocleavage reactions contained 38 μM bp pUC19 plasmid DNA, 20 μM of dyes **KI2**, **KI3**, or **KI4**, and 10 mM sodium phosphate buffer pH 7.0. Samples immersed in an ice bath were either irradiated at 850 nm or kept in the dark for 30 min. After the 30 min time interval, the samples were electrophorized on a non-denatured 1.3 % agarose gel for 60 min. A small amount of supercoiled plasmid DNA was converted to nicked DNA upon irradiation of reaction samples containing chlorinated dye **KI3** and **KI4** with 28 and 20 % yield respectively as shown in lanes 4 and 5 (Figure 3.5 A). Dye **KI2** produced the most cleavage yield that led to 64% yields level compared to the other two dyes (Figure 3.5 B).

Also, the negative control dark reactions revealed much lower levels of DNA strand breakage any dsDNA breakage at all as expected. A temperature analysis study was achieved by

recording the temperatures of the individual samples before and after the reactions to check for possible thermal DNA cleavage effect. Relative to dark controls, the temperatures of the irradiated samples appear not to increase after the 30 min irradiation. The result seems to rule against thermal DNA cleavage as a phenomenon; suggesting that the modest DNA strand breakage observed with dyes **KI2**, **KI3**, and **KI4** is photochemically driven. Both dyes **KI3** and **KI4** do not show a significant DNA cleavage activity. They show a reduced DNA cleavage effect that can be explained by a loss of their DNA cleavage activities. The inability of dyes **KI4** to photochemically induce a high DNA cleavage level at 850 nm correlates and is consistent with its UV-visible absorption spectra showing rapid auto-oxidation of the dye in aqueous buffer (Figure 3.2). In the case of dye **KI3**, concentrated stock solutions of the dye were observed to lose absorption over weeks. This result suggests that dyes **KI3** and **KI4** should be discontinued and only dye **KI2** will be employed for the remaining studies.

3.3.2.1 DNA Photocleavage at Different Wavelengths

This study was performed to examine whether DNA photocleavage by dye **KI2** is not thermal in nature at 830 nm and 905 nm wavelengths. Individual reaction mixtures consisted of 38 μM bp pUC19 plasmid DNA, 10 mM sodium phosphate buffer pH 7.0, or in the presence or absence of 20 μM dye **KI2**. Reactions were either irradiated with LED lasers light with a wavelength of 830 or 905 nm or kept in the dark (30 min). The temperatures were immediately recorded before and after the photocleavage reaction. After that, the resulted reactions samples were all electrophorized on a 1.3 % agarose gel to visualize the DNA bands. Dye **KI2** was able to markedly convert supercoiled DNA to nicked DNA upon irradiation of the samples containing dye 20 μM **KI2** and 38 μM bp of pUC19 plasmid DNA with 830 and 905 nm LED lasers light and

DNA. Intriguingly, 82 and 33% cleavage yields are respectively produced at 830 and 905 nm (Figure 3.6).

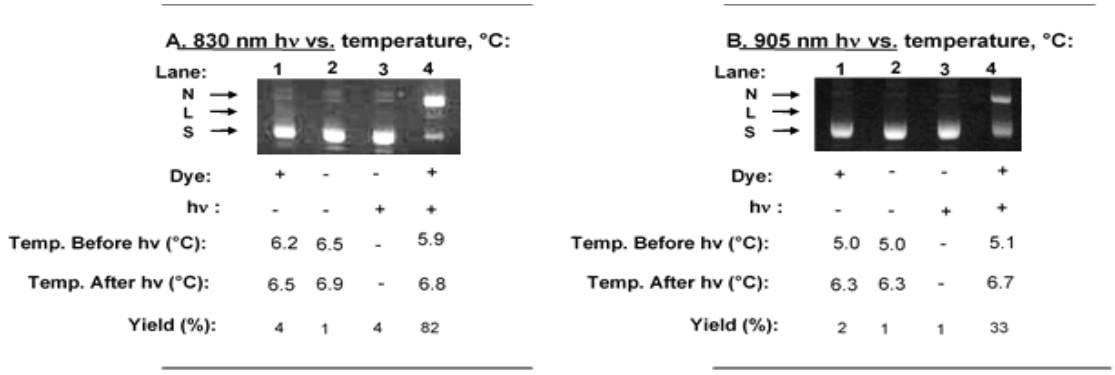

Figure 3.6: Representative ethidium bromide stained 1.3% agarose gel showing pUC19 plasmid DNA photocleavage. Reactions contained 10 mM sodium phosphate buffer pH 7.0, 38 μM bp pUC19 plasmid DNA in the presence and absence of 20 μM dye **KI2**. Individual reactions were irradiated for 30 min with laser light power of: (**A)** 350 mW 830 nm; **(B)** 50 mW 905 nm or kept in dark. A metal block holding the samples was immersed in an ice bath during the reaction. Sample temperature before and after the reaction was recorded with non-contact of the infrared thermometer. Abbreviations: Temp, temperature; N, nicked; L, linear; S, supercoiled.

On the other hand, very little DNA strand breakage is observed with dark control reactions in all cases (Figure 3.6). Also, the recorded temperature before and after the reaction shows the light from the lasers is not substantially heating the samples to induce DNA cleavage, suggesting that DNA photocleavage that is observed by dye **KI2** at wavelengths 830 and 905 nm is not thermally initiated, but rather mediated photochemically by the dye itself.

3.3.2.2 DNA Photocleavage Concentration Titration

The objective of this study was to determine the desired low concentration required for DNA photocleavage by the brominated dye **KI2**, which could minimize the risk of a potential side effects at high concentration of PS. Concentration titration DNA photocleavage was achieved with reactions consisting of 38 μM bp pUC19 plasmid DNA, 0-45 μM dye **KI2** in 10 mM sodium

phosphate buffer pH 7.0. Individual reactions were either heated at 37 °C, irradiated at 830 and 905 nm, or kept in the dark at (10 °C) for 30 min (Figure 3.7). Our results show that dye **KI2** does not cleave DNA at 37 °C, physiological temperature (Figure 3.7A). However, upon irradiation of the reactions with either 850 or 905 nm lasers light, a direct DNA strand break is observed (Figure 3.7 B, C).

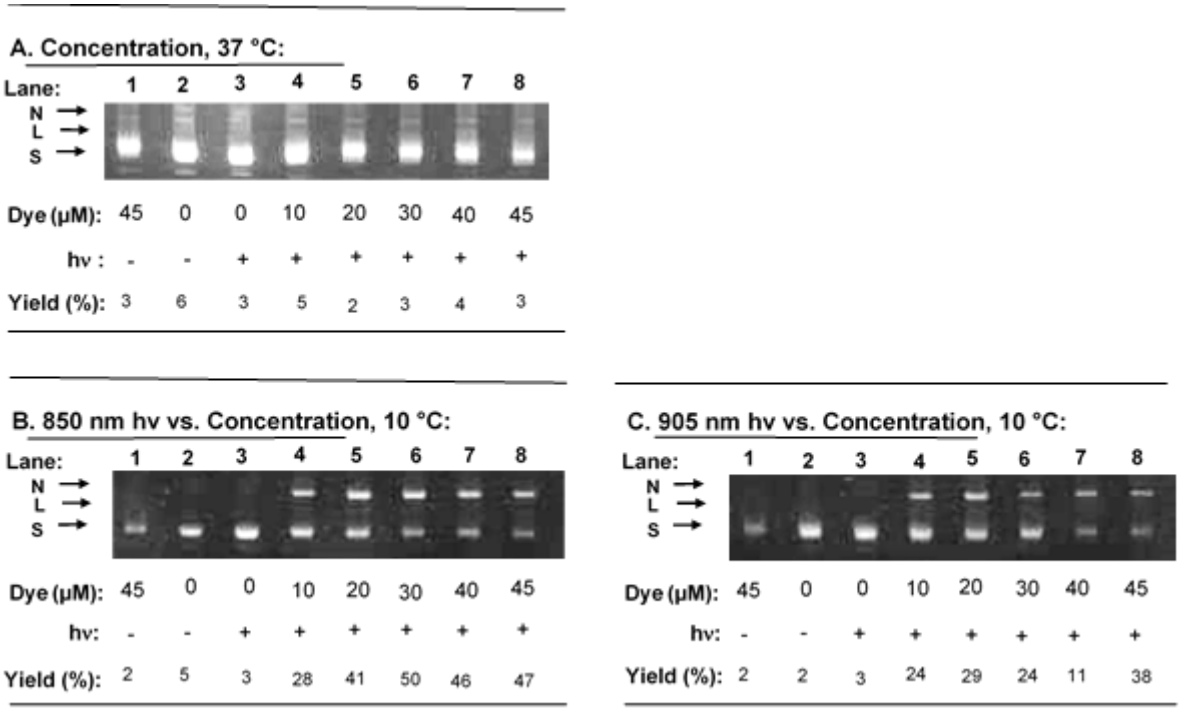

Figure 3.7: Representative ethidium bromide stained 1.3% agarose gel depicting pUC19 plasmid DNA photocleavage in presence of dye **KI2** concentrations ranging 0-45 μM. All reactions contained 10 mM sodium phosphate buffer pH 7.0 and 38 μM bp DNA. The reactions were either: **(A)** heated for 30 min at 37 °C or in dark; irradiated for 30 min with laser light powers of (**B)** 100 mW 850 nm; and **(C)** 50 mW 905 nm or in dark at 10 °C. Abbreviations: N, nicked; L, linear; S, supercoiled.

As expected, the cleavage yield tended to increase as a function of increasing concentrations of dye up to 20 or 30 μM. As the concentration of dye added to the reaction increases, more pUC19 plasmid supercoiled DNA strand is converted to the nicked form of DNA

with some variations at high dye concentration (Figure 3.7, C; lanes 5-7). The highest dye **KI2** concentrations display a low level of DNA cleavage with respect to the other concentrations. This artifact may be caused by a precipitation of the dye at high concentrations of 30, 40, and 45 μM of DNA complex. In all dark control reactions, pUC19 plasmid converted to substantial levels of nicked DNA for 30 mins. According to result seen in Figure 3.7, dye **KI2** can be used at the physiological body temperature and 20 μM is the optimum concentration of dye that can be utilized in the rest of one photocleavage experiments.

3.3.2.3 Time-Course DNA Photocleavage

In this investigation, we are accessing the ability of dye **KI2** to photocleave DNA in the short possible time frame. The irradiation time or the time required to photoactivate the photosensitizer is a key factor in PDT practice.

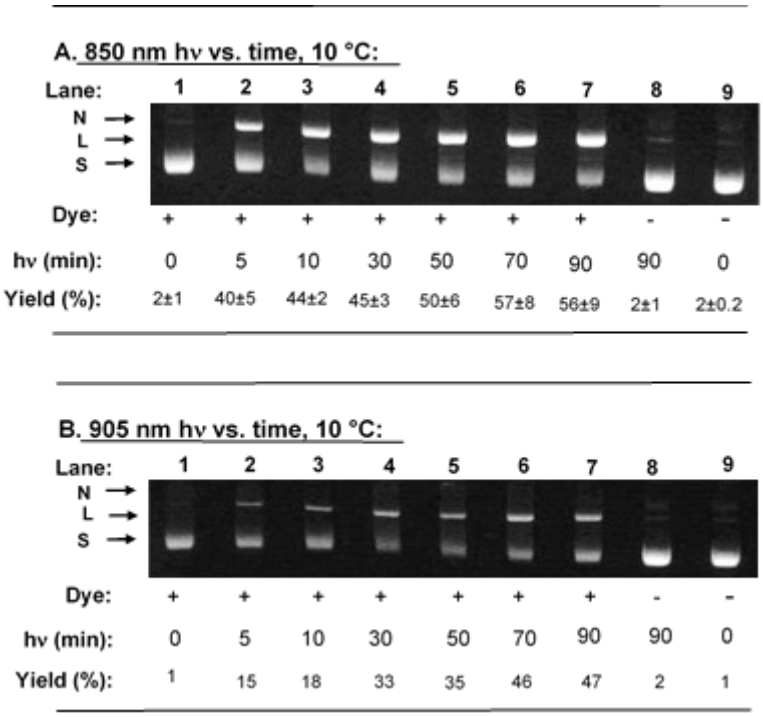

Figure 3.8: Representative ethidium bromide stained 1.3% agarose gel depicting cyanine dye **KI2** photocleavage of pUC19 plasmid DNA. Reactions contained 10 mM sodium phosphate buffer pH 7.0 and 38 μM bp DNA in the presence or absence of 20 μM of dye **KI2**. The reactions were irradiated for various times (0-90 min) with laser light powers of: **(A)** 100 mW 850 nm, **(B)** 50 mW 905 nm or kept in dark (10 °C). Abbreviations: N, nicked; L, linear; S, supercoiled.

In this DNA photocleavage experiment, samples contained 38 μM bp pUC19 plasmid DNA with 20 μM of dye **KI2** in 10 mM sodium phosphate buffer pH 7.0. The reactions were kept in the dark or irradiated with either LED light with power of 100 mW 850 nm or 50 mW 905 nm at time interval from 0-90 min (10 °C). After irradiation of individual samples, reactions were electrophorized on a non-denaturing 1.3% agarose gel to visualize the DNA bands resulted from the reaction. The gel image Figure 3.8 demonstrates that 4-quinolinium cyanine dye **KI2** cleaves pUC19 plasmid DNA upon irradiation with 850 nm and 905 nm lasers light as a function of time (0-90 nm). Upon light irradiation at 850 nm and 905 nm, supercoiled DNA was converted to the relax form nicked DNA, which is a clear indication of a breakage of the double strand plasmid DNA, and this is observed in Figure 3.8. The amount of damaged DNA increases as function of

time at both 850 nm and 905 nm. The light exposure time seems to be proportional to the cleavage yield. In both cases, cleavage occurs after 5 min and increases up until ~ 70 min of light exposure. This may be the saturated time because at this specific time, the cleaved DNA yield remains constant and is approximately the same as at 70 min. Based on the result seen in Figure 3.8, 30 min time as the optimum time was used in all the DNA photocleavage analysis. Interestingly, dye **KI2** markedly exhibited a pronounced DNA photocleave activity upon light irradiation with 850 nm laser light. Also, the cleavage yield was 40 ± 5% after only 5 min of irradiation. There is very little evidence of dark toxicity by the dye (Figures 3.8 A, B; lanes 8 and 9).

This study allowed us to probe the light exposure time required by the dye **KI2** to induce DNA cleavage using LEDs lasers with 850 nm and 905 nm wavelengths. The amount of cleaved DNA increases with the time at 850 nm and 905 nm (Figure 3.8). Importantly, dye **KI2** does not only exhibit the ability to cleave dsDNA but also cleaves DNA in the near-infrared range, above 830 nm. This is the first reported single-photon excitation DNA photocleavage at wavelengths of 850 and 905 nm.

3.3.3 DNA Binding Mode Analysis

Small molecules including cyanine dyes are well known to interact with biomolecules, such as DNA. They can interact with DNA in three common fashions as: intercalators, groove bindesr, or through electrostatic interactions (external binding). However, some small molecules randomly interact with DNA while other selectively bind in the DNA bases.[23, 24] Cyanine dyes possess distinctive properties that allow them to interact with DNA through one or more of the three common fashions. In the previous studies, UV-visible spectroscopy analysis and DNA photocleavage assays showed that dye **KI2** interacts with DNA and photocleaves DNA strands.

Still, little is known about the mechanism of interaction of dye **KI2** and DNA. In our next investigation, we will probe the binding mode of dye **KI2** to DNA through several optical methods

3.3.3.1 Circular Dichroism

We began our investigation of the mechanism of interaction between pentamethine carbocyanine dye **KI2** and DNA through circular dichroism (CD) spectroscopic analysis. CD spectra of dye **KI2** were recorded in 10 mM sodium phosphate buffer pH 7.0 at 22 °C in the presence or absence of either an increasing concentration range (31- 1283 μM bp) or 38 μM bp of CT-DNA. Data obtained from CD analysis show that **KI2** does not induce a CD signal upon binding to DNA. As expected, DNA molecule exhibits a CD signal between 200 and 300 nm due to its chirality that it owns from its structural properties. Also, there is no CD signal for the dye itself. This absence of ICD signals may be due to the way the dye **KI2** interacts with DNA.

A previously recorded UV-vis titration absorption spectra (Figure 3.4) suggested that dye weakly **i**nteracts with DNA. Cyanine dyes are usually prone to intercalate within DNA base pairs or bind in the DNA groove causing a change in DNA conformation can be characterized by the presence of cyanine dye ICD signals.[8, 26] Cyanine dyes that do not display induced CD signals usually bind to DNA by outside edge stacking to the DNA backbone (external binding).[8, 24] Data presented implies the possibility of external DNA binding by **KI2**.

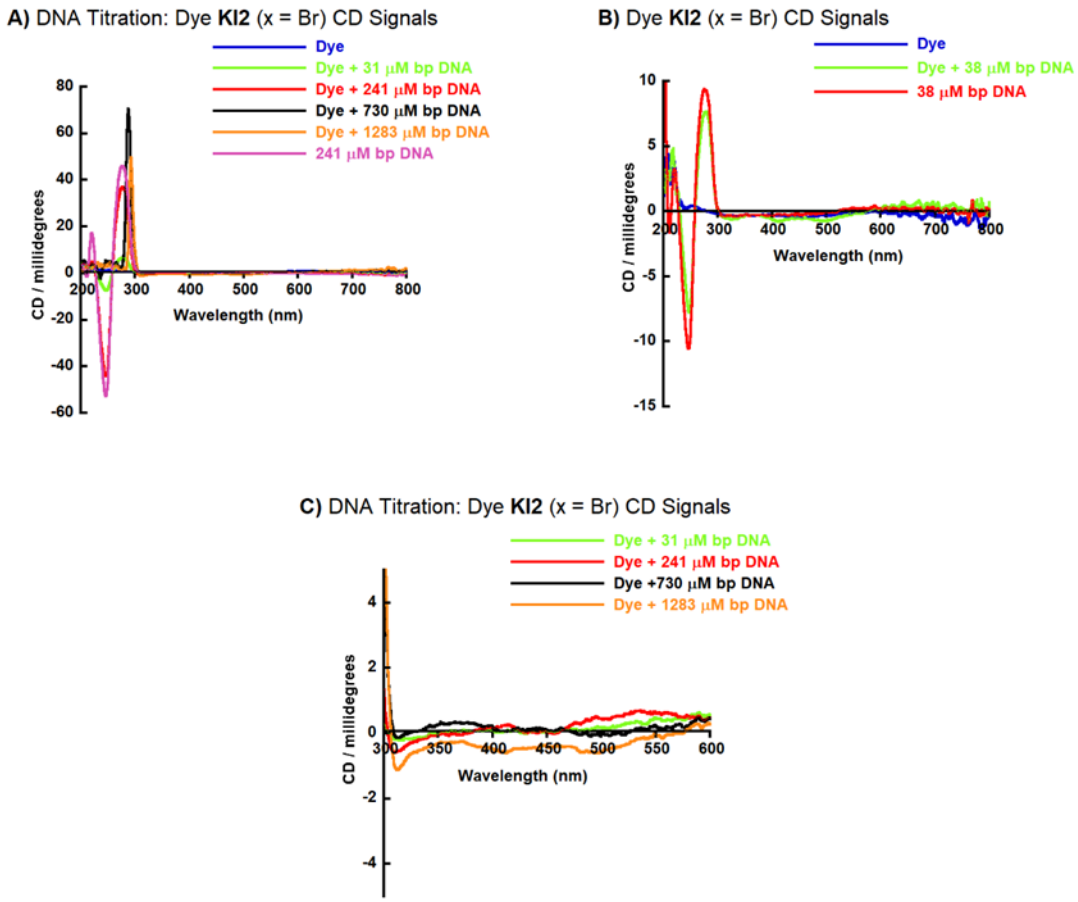

Figure 3.9: Circular dichroism spectra of dye **KI2**. Samples contained **(A) and (C)** 20 μM and **(B)** 45 μM of dye **KI2** in 10 mM sodium phosphate buffer pH 7.0 in the presence or absence of increasing concentrations (31-1,283) or 38 μM bp CT DNA (22 °C). CD spectra **(C)** from 3A and re-plotted from 300-600 nm for clarity.

3.3.3.2 Fluorescence Spectrophotometry

With the effort of further evaluating the mode of interaction of dye **KI2** and DNA, fluorescence spectra 10 μM of dye **KI2** were recorded in 10 mM sodium phosphate buffer pH 7.0 in the absence and presence of an increasing concentration of CT DNA from 31 to 1283 μM bp (Figure 3.9) or at 1283 μM bp CT DNA with various excitation and emission wavelengths. In absence of DNA, the reactions were excited with two distinct excitation wavelengths (λex/ λem = 684, 800 nm/694, 810 nm, respectively) to target the maximal absorptions of the free dye. In the

presence of DNA, the samples were excited with wavelengths (λex /λex = 600, 660, 800 nm/610, 670, 810 nm) to target DNA-dye complex (Figure 3.9). At all the excitation wavelengths, fluorescence emission was not observed. Instead, very sharp peaks are seen when the reactions were excited at 800 nm with an emission wavelength at 810 nm (Figure 3.9). The narrow emission bandwidth suggests that **KI2** might scatter the emitted light, which would result in an observation of the sharp peaks. A molecule can experience either fluorescence or light scattering when excited at specific wavelengths. The difference between light scattering and fluorescence is that fluorescence is long-lived electronic state phenomenon that can last between 10^{-8}-10^{-9} s, while light scattering occurs on via a very short-lived electronic state less than 10^{-15} s.[27] The recognition of the provenance of any observable peaks during fluorescence measurement is significant and must be identified because the nature of the peaks can be either florescence or light scattering. A close look is taken to pinpoint the nature of these apparent emission peaks to find the theory that governs the formation of these strange emission bands.

With the attempt of identifying possible light scattering, we lowered the 800 nm excitation wavelength by 10 nm to obtain 790 nm with reaction samples consisting of dye **KI2** or in the presence of 1283 μM bp CT-DNA shown in the supplemental information (Figure 3.18 in Supplementary Information). As a result, a Stoke shift is observed with the emission wavelengths being reduced from 810 nm to 800 nm, which is a characteristic fingerprint of a Raman light scattering effect. This formation of the very narrow bands of the free dye and DNA bound dye are observed when the samples are excited with wavelengths of 790 nm and 800 nm are not the result of fluorescence (Figure 3.18 in Supplementary information).

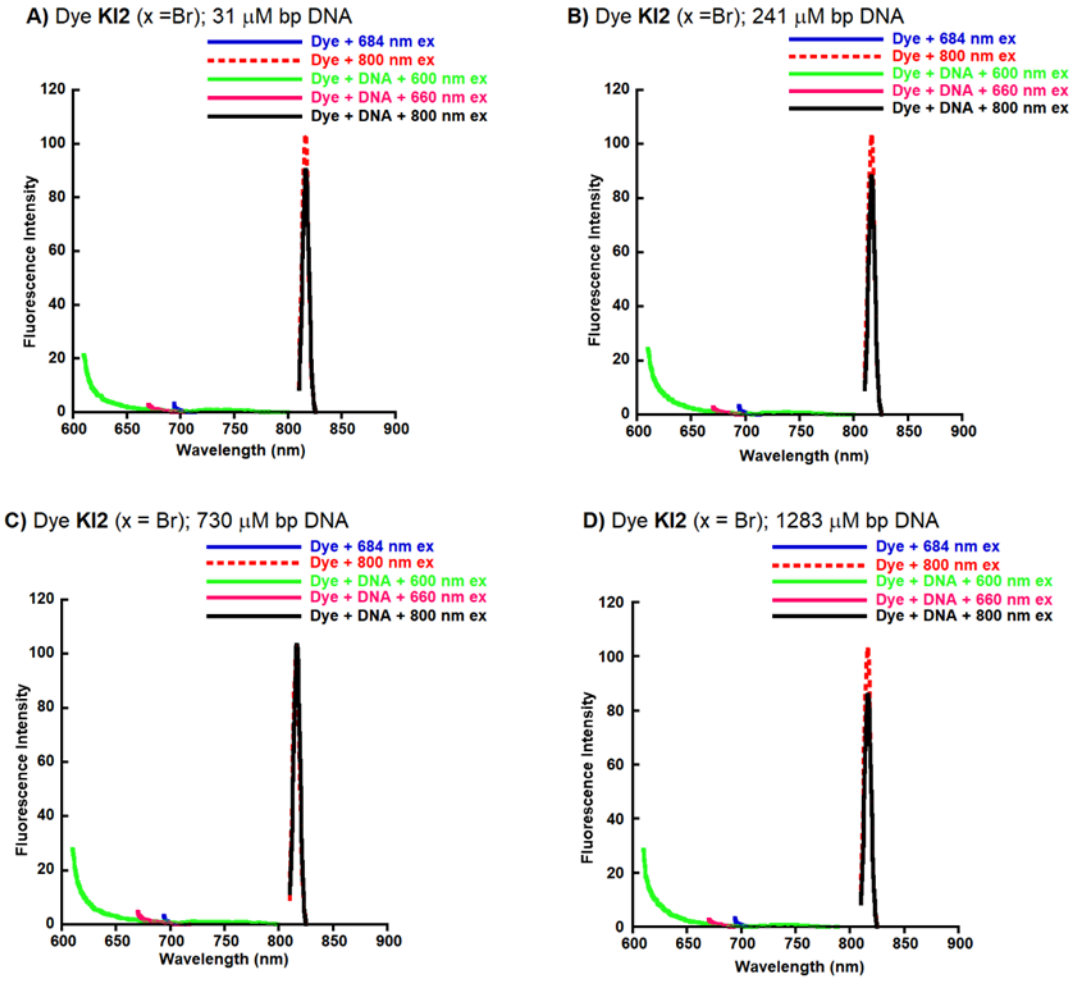

Figure 3.10: Fluorescence emission spectra (E_m)(showing light scattering) of 10 µM dye **KI2** in 10 mM sodium phosphate buffer pH 7.0 (22 ºC) in the presence and absence of: **(A)** 31 µM bp CT DNA to 1,283 µM bp; **(B)** 241 µM bp CT DNA; **(C)** 730 µM bp CT DNA; and **(D)** 1,283 µM bp CT DNA. Emission spectra were recorded at various excitation wavelengths (E_X) 684, 800, 600, and 660 nm with emission wavelengths of (E_m) 694, 810, 610, and 670 nm, respectively.

Raman scattering light peaks depends on the excitation wavelength.[27, 29]In fluorescence the kinetic energy of the incident photons is usually conserved. On the other hands, Raman light scattering does not conserve the energy present in the incident photon. Energy may decrease (anti-Stoke Raman) or increase (Stoke Raman) light scattering.[28] When the excitation wavelength was reduced by 10 nm, the apparent emission was raised by 10 nm (Figure 3.18 in Supplementary

Information), demonstrating an evidence of Raman light scattering effect with dye **KI2**. Thus, this is an example of Stoke Raman light scattering.

Since, no fluorescence emission was observed in any of our experiments, a positive control was needed towards this end. The fluorescence emission of methylene blue in pure ethanol was recorded with an excitation of 600 nm while the expected was 610 nm was observed, suggesting that the instrument was not malfunctioning (Figure 3.19 in Supplementary Information). The optical CD and fluorescence data of dye **KI2** suggest that dye **KI2** is neither an intercalative, nor a groove binder to the DNA double strand. Cyanine dyes that intercalate are fluorescent due to conformational mobility. Also, minor groove binders are usually fluorescent. Thus, the only remaining DNA binding mode is external binding.[14]

3.3.3.3 Competitive DNA Binding

Competitive DNA binding studies of dye **KI2** were carried out to clarify the mode of DNA binding of dye **KI2** through DNA photocleavage and UV-visible spectroscopic studies with the major groove binder methyl green[30] and the minor groove binder pentamidine.[31] Edwards and coworkers demonstrated in structural studies that pentamidine binds in a non-intercalative fashion in the minor groove of DNA.[32] In the present work, we prepared reactions containing 10 mM sodium phosphate buffer pH 7.0 and 38 μM bp DNA in the presence and absence of 50 μM of pentamidine or methyl green and 30 μM of dye **KI2.** The reactions at 10 °C were either irradiated with laser light of 100 mW 850 nm (left) or kept in the dark (right) (Figure 3.11) for 30 min then electrophorized in a 1.3% agarose for 60 min. With both LED lasers, very little breakage of DNA strand is observed in dark controls and when dye **KI2** is not present in lanes 3**.**

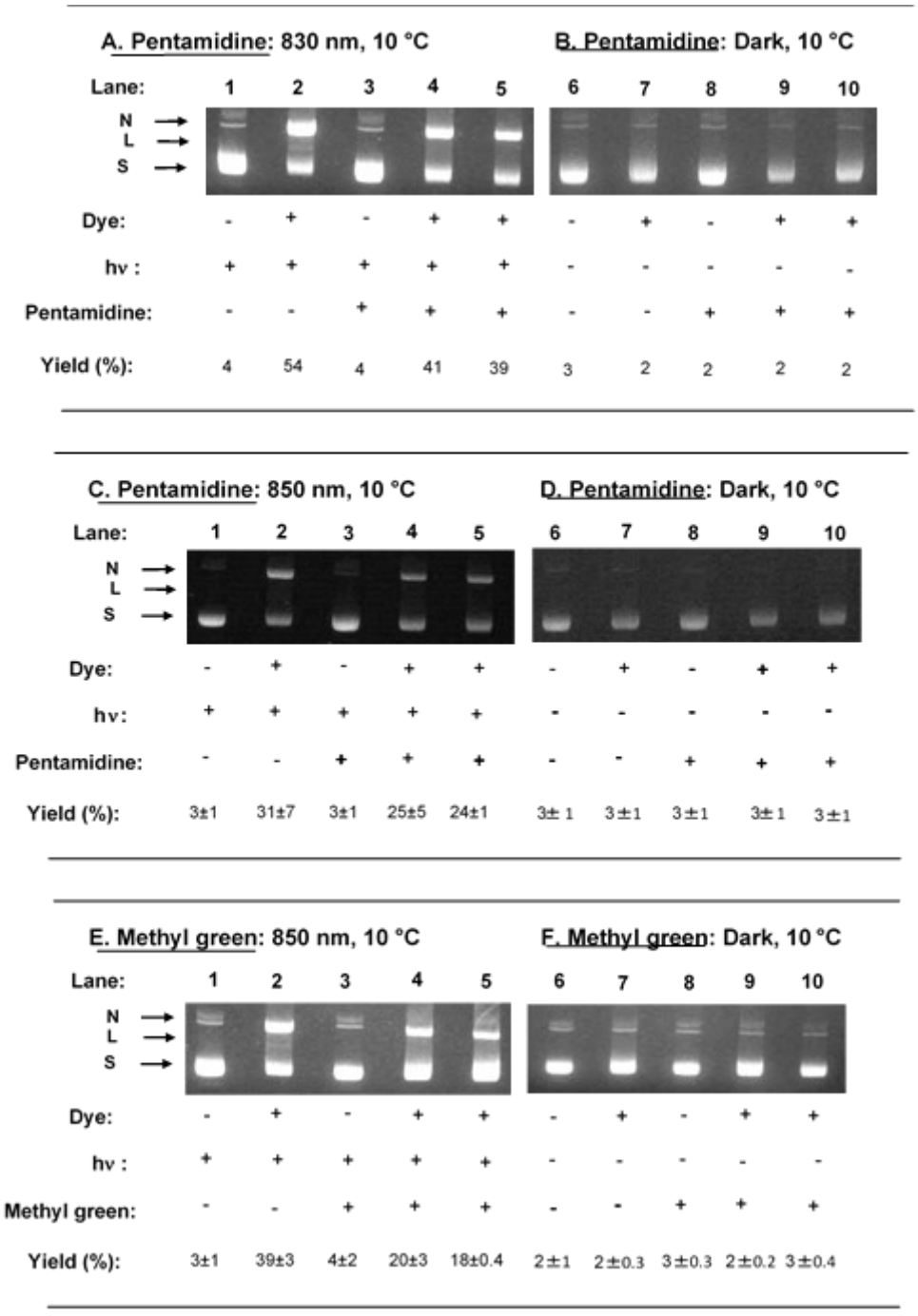

Figure 3.11: Representative ethidium bromide stained 1.3% agarose gel showing pUC19 plasmid DNA photocleavage. Reactions contained 10 mM sodium phosphate buffer pH 7.0, 38 μM bp pUC19 plasmid DNA equilibrated with 30 μM of dye **KI2** in the presence and absence of 50 μM pentamidine or methyl green. Individual reactions were irradiated for 30 min with laser light power of 350 mW 830 nm, 100 mW 850 nm, or kept in the dark (10 °C). Pentamidine or methyl green was added before dye **KI2** (lanes 4 and 9) and dye **KI2** was added before pentamidine or methyl green (lanes 5 and 10). Yields are averaged over 2-3 trials with errors reported as standard deviation (100 mW 850 nm laser light). Abbreviations: N, nicked; L, linear; S, supercoiled.

In separate photocleavage reactions, pentamidine or methyl green was added to the sample before and after adding dye **KI2**. Our result shows that the order of addition of both pentamidine and methyl green does not significantly affect DNA photocleavage (lanes 4 vs. 5 of Figure 3.11). Upon light irradiation at 830 and 850 nm, methyl green and pentamidine seem to interfere with dye **KI2** (Table 3.1), leading to less nicked DNA in all cleavage. DNA cleavage yield seems to be lower. This could be due to the interaction of KI2 with either methyl green or pentamidine in solution or the competitive binding to DNA and displacing the dye. Data in the Table 3.1 and Figure 3.11 reveal that methyl green seems to exhibit a more pronounced DNA cleavage pattern at 850 nm compared to pentamidine, leading to a decrease in DNA cleavage. Irradiation of the dye **KI2** in the presence of pentamidine and DNA with 830 nm laser power of 350 mW resulted in relatively higher inhibition (24% inhibition) than at 850 nm which is roughly 20% inhibition. To obtain a clear understanding and confirm our findings about the binding mode of **KI2**, UV-visible spectroscopic studies were performed using methyl green and pentamidine were. UV-visible spectra of samples containing 10 mM pH 7.0 sodium phosphate buffer pH 7.0, 30 μM (Figure 3.11) and 10 μM (Figure 3.20 in Supplemental Information) of dye **KI2**, and 50 μM pentamidine or methyl green in the presence or absence of 38 μM bp of CT DNA were recorded at 22 °C.

The Figure 3.12 A shows that pentamidine increases dye absorption and shifts the λ_{max} of the putative monomoric band from 812 nm to 817 nm in absence of DNA. This indicates that there may be some interactions between pentamidine and **KI2** when DNA is absent. When methyl green is added to aquous solutions of dye in the absence of DNA (Figure 3.12 C), there are some minor changes in dye absorption but they are more difficult to quantitate due to the overlap between the hypsochromic absorption band of dye **KI2** and methyl green absorption. In our next experiments, we wanted to determine the effects of adding pentamidine and methyl green to dye/DNA solutions.

Figure 3.12 B shows that pentamidine produces a major effect. When pentamidine is added, the λ_{max} of the bathochromic dye shifts from 813 nm to 819 nm and exhibits major hyperchromicity. This indicates that pentamidine changes the way **KI2** interacts with DNA. It's possible that pentamidine is formimg a complex with the monomer. The new hyperchromic peak could also be free monomeric dye hyperchromic with respect to DNA bound dye (Figure 3.20 E in Supplementary Information). Unfortunately, the λ_{max} of the free monomeric dye is difficult to determine because it appears as a shoulder of the major hypsochromic peak (Figure 3.20 E in Supplementary Information). Figure 3.20 D shows that the addition of methyl green to dye/DNA solution appears not to disrupt dye-DNA complex

Table 3.1: Inhibition of Dye KI2 photocleavage induced by chemical additives. Reactions contained 10 mM sodium phosphate buffer pH 7.0, 38 μM bp pUC19 plasmid DNA equilibrated with 30 μM dye **KI2** in the presence and absence of: **(A)** 50 μM of pentamidine or methyl green added before dye **KI2**; **(B)** Dye **KI2** added before 50 μM pentamidine or methyl green. The reactions were irradiated for 30 min with laser light power of 350 mW 830 nm or 100 mW 850 nm or kept in dark (10 °C). Data points are averaged over 2-3 trials with error reported as standard deviation (100 mW 850 nm laser light).

Reagents Added	Target	Cleavage Inhibition (%)	
hv		850 nm	830 nm
Pentamidine	Minor groove	**(A)** 19 ± 6	**(A)** 24
		(B) 21 ± 10	**(B)** 28
Methyl green	Major groove	**(A)** 49 ± 5	
		(B) 52 ± 2	

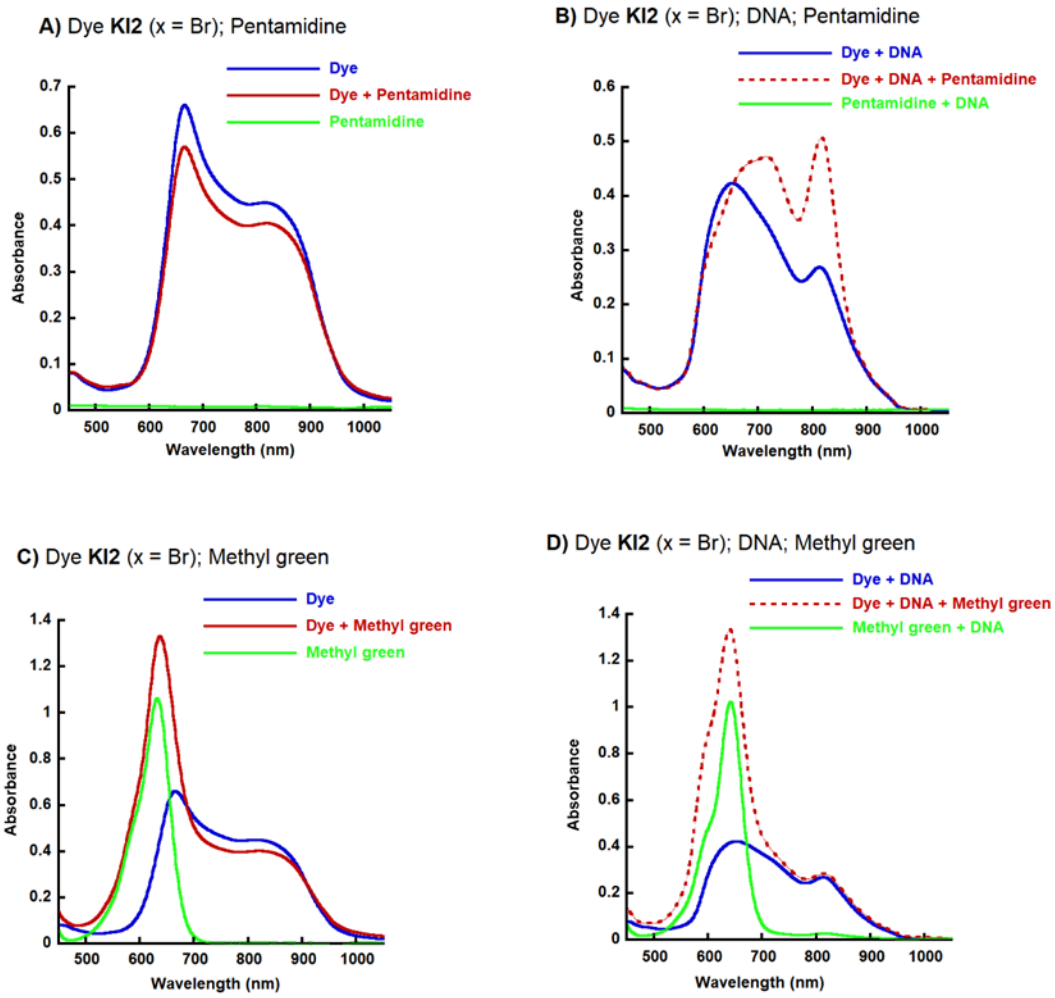

Figure 3.12: UV-visible absorption spectra of dye **KI2** recorded with pentamidine or methyl green. All samples contained 30 µM of dye **KI2** in 10 mM sodium phosphate buffer pH 7.0 (22 ^{o}C) in the presence or absence of 50 µM pentamidine or methyl green, and: **(A)** and **(C)** without 38 µM bp of CT DNA; **(B)** and **(D)** with 38 µM bp CT DNA. Dye **KI2** was added before pentamidine and methyl green (red lines in all cases).

In our next set of experiments, we lowered the dye concentration from 30 µM to 10 µM and kept DNA concentration constant at 38 µM bp. We compared the order of addition of the dye against competitor to DNA solutions (Figure 3.20 in Supplementary Information). When pentamidine or dye was added before and after **KI2**, Similar results were observed. A major hyperchromic peak at 819 nm appeared in both cases when DNA, dye, and monomer were present in combination. Figure 3.20 A, B in Supplementary Information). In the case of methyl green, there were slight

spectral changes when the order of competitor and dye was reversed (Figure 3.20 C, D in Supplementary Information). When the dye was added before the methyl green, there was a slight increase in the absorption of the monomeric peak when the methyl green was added (Figure 3.20 C in Supplemental Information). The λ_{max} of the bathochromic shifts from appeared at 616 nm. When methyl green was added first, the dye DNA complex appears not to be disprupted (Figure 3.20 D in Supplementary Information). In this case, the bathochromic peak appeared at 817 nm.

With the spectroscopy results, methyl green was not expected to inhibit the conversion of supercoiled DNA to cleaved DNA but did in this case (Table 3.1) with its related DNA cleavage (Figure 3.11). This result cannot be explained. On the other hand, the ability of pentamidine to inhibit DNA photocleavage by **KI2** could not be the result of the ability of this minor groove binder to alter dye-DNA interactions. Our findings demonstrate that there is minimal change in the dye-DNA duplex in the presence of major groove binder methyl green while pentamidine generated a pronounced peak of the monomeric dye inferring that dye **KI2** may associate with the DNA minor groove. Pentamidine may also form a complex with **KI2** itself.

3.3.3.1 Regent-Induced Change in DNA Photocleavage

In this experiment, the mechanisms underlying DNA photocleavage were explored. Three chemical agents sodium benzoate, a type I hydroxyl radical scavenger (•OH), deuterium oxide (D_2O), which increases the half-life of type II singlet oxygen, and the metal chelating agent ethylenediaminetetraacetic acid (EDTA) were used to modify direct DNA strand breakage by dye **KI2**. Reactions consisted of 10 mM sodium phosphate buffer pH 7.0, 38 μM bp pUC19 plasmid DNA in the presence and absence of 30 μM dye **KI2**, and 100 mM sodium benzoate, 100 mM EDTA, or 79% D_2O and were irradiated at 850 nm with an LED laser light. Sodium benzoate

seems to noticeably prevent direct DNA break by causing a decrease in the DNA cleavage yield Figure 3.14B (lane 3) by 49% (Table 3.2).

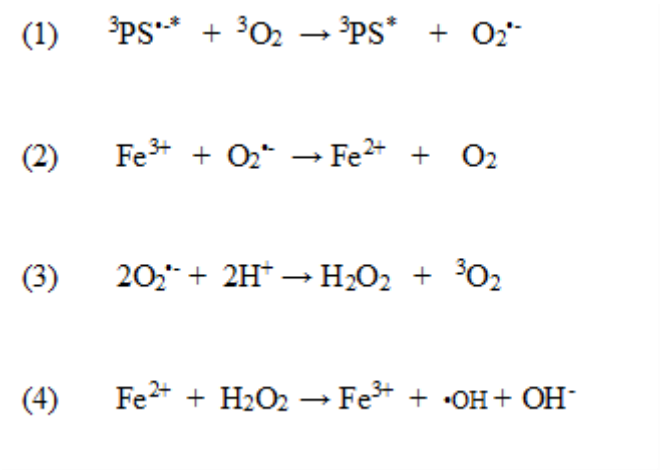

Figure 3.13: Hydroxyl radical generation through Fenton Chemistry. $^3PS^*$ stands for the triplet state photosensitizer and $^3PS^{\bullet -*}$ is the photosensitizer triplet state anion radical.

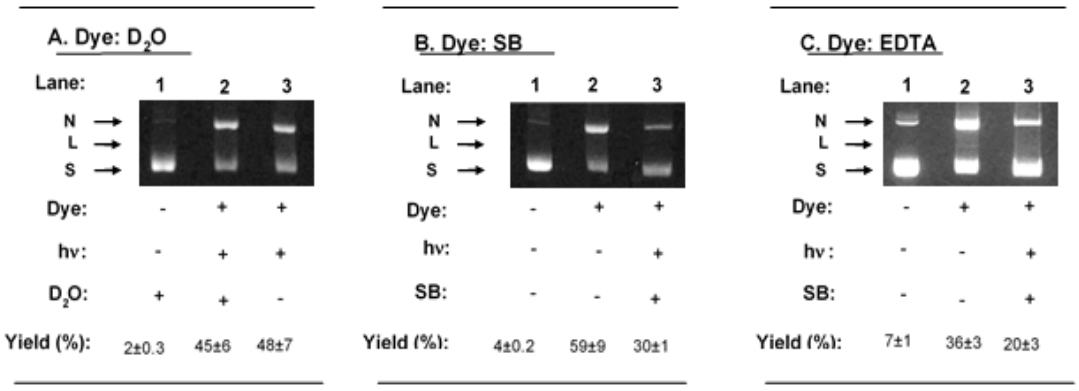

Figure 3.14: Representative ethidium bromide stained 1.3% agarose gel showing pUC19 plasmid DNA photocleavage. Reactions contained 10 mM sodium phosphate buffer pH 7.0 and 38 μM bp DNA in the presence or absence of: **(A)** 79% of deuterium oxide (D_2O); **(B)** 100 mM of sodium benzoate (SB); **(C)** 100 mM of ethylenediaminetetraacetic acid (EDTA) and 30 μM of dye **KI2**. Individual reactions were irradiated for 30 min with a laser light power of 100 mW 850 nm or kept in dark (22 °C). Data points are averaged over 3 trials with errors reported as standard deviation. Abbreviations: N, nicked; L, linear; S, supercoiled.

The metal chelating agent EDTA is known for its interruption of the Fenton reaction shown in Figure 3.13, a mechanism that governs the production of hydroxyl radical by chelating iron and

copper ions. Similarly, double strand DNA was relatively inhibited by EDTA Figure 3.14C (lane 3), corresponding to 45% inhibition (Table 3.2). We alternatively investigated the involvement of type II singlet oxygen by replacing water (H_2O) by 79% D_2O. Deuterium oxide enhances the lifetime of singlet oxygen, which would lead to an increase in DNA cleavage if singlet oxygen was being generated.[34, 35] However, in this study, 79% D_2O did not enhance but instead inhibited DNA strand cleavage as observed in Figure 3.14A (lane 2), which ultimately resulted in 7% inhibition (Table 3.2). Similar results were reported by Williams and coworkers during an investigation of DNA photocleavage activity by a copper-based DNA photosensitizer. In their study, D_2O also inhibited DNA photocleavage, which was attributed to the possibility that D_2O might be reducing hydroxyl radical production through an isotope effect.[34]

Table 3.2: Inhibition of Dye **KI2** photocleavage induced by chemical additives. Reactions contained 10 mM sodium phosphate buffer pH 7.0 and 38 μM bp pUC19 plasmid DNA in the presence and absence of 79% of D_2O (v/v); 100 mM of sodium benzoate; 100 mM EDTA, and 30 μM of dye **KI2.** The reactions were irradiated for 60 min with laser light power of 100 mW 850 nm or kept in dark (22 °C). Data points are averaged over 3 trials with error reported as standard deviation.

Reagents Added	Target	Cleavage Inhibition (%)
D_2O	$^1O_2$	7 ± 2
Na benzoate	•OH	49 ± 6
EDTA	Fe^{2+}, Fe^{+3}/Cu^{+1},Cu^{+2}	45 ± 4

3.3.4 Reactive Oxygen Species Detection

Grant and coworkers tested the selectivity of 3'-(4-hydroxyphenyl) fluorescein (HPF) and singlet oxygen sensor green (SOSG) by using prepared positive controls Fenton reagents and methylene blue. They used the Fenton reagent for to generate hydroxyl radicals and methylene blue photosensitize singlet oxygen production. Using HPF, they observed fluorescent signals for

both methylene blue and the reagent, suggesting that HPF detects both hydroxyl radical and singlet oxygen.[8] SOSG was reported to selectively detect singlet oxygen.[36, 37]As a result, in this analysis, HPF and SOSG probes were used to confirm the possible involvement of hydroxyl radicals and singlet oxygen in DNA photocleavage by dye **KI2**. The reactions contained 10 mM sodium phosphate buffer pH 7.0 in the presence and absence of 10 μM 4-quinolinium pentamethine carbocyanine dye **KI2**, 3 mM of HPF or 0.75 μM of SOSG, 100 mM sodium benzoate, 90% D_2O. Individual reactions were irradiated for 30 min with laser light of 850 nm or kept in dark (22 °C). Fluorescence emission spectra were then recorded using excitation wavelengths of 890 nm for HPF (Figure 3.15 A) and 480 nm for SOSG (Figure 3.15 B,C) with a 500 nm emission wavelength for both. HPF itself does not display any ROS production. However, a maximum fluorescent emission intensity is produced when dye **KI2** is added then irradiated at 850 nm (Figure 3.15 A), which is a sign of an ROS burst. After the addition of the hydroxyl radical scavenger sodium benzoate to the solution, the fluorescent intensity substantially decreased denoting that sodium benzoate visibly quenched the hydroxyl radical production (Figure 3.15 A). And this result is consistent with the scavenger experiment through DNA photocleavage analysis of dye **KI2** using sodium benzoate (Figure 3.14 A), suggesting that hydroxyl radicals mainly implicated in DNA cleavage by the dye **KI2**. A detail mechanism of HPF is illustrated in Figure 3.15.

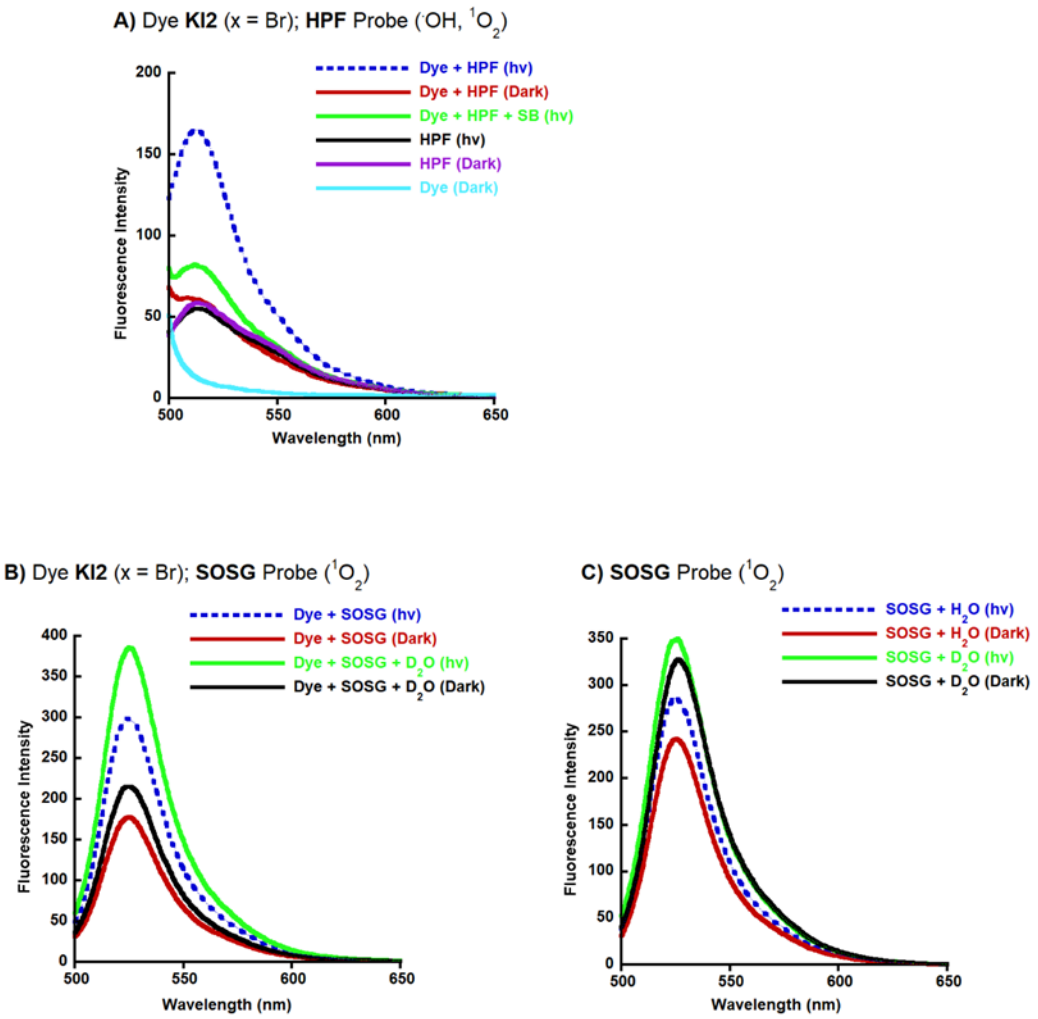

Figure 3.15: Fluorescence emission spectra depicting ROS production by dye **KI2**. Emission spectra were recorded for solutions containing 10 mM sodium phosphate buffer pH 7.0 and : **(A)** 10 µM dye, 3 mM of hydroxyphenyl fluorescein (HPF), 100 mM sodium benzoate (SB) excitation and emission wavelengths (E_X/E_m = 490/500 nm); **(B)** 10 µM dye **KI2**, 0.75 µM singlet oxygen sensor green (SOSG), 90% deuterium oxide (D_2O) or in 100% deionized water with E_X/E_m = 480/500 nm); **(C)** 0.75 µM SOSG, 90% D_2O or in 100% deionized water with E_X/Em = 480/500 nm. Reactions were either kept in the dark or irradiated at 850 nm for 30 min (22 °C). Percent increase of ROS using SOSG: **(B)** Dye and SOSG in H_2O; dye and SOSG in D_2O are respectively increased by 68 and 79%; **(C)** SOSG in H_2O, SOSG in D_2O are respectively increased by 18 and 7%.

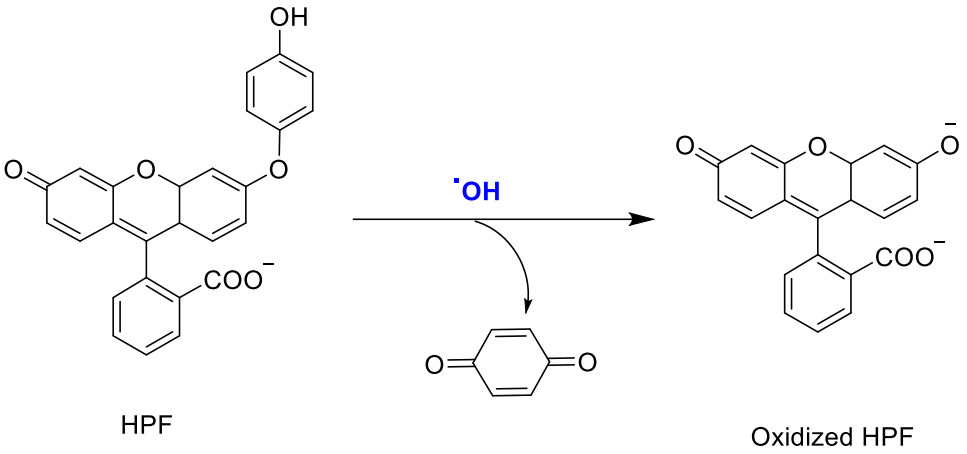

Figure 3.16: Mechanism of action of 3'-(4-hydroxyphenyl) fluorescein (HPF) showing a non-fluorescent HPF probe that becomes fluorescent when oxidized by hydroxyl radicals.

SOSG probe is a combinatory molecule of fluorescein and anthracene moities.[38-40] Before the reaction of SOSG, an internal electron transfer occurs between the anthracene and the fluorescein by quenching the SOSG fluorescence. Upon reaction with singlet oxygen, the SOSG is oxidized leading to the formation of SOSG-endoperoxide[41], which is substantially fluorescent.[39] The mechanism of SOSG is exemplified in Figure 3.17. ROS detection analysis of dye **KI2** using SOSG led to a fluorescence signal when irradiated at 850 nm with an LED laser light in the presence of dye as observed (Figure 3.15). Relative to dark controls in Figure 3.14 B, this signal increased by 79% for the D_2O reaction and 68% for the H_2O reaction, giving the impression that D2O increases singlet oxygen production. However, D_2O and H_2O signals are nearly equivalent in intensity to control spectra shown in Figure 3.15 C of parallel SOSG reactions conducted in the absence of dye. This comparison shows that the **KI2** dye does not generate substantial levels of singlet oxygen, and this is consistent with the conclusion drawn from DNA photocleavage reactions conducted in D_2O (Figure 3.14 A).

Merkel and coworker demonstrated in a study that deuteration enhances the lifetime of singlet oxygen by studying the effect of water and deuterium oxide on the lifetime of singlet oxygen. In the study, deuterium oxide significantly increased the lifetime of singlet oxygen approximately by 10-folds.[35] The data in Figures 3.14 and 3.15 suggest that type I hydroxyl radical are the main ROS causing photocleavage by dye **KI2**.

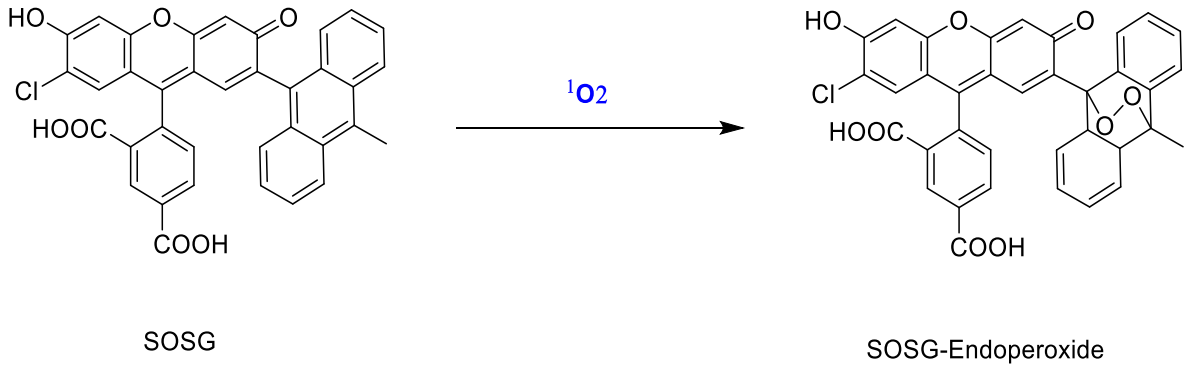

Figure 3.17: Mechanism of singlet oxygen sensor green (SOSG).

3.4 Materials and Methods

3.4.1 General

All reagents used in this experiment had high purity and were commercially brought except for pUC19 plasmid DNA and cyanine dyes **KI2**, **KI3**, and **KI4**. All DNA and buffer samples were prepared using deionized distilled water. XL-1 blue *E. coli* competent cells (Strategene) were used to clone pUC19 plasmid according to standard laboratory protocols. pUC19 plasmid was purified using QIAfilter Plasmid Mega Kit (QiagenTM, Cat. No. 12263) by following the manufacturer's instructions. Calf thymus DNA was obtained from Invitrogen (Cat.No.15633-019; 10 mg/mL, average size ≤ 2000 bp). Sodium phosphate buffer was made by utilizing monobasic and dibasic sodium phosphate provided by Thermo Fisher Scientific. Dimethyl sulfoxide (DMSO, ≥99.99%), and sodium benzoate (SigmaUltra, Minimum 99%) were supplied by Sigma-Aldrich. Deuterium

oxide (99.9%) and agarose were respectively obtained from Cambridge Isotope Laboratories and BioRad. UV-visible absorptions spectra of dyes **KI2**, **KI3**, and **KI4** were acquired utilizing a PerkinElmer Lambda 35 spectrophotometer. Circular dichroism (CD), and fluorescence emission spectra of dye **KI2** were respectively recorded using Jasco J-810 and PerkinElmer LS55 instruments.

3.4.2 UV-visible Spectroscopy

The UV-visible absorption time-course spectra of cyanine dyes **KI2**, **KI3**, and **KI4** were measured at 22 °C by utilizing a UV-visible spectrophotometer. All the cuvettes contained either 10 μM of the dye in 10 mM sodium phosphate pH 7.0, 10 μM of dye **KI2** in DMSO in the presence or absence of 150 μM bp CT DNA. Absorption spectra were recorded at a time interval of 0 min up to 30 min.

In the UV-visible DNA titration experiment of dye **KI2**, small volumes of an aqueous solution of 13,088 μM bp CT DNA were consecutively added to samples containing 20 μM dye **KI2** in 10 mM sodium phosphate pH 7.0 with an initial volume of 500 μL. Final concentrations of CT DNA present in the sample ranged from 34 μM bp up to 1328 μM bp. All titration absorption spectra were corrected for sample dilution.

3.4.3 DNA Photocleavage

DNA cleavage reactions samples contained various concentrations (0-45 μM) of dye **KI2** or with 20 or 30 μM of either dyes **KI2**, **KI3**, or **KI4** with 38 μM bp of PUC19 plasmid DNA, and 10 mM of sodium phosphate at pH 7.0 with a total volume of 40 μL. The reactions temperatures were kept constant by keeping them in a metal block that was immersed in an ice bath or at 10 °C and 37 °C (hv). Samples were kept in the dark or irradiated either for 30 or 60 min, or a time-course of 0, 5, 10, 30, 50, 70, 90 min using emitting diode (LED) laser light with wavelengths of 830 nm (350

mW), 850 nm (100 mW), and 905 nm (50 mW) or were heated at 37 degrees Celsius. Temperatures of individual reaction samples were recorded with a non-contact of a thermometer before and after the irradiation time or before and after 30 min in dark. After irradiation with respective laser lights, 3 µL of loading buffer containing 15.0% (w/v) ficoll and 0.025% (w/v) bromophenol blue were added to each sample and 20 µL of the resulting solution were loaded to the wells of 1.3% agarose gel containing 0.5 µg/mL ethidium bromide. A total of 10 µL of 0.5 µg/mL ethidium bromide was added to 1 × tris-acetate-EDTA (TAE) running buffer. The reaction was then electrophoresed at 100 V for 60 min in a Bio-Rad Laboratories gel box. The gels were then visualized at 302 nm with a VWR Scientific LM-20E transilluminator, photographed with a UVP PhotoDoc-It™ Imaging System and quantitated using ImageJ software. In the case of supercoiled DNA, integrated numerical values were multiplied by a correction factor of 1.22 to account for the decreased affinity of ethidium bromide for supercoiled vs. nicked and linear plasmid forms. DNA photocleavage percentages were calculated by using the following formula:

Percent Photocleavage = [(Linear + Nicked DNA)/(Linear + Nicked + Supercoiled DNA)] × 100.

3.4.4 Circular Dichroism

Samples used in the CD experiments consisted of 20 µM or 45 µM of cyanine dye **KI2** in 10 mM sodium phosphate pH 7.0 in the presence and absence of various concentrations of CT DNA (0, 31, 38, 241, 730, 1283 µM bp) with a total volume of 2000 µL. Spectra were acquired from 800 to 200 nm in 3 mL (1.0 cm) quartz (Starna) cuvettes using specific instrument setting as follow: Scan speed of 100 nm/min, response time and digital integration time (D.I.T) of 4 s, bandwidth of 2 nm, and sensitivity of 200 millidegrees. The temperature was kept constant at 22 °C and the resulted spectra were averaged over 12 acquisitions.

3.4.5 Fluorescence Spectrophotometry

Fluorescence of cyanine dye **KI2** was measured at 22 °C with a fluorescence spectrophotometer. Solutions contained 10 mM aqueous buffer (sodium phosphate) at pH 7.0, 10 μM of dye **KI2** in the presence or absence of 31, 241, 730, or 1283 μM bp CT DNA. Samples were individually prepared in quartz (Starna) cuvettes in a total volume of 2000 μL. Individual samples were excited at specific wavelength of 600, 660, 684, 790, and 800 nm with corresponding emission spectra that were respectively recorded at wavelengths of 610, 670, 694, 800, and 810 nm. In the case of methylene blue, 5 μM of the dye was dissolved in pure ethanol and the reaction was excited at 600 nm with emission of 610 nm. The scan speed was 100 nm/min, gain was medium, the excitation and emission slits were both 4.5 nm.

3.4.6 Regent-Induced Changes in DNA Cleavage

Reactions contained 10 mM of sodium phosphate buffer pH 7.0, 38 μM bp pUC19 plasmid DNA and 30 μM of dye **KI2** were prepared in the presence and absence of 100 mM of sodium benzoate, 79 % D_2O (v/v), or 100 mM EDTA. The reactions were then irradiated with LED laser light power of 100 mW 850 nm for 60 min. The reactions temperatures were kept constant 22 °C. After the irradiation, the reactions were resolved on 1.3% non-denaturing agarose gels and visualized and quantitated as previously described. The percent inhibition of DNA photocleavage was calculated using the following formula, where the additive was either D_2O, sodium benzoate, or EDTA:

Percent Inhibition = [(% Total of Linear and Nicked DNA with additive - % Total of Linear and Nicked DNA without additive)/(% Total of Linear and Nicked DNA without additive)] × 100.

3.4.7 Competitive DNA Binding Mode

In competitive DNA binding photocleavage, experiments reactions contained 10 mM of sodium phosphate buffer pH 7.0, 38 μM bp pUC19 plasmid DNA and 30 μM of dye **KI2** and were

prepared in the presence and absence of 50 μM of methyl green or pentamidine, which were added before the dye in lanes 5 and 9 of Figure 3.10. The reactions were either irradiated with LED laser light power of 350 mW 830 nm or 100 mW 850 nm, or kept in dark for 30 min. The reactions temperatures were cooled in ice bath at 10 °C. After the irradiation, the reactions were resolved on 1.3% non-denaturing agarose gels for 60 min and quantitated as just described. The percent inhibition of DNA photocleavage was calculated as previously stated, but the additives in this case were pentamidine and methyl green.

In the competitive DNA binding UV-visible spectroscopy study using pentamidine or methyl green, the absorbances of the cyanine dye **KI2** were measured at 22 °C by utilizing a UV-visible spectrophotometer. All the cuvettes contained either 10 or 30 μM of dye **KI2** in 10 mM sodium phosphate buffer at pH 7.0 in the presence and absence of 50 μM of pentamidine or methyl green, and 38 μM bp CT DNA. Absorption spectra were recorded immediately.

3.4.8 ROS Detection

Reactions contained 10 mM of sodium phosphate buffer pH 7.0, 38 μM bp pUC19 plasmid DNA and 10 μM of dye **KI2** and were prepared in the presence and absence of 3 mM of HPF or 0.75 μM SOSG, and sodium benzoate. The reactions were then irradiated with laser light power of 100 mW 850 nm for 30 min or in dark at (22 °C). After the irradiation, fluorescence emission spectra were recorded by exciting the sample at 490 nm with emission 500 nm for HPF or at 480 nm with emission of 500 nm for SOSG.

3.5 Conclusion

UV-visible absorption spectra show that 4-quinolinium pentamethine cyanine dyes *meso*-substituted with either bromine and chlorine (**KI2** and **KI3**) respectively are stable in DMSO and aqueous buffer pH 7.0, and in the presence of DNA. In contrast, the cyanine dye substituted with

hydrogen (**KI4)** is stable in DMSO, but less stable in aqueous buffer and even when DNA is present. Data presented reveal evidence of the interaction of the dyes **KI2, KI3**, and **KI4** with DNA. Recorded UV-visible absorption spectra of dye **KI2** show that high DNA concentrations promote the conversion of aggregated dye to monomeric cyanine dye. Because aggregated and monomeric DNA-dye forms are non-fluorescent, it is likely that cyanine dye **KI2** interacts with DNA in a non-intercalative way. UV-visible spectra and DNA photocleavage examining competitive binding using the minor groove binder pentamidine and methyl green as a major groove binder indicate that dye **KI2** may be associated with the DNA minor groove, which is surprising in light of our observation that the aggregated and monomeric dye forms of **KI2** do not generate ICD signals when bound to DNA. The absence of ICD signals points to possible external DNA interactions.

In this study, we showed that symmetrical 4-quinolinium cyanine dyes **KI2, KI3 and KI4** displayed DNA cleavage activities upon irradiation with 830, 850, and 905 nm LED lasers. This result represents the first reported example of DNA photocleavage upon single-photon excitation of a chromophore at wavelengths above 830 nm.

DNA photocleavage experiment in the presence of the chemical additives deuterium oxide, sodium benzoate, and EDTA demonstrated that DNA strand breakage by dye **KI2** with near-infrared light at 850 nm involves a major contribution from type I hydroxyl radicals. Also, dye **KI2** upon irradiation displayed ROS burst with the HPF hydroxyl radical probe (HPF).

In the future, the photocytotoxicity studies of dye **KI2** will be explored in cancer cells. Moreover, we will continue to develop new and improved symmetrical 4-quinolinium carbocyanine dyes that absorb in the near-infrared wavelength range. Our long-term goal is to develop near-infrared cyanine dyes for use in photodynamic cancer treatment. The therapeutic

benefit of using infrared light rests in its ability to penetrate biological tissues leading to more effective elimination of cancer cells. Based on our results, we envisage that cyanine dye **KI2** might be an important photosensitizer for PDT practice one day.

3.6 Supplementary Information

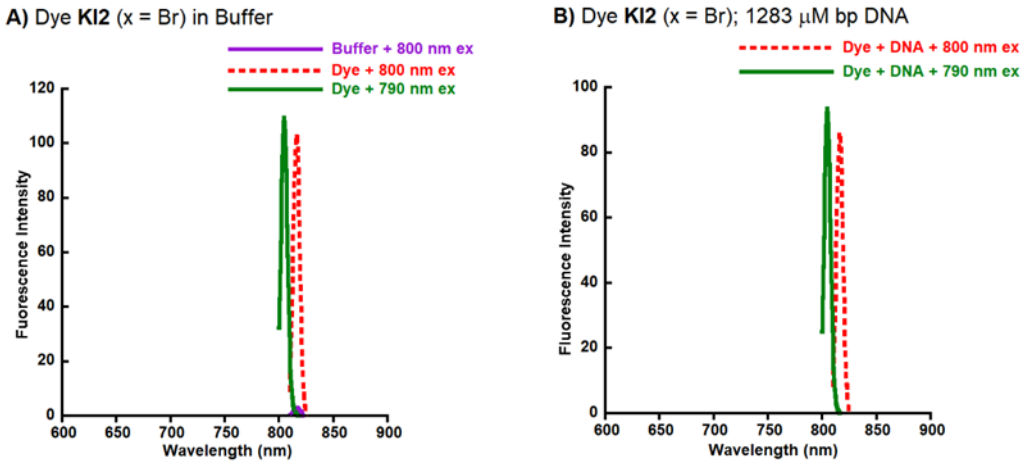

Figure 3.18: Fluorescence emission spectra showing light scattering of 10 µM dye **KI2** in 10 mM sodium phosphate buffer pH 7.0 (22 ºC) in the: **(A)** absence of 1,283 µM bp CT DNA and **(B)** presence of 12,83 µM bp CT DNA. Emission spectra were recorded at excitation wavelengths (E_X) 800 and 790 nm with emission wavelengths (E_m) 810 and 800 nm, respectively ΔE_X =10 and ΔE_m=10 (red and green lines)

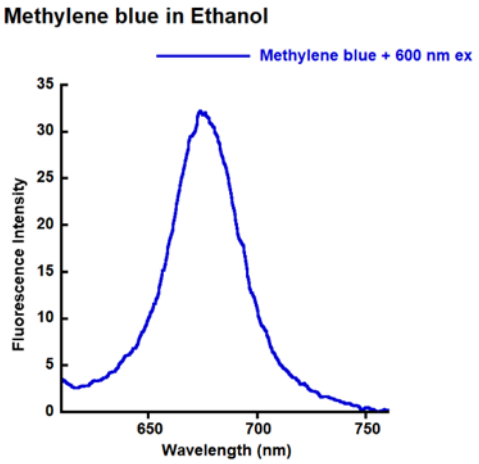

Figure 3.19 Fluorescence emission spectrum of 5 μM methylene blue in pure ethanol. The emission spectrum of methylene blue was recorded at an excitation wavelength (E_X) of 600 nm with an emission wavelength (E_m) of 610 nm (22 ºC).

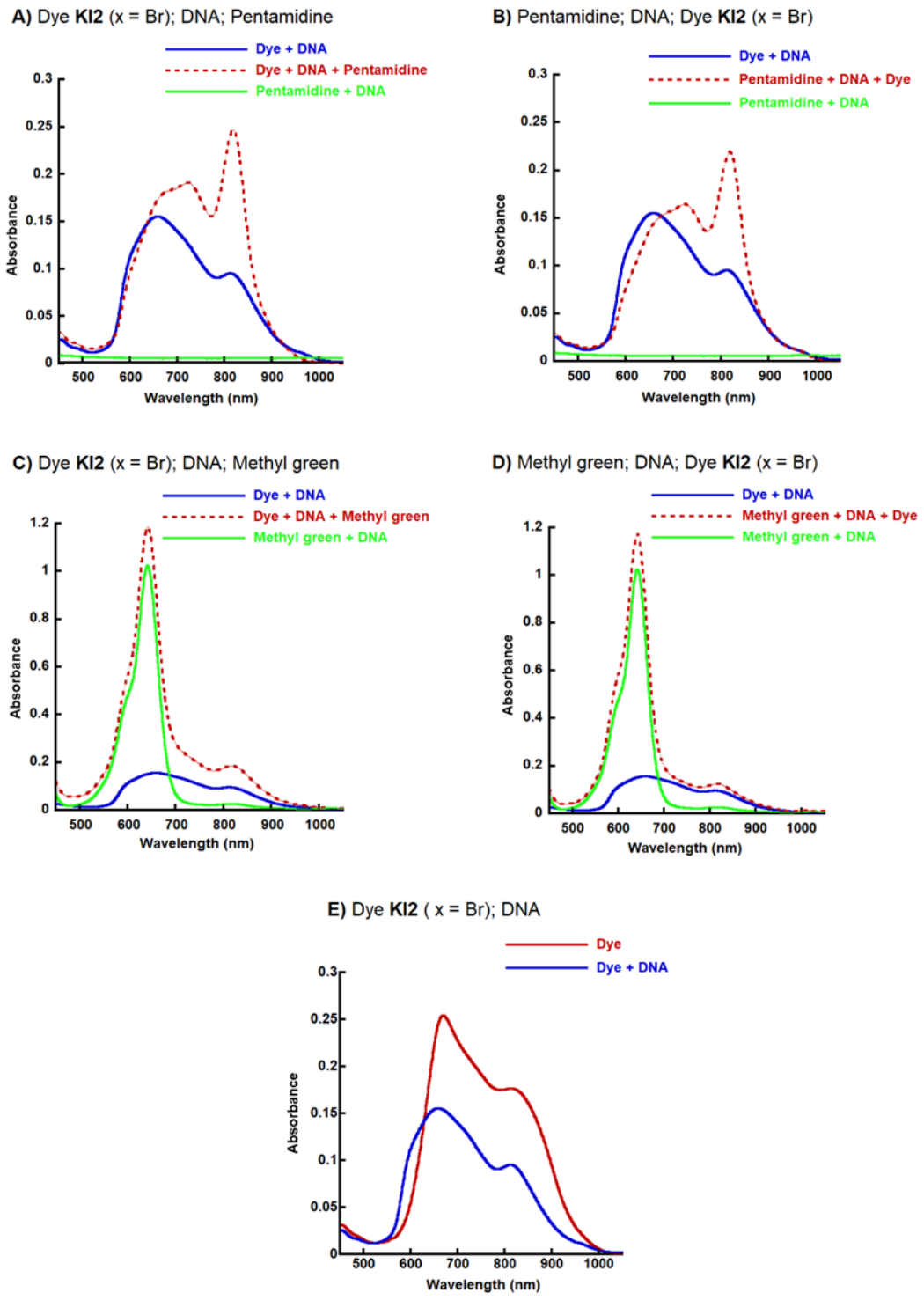

Figure 3.20: UV-visible absorption spectra of dye **KI2** recorded with pentamidine or methyl green. Samples contained 10 µM of dye **KI2**, 10 mM sodium phosphate buffer pH 7.0, 38 µM bp of CT DNA, and **(A)** and **(B)** 50 µM pentamidine; **(C)** and **(D)** 50 µM methyl green: (left panels) dye was added before pentamidine or methyl green, (right panels) dye was added after pentamidine or methyl green (22 ºC).

3.7 References

1. Dąbrowski, J. M.; Pucelik, B.; Regiel-Futyra, A.; Brindell, M.; Mazuryk, O.; Kyzioł, A.; Stochel, G.; Macyk, W.; Arnaut, L. G. Engineering of relevant photodynamic processes through structural modifications of metallotetrapyrrolic photosensitizers. *Coordination Chemistry Reviews.* **2016,** *325*, 67-101.
2. Zhang, J.; Jiang, C.; Figueiró Longo, J. P.; Azevedo, R. B.; Zhang, H.; Muehlmann, L. A. An updated overview on the development of new photosensitizers for anticancer photodynamic therapy. *Acta Pharmaceutica Sinica B.* **2018,** *8* (2), 137-146.
3. Baskaran, R.; Lee, J.; Yang, S.-G. Clinical development of photodynamic agents and therapeutic applications. *Biomaterials Research.* **2018,** *22* (1), 25.
4. Zepp, R. G.; Faust, B. C.; Hoigne, J. Hydroxyl radical formation in aqueous reactions (pH 3-8) of iron(II) with hydrogen peroxide: the photo-Fenton reaction. *Environmental Science & Technology.* **1992,** *26* (2), 313-319.
5. Abrahamse, H.; Hamblin, M. R. New photosensitizers for photodynamic therapy. *Biochemical Journal.* **2016,** *473* (4), 347-64.
6. O'Connor, A. E.; Gallagher, W. M.; Byrne, A. T. Porphyrin and Nonporphyrin Photosensitizers in Oncology: Preclinical and Clinical Advances in Photodynamic Therapy. *Photochemistry and photobiology.* **2009,** *85* (5), 1053-1074.
7. Ormond, A. B.; Freeman, H. S. Dye Sensitizers for Photodynamic Therapy. *Materials (Basel).* **2013,** *6* (3), 817-840.
8. Basnet, K.; Fatemipouya, T.; St Lorenz, A.; Nguyen, M.; Taratula, O.; Henary, M.; Grant, K. B. Single photon DNA photocleavage at 830 nm by quinoline dicarbocyanine dyes. *Chemical Communications. (Camb)* **2019,** *55* (84), 12667-12670.
9. Escobedo, J. O.; Rusin, O.; Lim, S.; Strongin, R. M. NIR dyes for bioimaging applications. *Current Opinion in Chemical Biology.* **2010,** *14* (1), 64-70.
10. Oushiki, D.; Kojima, H.; Terai, T.; Arita, M.; Hanaoka, K.; Urano, Y.; Nagano, T. Development and Application of a Near-Infrared Fluorescence Probe for Oxidative Stress Based on Differential Reactivity of Linked Cyanine Dyes. *Journal of American Chemical Society.* **2010,** *132* (8), 2795-2801.
11. Bosson, J.; Labrador, G. M.; Besnard, C.; Jacquemin, D.; Lacour, J. Chiral Near-Infrared Fluorophores by Self-Promoted Oxidative Coupling of Cationic Helicenes with Amines/Enamines. *Angewandte Chemie International Edition.* **2021,** *60* (16), 8733-8738.
12. Karton-Lifshin, N.; Segal, E.; Omer, L.; Portnoy, M.; Satchi-Fainaro, R.; Shabat, D. A Unique Paradigm for a Turn-ON Near-Infrared Cyanine-Based Probe: Noninvasive Intravital Optical Imaging of Hydrogen Peroxide. *Journal of American Chemical Society.* **2011,** *133* (28), 10960-10965.
13. Yang, X.; Bai, J.; Qian, Y. The investigation of unique water-soluble heptamethine cyanine dye for use as NIR photosensitizer in photodynamic therapy of cancer cells. *Spectrochimica Acta Part A: Molecular and Biomolecular Spectroscopy.* **2020,** *228*, 117702.
14. Ahoulou, E. O.; Drinkard, K. K.; Basnet, K.; St Lorenz, A.; Taratula, O.; Henary, M.; Grant, K. B. DNA Photocleavage in the Near-Infrared Wavelength Range by 2-Quinolinium Dicarbocyanine Dyes. *Molecules.* **2020,** *25* (12).
15. Mapp, C. T.; Owens, E. A.; Henary, M.; Grant, K. B. Oxidative cleavage of DNA by pentamethine carbocyanine dyes irradiated with long-wavelength visible light. *Bioorganic & Medicinal Chemistry Letters.* **2014,** *24* (1), 214-9.

16. Mahon, K. P., Jr.; Ortiz-Meoz, R. F.; Prestwich, E. G.; Kelley, S. O. Photosensitized DNA cleavage promoted by amino acids. *Chemical Communications (Camb).* **2003,** (15), 1956-7.
17. Biton, A.; Ezra, A.; Kasparkova, J.; Brabec, V.; Yavin, E. DNA photocleavage by DNA and DNA-LNA amino acid-dye conjugates. *Bioconjugate Chemistry.* **2010,** *21* (4), 616-21.
18. Akerman, B.; Tuite, E. Single- and double-strand photocleavage of DNA by YO, YOYO and TOTO. *Nucleic Acids Research.* **1996,** *24* (6), 1080-90.
19. Kanony, C.; Akerman, B.; Tuite, E. Photobleaching of asymmetric cyanines used for fluorescence imaging of single DNA molecules. *Journal of American Chemical Society.* **2001,** *123* (33), 7985-95.
20. Ishihara, M.; Fujisawa, S. Review. Photooxygenation, photodegradation and antioxidative activity of platonin, a cyanine photosensitizing dye. *In vivo (Athens, Greece).* **2007,** *21* (2), 163-73.
21. Henary, M.; Mojzych, M. Stability and Reactivity of Polymethine Dyes in Solution. In *Heterocyclic Polymethine Dyes*, Strekowski, L., Ed. Springer Berlin Heidelberg: Berlin, Heidelberg. **2008**, pp 221-238.
22. Renikuntla, B. R.; Rose, H. C.; Eldo, J.; Waggoner, A. S.; Armitage, B. A. Improved photostability and fluorescence properties through polyfluorination of a cyanine dye. *Organic Letters.* **2004,** *6* (6), 909-12.
23. Williams, A. K.; Dasilva, S. C.; Bhatta, A.; Rawal, B.; Liu, M.; Korobkova, E. A. Determination of the drug-DNA binding modes using fluorescence-based assays. *Analytical Biochemistry.* **2012,** *422* (2), 66-73.
24. Aleksić, M. M.; Kapetanović, V. An overview of the optical and electrochemical methods for detection of DNA - drug interactions. *Acta chimica Slovenica.* **2014,** *61* (3), 555-73.
25. Jiang, Q.; Xu, X.; Yin, P. A.; Ma, K.; Zhen, Y.; Duan, P.; Peng, Q.; Chen, W. Q.; Ding, B. Circularly Polarized Luminescence of Achiral Cyanine Molecules Assembled on DNA Templates. *Journal of American Chemical Society.* **2019,** *141* (24), 9490-9494.
26. Sovenyhazy, K. M.; Bordelon, J. A.; Petty, J. T. Spectroscopic studies of the multiple binding modes of a trimethine-bridged cyanine dye with DNA. *Nucleic Acids Research.* **2003,** *31* (10), 2561-9.
27. Clarke, R. J.; Oprysa, A. Fluorescence and Light Scattering. *Journal of Chemical Education.* **2004,** *81* (5), 705.
28. Smith, Z. J.; Huser, T. R.; Wachsmann-Hogiu, S. Raman scattering in pathology. *Analytical cellular pathology (Amst).* **2012,** *35* (3), 145-63.
29. Masilamani, V.; Ghaithan, H. M.; Aljaafreh, M. J.; Ahmed, A.; al Thagafi, R.; Prasad, S.; Alsalhi, M. S. Using a Spectrofluorometer for Resonance Raman Spectra of Organic Molecules. *Journal of Spectroscopy.* **2017,** *2017*, 1-7.
30. Kim, S. K.; Nordén, B. Methyl green. A DNA major-groove binding drug. *FEBS letters.* **1993,** *315* (1), 61-4.
31. Lauria, A.; Montalbano, A.; Barraja, P.; Dattolo, G.; Almerico, A. M. DNA Minor Groove Binders: an Overview on Molecular Modeling and QSAR Approaches. *Current medicinal chemistry.* **2007,** *14* (20), 2136-60.
32. Edwards, K. J.; Jenkins, T. C.; Neidle, S. Crystal structure of a pentamidine-oligonucleotide complex: implications for DNA-binding properties. *Biochemistry.* **1992,** *31* (31), 7104-9.

33. Prieto, D.; Aparicio, G.; Morande, P. E.; Zolessi, F. R. A fast, low cost, and highly efficient fluorescent DNA labeling method using methyl green. *Histochemistry and cell biology.* **2014,** *142* (3), 335-45.
34. Williams, D. E.; Fischer, C. M.; Kassai, M.; Gude, L.; Fernández, M.-J.; Lorente, A.; Grant, K. B. An unlikely DNA cleaving agent: A photo-active trinuclear Cu(II) complex based on hexaazatriphenylene. *Journal of Inorganic Biochemistry.* **2017,** *168*, 55-66.
35. Merkel, P. B.; Kearns, D. R. Radiationless decay of singlet molecular oxygen in solution. Experimental and theoretical study of electronic-to-vibrational energy transfer. *Journal of American. Chemical Society.* **1972,** *94* (21), 7244-7253.
36. Huang, L.; Xuan, Y.; Koide, Y.; Zhiyentayev, T.; Tanaka, M.; Hamblin, M. R. Type I and Type II mechanisms of antimicrobial photodynamic therapy: an in vitro study on gram-negative and gram-positive bacteria. *Lasers in Surgery and Medicine.* **2012,** *44* (6), 490-9.
37. Prasad, A.; Sedlářová, M.; Pospíšil, P. Singlet oxygen imaging using fluorescent probe Singlet Oxygen Sensor Green in photosynthetic organisms. *Scientific Reports.* **2018,** *8* (1), 13685.
38. Kiesslich, T.; Gollmer, A.; Maisch, T.; Berneburg, M.; Plaetzer, K. A comprehensive tutorial on in vitro characterization of new photosensitizers for photodynamic antitumor therapy and photodynamic inactivation of microorganisms. *BioMedical research international.* **2013,** *2013*, 840417.
39. Kim, S.; Fujitsuka, M.; Majima, T. Photochemistry of Singlet Oxygen Sensor Green. *The Journal of Physical Chemistry B.* **2013,** *117* (45), 13985-13992.
40. Koh, E.; Fluhr, R. Singlet oxygen detection in biological systems: Uses and limitations. *Plant Signal Behavior.* **2016,** *11* (7), e1192742-e1192742.

4 GENERAL SUMMARY AND CONCLUSION

Photosensitizing agents that can be light activated in the near-infrared phototherapeutic window are of a great importance for photodynamic therapy, by allowing an enhanced penetration depth of the incident light through biological tissues. In this study, we showed that symmetrical 2-quinolinium and 4-quinolinium pentamethine carbocyanine dyes substituted with either hydrogen (**3** and **KI4**), bromine (**4** and **KI2**), or chlorine (**KI3**) generated DNA cleavage when irradiated in the near-infrared range. The electron withdrawing *meso*-bromine atom of 2 -quinolinium (**4**) and 4-quinolinium (**KI2**) carbocyanine dyes enhances their interactions with dsDNA by preventing them from becoming auto-oxidized in aqueous solution. UV-visible spectra of the brominated carbocyanine dyes reveal that DNA has a major effect on dye aggregation. Low DNA concentrations encouraged the formation of a high order hypsochromic aggregated form of dyes **4** and **KI2**, while high DNA concentrations promoted the formation of a putative bathochromic dye monomer through a intermediate of low-order aggregated dye forms.

The monomeric form of dyes **4** and **KI2** seems to interact with DNA in a non-intercalative way due to lack of fluorescence emission with a possibility of external binding. Moreover, competitive DNA binding using pentamidine shows that dyes **4** and **KI2** might also interact with the DNA minor groove. Reactions of the dyes run in the presence and absence of fluorescent ROS probes, and DNA photocleavage experiments of chemical additives reveal that irradiation of the DNA-bound form of dyes **4** and **KI2** with 707–759-nm and 850 nm near–infrared light generates Type I $OH^{\bullet}$ radicals that create direct strand breaks in plasmid DNA in high yield (pH 7.0, 22 °C). Also, DNA photocleavage reactions of the brominated 4-quinolinium cyanine **KI2** show that irradiation of DNA-bound dye at 905 nm leads to direct DNA strand breakage. The results

presented in this thesis represent the first report of DNA photocleavage upon single-photon excitation of a chromophore at wavelengths above 830 nm.

Fluorescence microscopic data reveal that brominated cyanine dye **4** is taken up by ES-2 ovarian cancer cells by localizing in the cytosolic and perinuclear regions with a possibility of cell nuclei localization. Dye **4** is found to be non-toxic in the dark. Also, when irradiated with 694 nm laser light, cyanine dye **4** shows high levels of phototoxicity by reducing ES-2 ovarian cancer cell viability from 100 ± 10% to 14 ± 1%.

In the future, the photocytotoxicity studies of dye **KI2** will be conducted. Moreover, we will continue to develop novel symmetrical 2-quinolinium and 4-quinolinium carbocyanine dyes that absorb in the near-infrared wavelengths range with the goal of developing near-infrared phototherapeutic agents. The benefit of using near-infrared light is that it allows deep penetration of the incident irradiation into biological tissue to eliminate cancer cells more effectively. Based on our results, cyanine dyes **4** and **KI2** might one day be important as photosensitizing agents in photodynamic cancer therapy.